U.S. Department
of Transportation
National Highway
Traffic Safety
Administration

NHTSA

DOT HS 813 177

September 2021

An Applied Review of Simulation Validation Approaches on a Vehicle Dynamics Model

DISCLAIMER

This publication is distributed by the U.S. Department of Transportation, National Highway Traffic Safety Administration, in the interest of information exchange. The opinions, findings, and conclusions expressed in this publication are those of the authors and not necessarily those of the Department of Transportation or the National Highway Traffic Safety Administration. The United States Government assumes no liability for its contents or use thereof. If trade or manufacturers' names or products are mentioned, it is because they are considered essential to the object of the publication and should not be construed as an endorsement. The United States Government does not endorse products or manufacturers.

NOTE: This report is published in the interest of advancing motor vehicle safety research. While the report may provide results from research or tests using specifically identified motor vehicle models, it is not intended to make conclusions about the safety performance or safety compliance of those motor vehicles, and no such conclusions should be drawn.

Suggested APA Format Citation:

Salaani, K., Rao, S. J., Howe, J. G., Elsasser, D., & Schnelle, S. (2021, September). *An applied review of simulation validation approaches on a vehicle dynamics model* (Report No. DOT HS 813 177). National Highway Traffic Safety Administration.

Technical Report Documentation Page

1. Report No. DOT HS 813 177	**2. Government Accession No.**	**3. Recipient's Catalog No.**
4. Title and Subtitle An Applied Review of Simulation Validation Approaches on a Vehicle Dynamics Model		**5. Report Date** September 2021 **6. Performing Organization Code** NHTSA/NSR-120
7. Authors Kamel Salaani, Ph.D., Sughosh J. Rao Ph.D., and J. Gavin Howe, Transportation Research Center Inc. Devin Elsasser and Scott Schnelle, Ph.D., NHTSA		**8. Performing Organization Report No.**
9. Performing Organization Name and Address National Highway Traffic Safety Administration Vehicle Research and Test Center P.O. Box B37 East Liberty, OH 43319		**10. Work Unit No. (TRAIS)** **11. Contract or Grant No.**
12. Sponsoring Agency Name and Address National Highway Traffic Safety Administration 1200 New Jersey Avenue SE Washington, DC 20590		**13. Type of Report and Period Covered** **14. Sponsoring Agency Code** NHTSA/NSR-120
15. Supplementary Notes		

16. Abstract

This report presents an approach to vehicle dynamics modeling and validation of a Class 6 International 4300 SBA 4x2 truck, model year 2017, with pneumatic brakes. The model was developed using dSPACE Automotive Simulation Models for heavy vehicles with a hardware-in-the-loop pneumatic brake test bench. The report discusses vehicle model validation techniques and applies methodologies found in literature, which include both subjective and objective approaches. This report finds the error quantification method through the use of empirical cumulative distribution methods that estimate the probability of the error between simulation and test track data to have the potential to facilitate thresholds for model acceptance. The goal is to assess vehicle dynamics simulation fidelity with probabilistic metrics within a certain error tolerance.

17. Key Words vehicle dynamics simulation, simulation validation, simulation, simulation scenario, HiL, MiL, SiL, ViL,		**18. Distribution Statement** This document is available to the public from the National Technical Information Service, https://www.ntis.gov/.	
19. Security Classification (of this report) Unclassified	**20. Security Classification (of this page)** Unclassified	**21. No. of Pages** 84	**22. Price**

Form DOT F 1700.7 (8-72) Reproduction of completed page authorized

Table of Contents

List of Figures and Tables

Figures

Tables

Acronyms, Abbreviations, and Initialisms

ADS	automated driving system
ADAS	advanced driver-assistance systems
ABS	antilock braking system
ASM	Automotive Simulation Model (dSPACE model)
CG	center of gravity
CIB	crash imminent braking
ECDF	empirical cumulative distribution function
ESC	electronic stability control
FCW	forward crash warning
FHWA	Federal Highway Administration
FMVSS	Federal Motor Vehicle Safety Standard
GAWR	gross axle weight rating
GVWR	gross vehicle weight rating
HiL	hardware-in-the-loop
ISO	International Standards Organization
JPO	Joint Program Office
LLVW	lightly loaded vehicle weight
MiL	model-in-the-loop
OEM	original equipment manufacturer
SAE	SAE International
SiL	software-in-the-loop
SIS	slowly increasing steer
SUT	single-unit truck
SWA	steering wheel angle
VDS	vehicle dynamics system
ViL	vehicle-in-the-loop
TTC	time to collision

Executive Summary

Simulation has long become an integral part of the vehicle development and validation process. It is routinely used in designing, parametrizing, and testing various vehicle systems in conjunction with track-based and on-road testing. However, simulation is commonly believed to face some challenges; among them is verifying that the simulated virtual world representation is a reasonably accurate approximation of the real-world results. In this report, a vehicle dynamics validation process is presented. The primary goal of the study was to assess vehicle dynamics simulations fidelity with objective, probabilistic metrics within a certain error tolerance, while also considering some subjective evaluations proposed in the literature. These findings may help address the common simulation fidelity research question related to vehicle dynamics quality and reliability.

To facilitate the assessment of simulation fidelity, a methodology is documented for adjusting, calibrating, and validating an existing heavy vehicle dynamics model provided in the dSPACE Automotive Simulation Models based on limited vehicle measurements and field test data. Also, a hardware-in-the-loop pneumatic brake test bench was incorporated into the heavy vehicle dynamics model. Starting with the nominal model provided by dSPACE, vehicle parameters such as mass and center of gravity lateral and longitudinal positions measured for a Class 6 single-unit truck were input into the simulation model. Other vehicle parameters for the model can also be identified through additional testing and vehicle measurements like suspension tests, tire characterization tests, and inertia measurements. However, these is always an important question with respect to what level of simulation fidelity model may be necessary and adequate for the intended purpose. The process used for setting some vehicle model parameters is detailed in this report.

Due to the limited availability of vehicle measurements and field test data, validation research was conducted for steady-state lateral performance, longitudinal deceleration performance, and driving scenario-based validation. For steady-state lateral performance, “slowly increasing steer” field test data were used. Longitudinal braking test data were used to validate longitudinal deceleration performance. The data partially validate the primary longitudinal and lateral modes of vehicle motion. In addition, J-turn driving scenario-based maneuver (Federal Motor Vehicle Safety Standard No. 136) (49 CFR, 2017) test data were used to evaluate vehicle lateral responses with a driver model applying steering to follow the center of the lane, while attempting to maintain a constant speed.

The validation process involved using objective and subjective evaluation methodologies identified in literature. The objective validation involved the use of statistical hypothesis tests, mathematical procedures, and confidence intervals, and was combined with objective performance metrics rather than a subjective assessment of adequacy or satisfaction. In this study, three methods were applied: the 95% confidence interval statistical method, International Standards Organization 19364 (2016), and empirical cumulative distribution function. Subjective evaluations involved computer animation, visual comparison, and inspection of plotted results. Its metrics include indicators of level of appropriateness such as “good,” “excellent,” or “poor.” For the SUT subjective model evaluation, graphical comparison, analytical comparison, and verification were used. The analytical evaluations used the rules of kinematics to check steady-state values of lateral motion and longitudinal braking distance. Gradients were calculated within

the linear range to check roll gradient (vehicle resistance to roll motion), lateral acceleration gradient (acceleration to steering input), understeer gradient, and yaw rate gradient (yaw rate to steering input). The results from the linear analytical comparisons and inspection of graphs/plots demonstrate that the planar moments and forces on the vehicle from the ground forces were adequately formulated and modeled, as were the CG and suspension parameters.

For lateral dynamics, the confidence interval validation methodology, the empirical cumulative distribution function, and ISO 19364 (2016) methods provided consistent validation metrics. For longitudinal dynamics, the ISO 19364 method was not applicable because it is exclusively formulated to address lateral dynamics validity. The ECDF validation methodology was applied to all tests and provided an objective statistical metric for validation.

1 Introduction

This report presents a process of modifying, calibrating, and validating a general heavy truck vehicle dynamics simulation model for use in conjunction with a pneumatic brake hardware-in-the-loop set-up using limited vehicle measurements and test track data. Detailed vehicle models have numerous parameters that need to be modified to fit a specific vehicle. These parameters can be adjusted based on directly measurable vehicle characteristics or calibrated using experimental data. Some vehicle parameters are easily measured, such as vehicle dimensions, mass, CG, and tire corner weights, while others can be obtained through expensive and time-intensive measurements like suspension tests, tire characterization tests, and inertia measurements. There is a natural correlation between the simulation fidelity of a vehicle model, and the cost, resources, and time it takes to tune and validate it. It is often an important and early stage question to address as to what level of simulation fidelity may be adequate and appropriate for the given research objective. Once these directly measurable vehicle model parameters are obtained, further model calibration based on experimental data is necessary to further tune the model parameters to achieve a level of fidelity. This report considers a methodology for modifying, calibrating, and assessing some performance aspects of a heavy truck vehicle dynamics model using measured and estimated vehicle parameters and test track data.

1.1 Literature Review

Models are approximating the system being simulated. The utility of any simulation model depends on its use case, accuracy, and fidelity. The extent to which a model is validated determines its level of accuracy. A computerized mathematical model of a physical system, such as vehicle dynamics, can be considered valid if a simulation's predictions of the system's responses to specified inputs agree with the actual physical system's responses to the same inputs, within some specified level of accuracy (Garott et al., 1997). The inconsistencies between computer models and actual vehicle response could be due to problems in several areas that include model formulation, simulation programming/solver, vehicle parameter identification, numerical accuracy and stability, and low-quality experimental data. A review of vehicle dynamics simulation validation was published by Kutluay (2012), whose dissertation work provides detailed review of objective and subjective vehicle dynamics simulation validation methodologies used by OEMs, the National Highway Traffic Safety Administration, and other research centers.

Validation of the accuracy and fidelity of vehicle dynamics models is an active area of research and standards development. An example is ISO/AWI 22140 (ISO, 2020)**,** which addresses vehicle dynamic simulation and validation for lateral transient response. Another ISO standard ISO/AWI 11010-1 (ISO, 2020) was developed in response to worldwide demand for standardization of simulation models and their fidelity requirements for specific driving maneuvers. During development and testing of road vehicles in simulation, it must be decided beforehand how much fidelity is needed for performing certain driving maneuvers. Without standardization, experts in different organizations develop their own methods and processes to answer this question. Process standardization is useful for model comparability, exchange between project partners and data sharing. As drafted, the main purpose of this ISO standard is to provide a framework that enables a systematic assignment of simulation model characteristics for

certain driving maneuvers. The simulation models are classified into certain model classes, their fidelity level, and related characteristics. The assignment is the responsibility of the user or can be specified by other regulations and standards. The ISO standard contains recommendations of an appropriate simulation quality in terms of performance tests.

ISO 19365 (2016) provides methods for validating vehicle dynamic performance for the sine with dwell maneuver. The validation is based on assessing the tolerances between metrics obtained from physical testing and simulation. For different metrics, the tolerance ranges from ±15% (first peak of yaw rate) to ± 25% (second peak of yaw rate).

The following section provides a review of vehicle dynamic maneuvers that can be used to validate vehicle models.

1.1.1 Vehicle Dynamics Validation Maneuvers Review

Vehicle dynamics simulation validation involves comparing a simulation's predictions of a vehicle's responses to open-loop control inputs (steering, braking, and throttle) and disturbance inputs (wind, surface friction, etc.) to the actual vehicle's responses to the same inputs. There are standardized maneuvers that can be performed during experimental testing that cover a broad range of vehicle operations. These include vehicle longitudinal and lateral primary modes briefly listed as follows:

1. Steady-state lateral performance: These types of standard maneuvers are used to estimate the vehicle's quasi-steady-state lateral kinetic gains and understeer and provide data for characterizing the lateral handling mode of the test vehicle. One of the commonly used maneuvers is the SIS. This maneuver is performed at a constant speed, with handwheel steering rate not exceeding 13.5 deg/s (or corresponding road wheel steering rate), and up to the lateral limit. The model outputs compared to experimental results are lateral acceleration at the vehicle CG, vehicle yaw rate, and vehicle roll angle. These are the primary variables of vehicle motion that can be validated using this maneuver. Vehicle planar positions are not compared in this test, because a small error in accelerations at the start of the test can propagate monotonically through the integration of the equations of motions. Positions may be compared when a closed loop positional control is applied in the vehicle system. Vehicle standards provide more details to characterize vehicle lateral steady-state performances like ISO 19364 (2016), SAE J266 (2018), and FMVSS No. 126 (CFR, 2011)(49 CFR, 2011). These standards provide details of SIS experimental testing and vehicle conditions. An alternative method to the SIS provided in ISO 19364 is the steady-circular driving tests specified in ISO 4138 (2012).

2. Transient lateral performance: These types of standard maneuvers are used to estimate the vehicle's transient response. Handwheel or road wheel inputs are varied in the frequency domain and applied over a broad range of controlled speeds. Typical measures include steering input to lateral acceleration gains, yaw rate gains, and phase delays. The gains define the vehicle response bandwidth, and the phase provides a measure of vehicle responsiveness or agility to steering inputs. These three dynamic factors can be used to help grossly define vehicle agility and dynamic performances (Salaani, 1996) (Starkey, 1993). Steering inputs can be formulated with a sweep sine function, pulse steer, or

multiple sine steering tests at different frequencies and amplitude (Heydinger et al., 1993). Frequency domain analysis is appropriate to use only in the linear range of vehicle motion, typically under 0.3~0.4 g of lateral acceleration. Another transient test, like that specified by ISO 7401 (2011) Lateral Transient Methods, is a step steering input test (steering input increases from zero to a specified number in a very short time).

3. Longitudinal deceleration performance: These types of maneuvers can be used to characterize the vehicle's deceleration response to rolling resistance (coast down), regenerative brake system, and primary brake application inputs. These maneuvers can contain steady-state and transient effects, depending on the control strategy and severity of the brake application. An example for this type of maneuver is the FMVSS No. 121 (49 CFR, 2009) brake test procedure. The typical measures for this type of maneuver are stopping distance, vehicle speed, and longitudinal deceleration. If the simulation is to be used in driver-in-the-loop simulation, then the vehicle pitch angle may need to be examined and compared with experimental data.

4. Longitudinal acceleration performance: These maneuvers are performed to measure vehicle responses to powertrain control inputs. These tests usually apply a step powertrain input from zero speed (traditionally the input is called throttle input for a combustion engine) and the resulting longitudinal speed and acceleration can be compared to those obtained from simulation. These maneuvers contain steady-state and transient effects. Vehicle stability and control studies are dominated by either steering or braking control inputs, therefore no such standards are developed to validate this mode of vehicle operations. This mode is important in the development of vehicle driving simulators or driver in the loop simulations (Salaani & Heydinger, 1998).

5. Road disturbance input: These maneuvers are used to estimate vehicle vertical responses to road irregularities. Ride quality is normally associated with the level of comfort experienced when traveling in a vehicle. The vehicle experiences a broad spectrum of vibrations in response to excitation inputs that include road roughness, and tire/wheel, drive line, and engine vibrations. Road disturbance input maneuvers are typically used to test vehicle models for driver in the loop simulation studies where vertical motion cues are important feedback to the driver. This is important to vehicle developers/designers but secondary for vehicle handling and directional control and therefore not covered in this report.

6. Driving scenario-based validation: For the purposes of this research, these types of maneuvers can be used to build confidence in vehicle models developed with test track characterization data. Examples of driving scenario-based maneuvers for lateral dynamics validation are lane changes, obstacle avoidance maneuvers, such as the sine with dwell (FMVSS No. 126) (49 CFR, 2011), and curve negotiation maneuvers, such as the J-turn used in FMVSS No. 136 (49 CFR, 2017). Braking-in-a-turn maneuvers can be used to provide data for characterizing the interaction between the lateral and longitudinal handling modes of the test vehicle. These maneuvers can be used to evaluate the tire-ground complex phenomena. Steering systems can be tested with the on-center weave

maneuvers, and flick tests (Salaani et al., 2004). These can be used to help characterize the on-center handling of the vehicle and driver-in-the-loop systems.

1.1.2 Comparison Methodology Review

Simulation output can be compared with experimental results either subjectively or objectively. Subjective evaluation can be done with computer animation, visual comparison, and inspection of plotted results. Subjective metrics include indicators of level of appropriateness such as "good," "excellent," or "poor." Subjective numerical metrics might include general descriptive statistics like mean values, maximum or minimum values, or data at specific sub-sections combined with the experimenter's opinion of what is poor, good enough, or excellent.

Objective validation involves the use of statistical hypothesis tests, mathematical procedures, and confidence intervals, and is combined with numerical measures of agreement rather than an individual's assessment of adequacy or satisfaction. This process uses repetitive experimental testing of the actual vehicle to allow statistical methods to be used to determine the random uncertainty present in the experimental testing and measurement process. Every experimental measurement involves random error superimposed onto the signal. Random errors can be induced by road roughness, tire non-uniformity, changes due to tire wear, changes in the brakes (due to brake temperature and wear), transducer measurement error, and other unaccounted for variations disturbing the vehicle. The easiest way to determine the experimental random error level present in data is to average experimental data over several repetitions. One statistical method to validate vehicle model performance that has been used since the 1990's is the confidence interval (CI) methodology (Salaani, 1996) (Heydinger et al., 1990). In this method, simulation results are checked to see if they fall within the 95% CI of experimental runs (10 tests are recommended to be performed for statistically significant results).

ISO 19364 (2016) provides a methodology for comparing computer simulation results from a vehicle mathematical model with measured test data for a physical vehicle, according to steady-state circular driving tests as specified in ISO 4138 (ISO 4138, 2012)(2012) or the SIS test as described by FMVSS No. 126 (49 CFR, 2011). The standard states that the physically tested vehicle should be tested at least three times to allow the test data to be compared with the simulation results. As described in ISO 19364, the simulation results are used to define graphical boundaries for overlaid cross-plots (lateral acceleration in the X-axis). The data from physical testing are overlaid on the cross-plots to check if the measurements fall within the acceptable ranges. Lateral acceleration, steering wheel angle, sideslip angle, and roll angle are compared. The simulation is deemed valid if the experimental results fall within the boundaries. It is essentially a visual inspection based on a predetermined boundary with offsets and gains. This method relies on normalization of different units on the X and Y axes, and boundary values are subjectively set. This validation exercise is to test if experimental results fall closely to simulated results with a defined threshold error boundary.

The ECDF is a complementary method for objective assessments of vehicle dynamics models. The ECDF provides a numerical grading to the quality of simulation accuracy. It is not based on graphical comparisons but provides the probability that a model meets a predefined error tolerance. The error is the difference between the measured experimental variables (e.g., acceleration, yaw rate) and the corresponding values from the simulation results. This method

must be enhanced with an analytical comparison within the linear range, to avoid masking errors. The application of ECDF is explored and discussed in further detail in the following sections of this report.

1.2 Simulation Validation and Limitations

Depending on the intended application of the simulations, validations should include primary modes in longitudinal or lateral directions, or both. Other validation cases like the effects of wind gusts and other environmental conditions that affect vehicle stability and control can be addressed independently. Even if a modeled vehicle shows acceptable simulation accuracies when compared with experimental data in both longitudinal and lateral modes, it may not hold the same level of validity for combined longitudinal and lateral modes. Multi-directional secondary tests like the sine with dwell steering test (i.e., FMVSS No. 126, 49 CFR, 2011), the J-Turn test (i.e., FMVSS No. 136) (49 CFR, 2017), and other tests can be compared to gain more confidence in the model for combined lateral and longitudinal modes and to better understand the model limitations.

Vehicle dynamics operating range of the intended application can be defined using maximum performance acceleration and the frequency bandwidth of the controlled input. The frequency bandwidth of the model is defined by the maximum frequency at which the simulated control input will operate. The maximum dynamic performance is systematically addressed by applying the concept of the g-g diagram, a graph of longitudinal acceleration versus lateral acceleration, as shown in Figure 1-1. The acceleration severity level defined by this planar acceleration graph and the rate of change of controlled inputs define the operational envelope of the simulation at which it is evaluated and rated for trustworthiness.

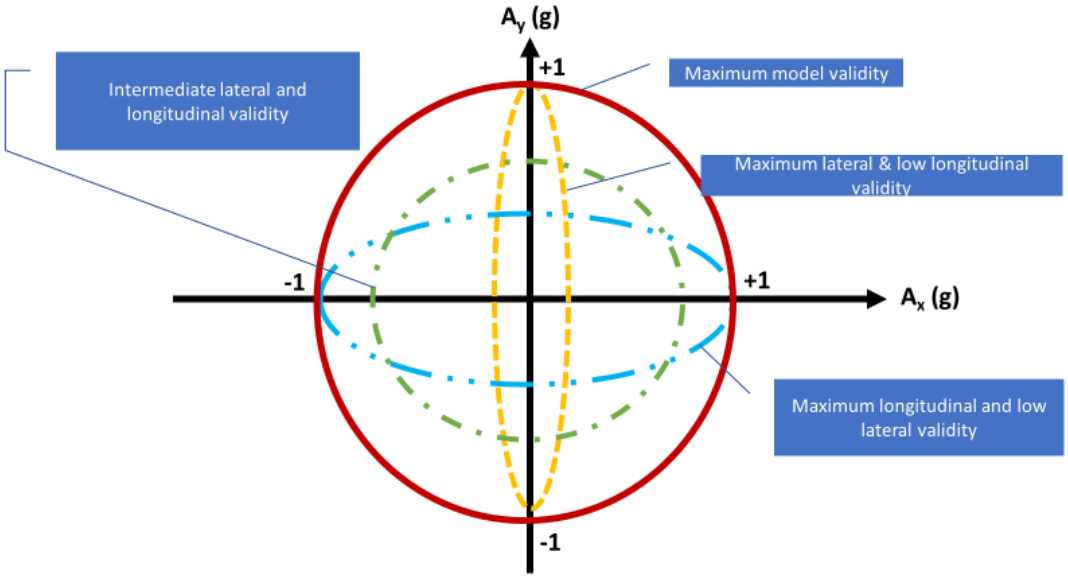

Figure 1-1. Vehicle Model Trustworthiness Examples

Vehicle dynamics simulation evaluation is a comparison of simulation results with test track measurements using the same control inputs, like steering, braking, or throttle (accelerator) inputs. It is an open-loop simulation process where the automated driving system is not part of the dynamics to be evaluated. This direct comparison with experimental data is compelling and sound, but measuring the actual physical responses is not an error-free exercise due to the inherent systematic and random errors within the vehicle system, like changes in tire forces due to wear from repeated testing, brake friction changes due to temperature and wear, road friction in relation to the viscoelastic nature of tire rubber compounds, and the laws of metallic friction as they are inadvertently misapplied to rubber products (Smith, 2008).

A simulation prediction will, in general, only be correct within some portion of the physical system's operating range. For example, vehicle dynamics simulations' prediction may be accurate for low lateral acceleration maneuvers but become progressively worse as lateral acceleration increases due to non-linear effects from tire mechanics and flexible elements in the model not being correctly modeled. A second example is incorrect modeling of the steering compliances or kinetic Ackerman effect, where the simulation's predictions could get worse as steer angle increases. A third example is a brake model being well suited for a specific range of vehicle speed, but not at low or high-speed due to brake sensitivity to wheel speed or kinetic energy of the rotating parts that have not been properly modeled for low/high speed operation.

Similarly, a simulation's predictions may only be accurate for control inputs that predominantly contain frequencies within some specified range. Vehicle lateral motion frequency content (measurable responses) can be up to 4 Hz for light vehicles, and 3 Hz or lower for heavy vehicles. For example, if vehicle dynamics simulations are compared only with test data from low frequency input maneuvers, then it might not be appropriate for maneuvers with fast transient inputs with high frequencies.

Moreover, simulations are valid only for specified input/output groups. For example, simply because the simulation has been shown to be valid for braking and steering control inputs, does not imply that the response to a road disturbance (such as road bump or pothole) will be correctly predicted. Similarly, a simulation that successfully predicts lateral sprung mass acceleration might fail to predict vertical sprung mass acceleration and vehicle ride performance. Also, when a vehicle is validated for longitudinal and lateral modes independently, it may not hold the same level of validity for combined longitudinal and lateral modes.

The level of fidelity required to classify a simulation vehicle model as valid depends on the range of perturbations/inputs and their severity utilized in driving scenarios during simulation. If the simulation vehicle model is to be used for navigation purpose only, then a valid linear model may be good enough (accelerations under 0.3 g). If incidents where stability control or automatic emergency braking systems are to be deployed, then validations at higher lateral and longitudinal accelerations are needed. In the work presented herein, validation was performed for up to the limit, so that advanced emergency control systems, like ESC or AEB, can be verified with simulation tests.

1.3 Applied Test Maneuvers and Validation Methods

To provide an example for how applied test maneuvers and validation methods can be used to validate vehicle models, an SUT vehicle model was built with dSPACE ASM software. Model development is described in detail in Appendix A. Due to the limited vehicle measurements and field test data available, the validation was only assessed for steady-state lateral performance, longitudinal deceleration performance, and a driving scenario-based validation. For steady-state lateral performance, SIS field test data were used, and longitudinal braking test data were used to validate longitudinal deceleration performance. The data partially validate the primary longitudinal and lateral modes of vehicle motion. In addition, J-turn driving scenario-based maneuver (FMVSS No. 136) (49 CFR, 2017) test data were used to evaluate vehicle lateral responses with a driver model. Transient lateral performance and longitudinal acceleration performance were not assessed due to the limited data available. Road disturbance modeling, as noted earlier, was considered beyond the scope of this evaluation.

Objective and subjective evaluations, which were used to validate the SUT model, include direct graphical comparison, analytical comparison and verification, CI statistical methods, ISO 19364 (2016), and the ECDF method.

2 Test Vehicle and Model

This chapter discusses the SUT vehicle used for vehicle dynamics testing, field tests conducted, and model development. In the interest of time and resources, for this research, approximate values were used for parameters that were not measured for the vehicle model. The focus of this research is objective and subjective validation techniques and not exact component level modeling of the vehicle. Hence a reasonable vehicle dynamics model representative of the test vehicle was arrived at using the approximations described in this section.

2.1 Test Vehicle

A Class 6 SUT was selected as the test vehicle for comparing results from the test track research with computer simulation. Vehicle properties and descriptions are given in Table 2-1. The SUT was evaluated at GVWR. Axle weights are given in Table 2-2. The SUT was a 2017 International 4300 SBA 4x2 and is shown in Figure 2-1 with outriggers and load frame installed. It was equipped with a Bendix Wingman Fusion^{T} system, pneumatic brake system, ABS, Bendix ESP EC-80 Controller (ESC), Bendix Wingman FLR21 Radar, and Bendix AutoVue FLC20 Camera.

Table 2-1. Test Vehicle Description

2017 International 4300 SBA 4x2	
Configuration	Cab and Chassis
Brake System	S Cam Drum Air Brakes
Model Year, Make, Model	International 4300 SBA 4x2
Drive GAWR	10,000 lbs.
Front GAWR	19,000 lbs.
GVWR	25,999 lbs.
Wheelbase	177 in.
Track - Steer Axle	67.5 in. inside 91.5 in. outside
Track - Drive Axles	48.25 in. inside 98.5 in. outside
Overall Length	282 in.
Overall Width	119 in.
Overall Height	102 in.
Steering Ratio	18.3 deg/deg
ABS System	Bendix ABS/ Auto Traction Control/ESP
Active Safety System	Bendix Wingman Fusion
Front Suspension	Dead rigid axle leaf spring suspension
Rear Suspension	Rigid live axle air ride suspension
Steer Axle Tire	11R22.5 Continental HS3 EcoPlus
Drive Axle Tire	11R22.5 Continental HDR2

Table 2-2. Truck Measured Weight at GVWR

Truck Weight at GVWR kg (lbs.)						
Steer – Left	**Steer – Right**	**Steer Axle TOTAL**	**Rear Drive Axle – Left**	**Rear Drive Axle – Right**	**Drive Axle TOTAL**	**Testing Weight**
2168 (4,780)	1877 (4,138)	4045 (8,918)	3942 (8,690)	3783 (8,340)	7725 (17,030)	11770 (25,948)

Figure 2-1. The 2017 International 4300 SBA 4x2

2.2 Test Data

Test data were collected using an RT 3000 that was mounted on the vehicle and from the vehicle CAN bus. The RT3000 measurement device is manufactured by Oxford Technical Solutions and provides six degree of freedom inertial data and highly accurate real-time differential GPS

positioning. The data were then processed, which included data filtering and acceleration correction to the roll angle and CG offsets. The tests that were used to validate the vehicle model are listed in Table 2-3. All tests were performed at the proving grounds of Transportation Research Center Inc.

Table 2-3. Speed and Number of Experimental Tests

Tests	Speed km/h (mph)	Direction_1	Direction_2	Total
SIS	48.3 (30)	3 Left	3 Right	6
Brake – FMVSS No. 121	48.3 (30)	3 North	3 South	6
Brake – FMVSS No. 121	96.6 (60)	3 North	3 South	6
JTurn – FMVSS No. 136	32.8 (20.5) to 64.8 (40.3)	18 Left	18 Right	36

2.3 SUT Vehicle Dynamics Modeling

A vehicle dynamics simulation is based on a set of equations derived from a model of the vehicle being simulated. Adjustable values, known as vehicle parameters, in these equations describe the specific vehicle configuration being modeled. During the development of the parametrization process, each vehicle model parameters should be unambiguously defined, with methods developed to measure these parameters. Parameters that are not clearly defined or for which there is no means for measuring/obtaining hinder the objective validation process.

Vehicle model parameters should be obtained independently when possible and when practical. While the ability to adjust the vehicle's parameters to make a simulation prediction match experimental data is a strong argument for the correctness of the model, it is preferable to match simulation predictions made with independently measured, non-adjusted, vehicle parameters. This would independently validate both the modeling methodology as well as the measured parameters. Certain parameters are difficult to measure and if no data are available, like suspension compliances (elasticity), then estimation methods could be used, and parameters can be varied within a reasonable range to fit experimental data. As an example, tire force peak saturation levels are surface dependent; that is, the same tire behaves slightly different if it is on a concrete or asphalt surface, and the measured forces from the test machine are certainly different. In this case, adjustments of friction levels are expected.

The SUT model development is briefly discussed in this chapter. The details of model development and parameter setting for vehicle mass and inertial properties, suspension geometries and force properties, suspension compliances, tire forces and moments, steering system, and brake system are all discussed in Appendix A.

2.3.1 Vehicle Mass, CG, and Inertia Properties

SUT mass and CG lateral and longitudinal positions were measured for the tested vehicle. However, vertical CG position and inertia were assumed from a different vehicle of similar size (data obtained from a measurement conducted on a 2006 Volvo 6X4 VNL 64T630 at AMSRD-

TAR-D, US Army TARDEC). The vehicle model uses four unsprung masses, one at each corner. Each of this unsprung mass at the corner is composed of the wheel assembly and half of the solid axle. The masses and inertia were measured for all these components and assembled into one mass. The values of their masses and inertia were adopted from a prior SUT model (2011 International Durastar 4300M7 SBA 4x2) in different software (Salaani et al., 2016).

2.3.2 Tire Model

The SUT model used dSPACE ASM *EasyToUse* (TMeasy) tire model. This is a semi empirical tire model for describing lateral and longitudinal forces and self-aligning torque. The model parameters were set by modifying data from typical heavy vehicle tires. The modifications were based on setting the three fundamental properties of tire force generation processes (stiffnesses, peak, and sliding frictions) to get simulations close to experimental results.

Two main drawbacks of this model were observed. The first was its linear dependency on normal load variations, and the second was the lack of tire relaxation or force delays. These limitations would make the simulated vehicle response not accurate in the high nonlinear region (typically higher than 0.5 g of acceleration), because at these dynamic states the effects of load shifting laterally or longitudinally would not be accurately accounted for. The lack of force delays would make the simulated transient dynamics not in phase of what would be expected and limits the frequency bandwidth validity region.

2.3.3 Suspension Geometries and Compliances

The suspension compliances and geometries model data were adopted from a similar SUT truck model provided in dSPACE and modified to match the tested SUT. In this suspension modeling process, the default values were used as a starting point to see how well the model performed in comparison to the test track data. If disagreements were encountered, adjustments were made based on observed vehicle dynamics. Many of the properties were set to reflect solid axle rigidity at the front and rear, and to account for most important effects like roll steer, or lateral compliances that affect the resultant road wheel steer angles. As noted earlier, none of these suspension properties were measured for the modeled SUT.

2.3.4 Steering Subsystem

The SUT model used dSPACE ASM Pitman-arm steering system model. The handwheel to road wheel steering angle ratio was measured for the test vehicle and incorporated in the dSPACE ASM model. None of the other parameters were modified from the original dSPACE ASM Pitman-arm steering system model.

2.3.5 Brake Model

The dSPACE ASM pneumatic brake model was not applied in this SUT model since it required numerous brake component parameters not available for the test vehicle. The model used the HiL brake system developed at NHTSA (Salaani et al., 2016) with adjustments to accommodate a two-axle truck system. The ASM Simulink model was modified to integrate brake line pressures measured at the wheel chambers in the HiL setup as well as the electronic control units on the HiL setup.

For this simulation, the electronic control unit (Bendix EC-60) was used to primarily activate the ABS system during hard braking, with no stability and control effects. Brake parameters were adopted from prior NHTSA research (Ashley, 2003). The values of the brake torque curves were adjusted to get the simulation braking responses (acceleration, speed, and stopping distance) during deceleration events closer to experimental measurements. A first-order dynamic delay with a time constant of 0.05 seconds was incorporated at each brake line to introduce additional brake delays and to filter brake line data from measurement noise.

2.3.6 Powertrain and Aerodynamics

The SUT powertrain model and aerodynamics were adopted from dSPACE ASM heavy track model of same type.

2.4 Simulation Data and Test Data Comparison Tools and Techniques

In this simulation research, only one test is used because the model response is assumed to be deterministic, or nearly deterministic with small imperceptible differences in output from test-to-test. The simulation data was collected using dSPACE ControlDesk data logger and exported to MATLAB data files. Each of the data files has a complex data structure (data standard) that was converted using an in-house MATLAB routine to multiple simple data channels that could be compared directly to the corresponding channels from experimental data.

A data processing program was developed using MATLAB which took both the simulation data and the experimental test track data as inputs and performed the following processes:

- Data synchronization: Simulation and experiment test track data were synchronized to the same starting condition of the test experiment. Different scenarios used different sync-reference points. The J-Turn scenario used the 150-feet circle entrance gate as the sync-reference point. The Brake-Stop scenario used brake treadle pushing point. The SIS used the steering start point.
- Data grouping: Vehicle experiments were often conducted with multiple repeated tests for one test condition. To compare with the simulation data, the program grouped multiple tests and calculated statistical values like the mean, standard deviation, and confidence level.
- Data comparison: The simulation data and the experiment data were compared, and the results were listed in tables and plotted as figures.
- Automated validation document generation: All the results of each scenario were put in a document by the data processing program.

3 Model Validation

This chapter presents the comparison between test and simulation data to validate the vehicle model. The process included validating the steady-state lateral response of the model, followed by a driving scenario-based lateral dynamics validation. Finally, the longitudinal braking behavior was validated using experimental data. The maneuvers used and the data comparison are presented in the sections below.

3.1 Steady-State Lateral Performance – Slowly Increasing Steer Maneuver

The steady-state lateral dynamics were validated using the SIS maneuver. The SIS maneuver is a gradual handwheel angle input at a constant rate of 13.5 deg/s while maintaining a constant vehicle speed, up to the nonlinear response region of the vehicle. Measurements showed that the SUT test vehicle lateral dynamics were consistently linear up to a lateral acceleration of 0.35 g, even when loaded to GVWR.

3.1.1 Subjective Evaluation

Figure 3-1 shows the results of SIS maneuvers conducted at 30 mph (48 km/h) with the truck loaded to its GVWR. At a constant speed and with a slowly increasing steer, the key vehicle variables to be examined are lateral acceleration, yaw rate, and roll angle. Table 3-1 provides a general comparison between experimental results and simulation, and lists entry speed (u_0), steer angle (θ) at 0.3 g of lateral acceleration, and maximum lateral acceleration achieved during each test. The graphs and the tabulated data indicate that the simulation through visual inspection matched well with the experimental data up to nearly 0.55 g of lateral acceleration.

It is to be noted that the experimental data show asymmetrical behavior of the test vehicle when comparing the left and right SIS maneuvers. For left steering direction, the steady-state curve (Figure 3-1) is asymptotic to some limit of lateral acceleration, which is an indication of limit understeer behavior. The plot indicates that both simulation and experimental vehicle followed similar trends up to maximum lateral acceleration.

However, for the right steering direction, oversteer behavior was consistently observed for the test vehicle, as evidenced by the yaw rate and lateral acceleration plots in Figure 3-1. The lateral acceleration drops suddenly (from 0.5 g) accompanied by an increase in yaw rate in excess of 20 deg/s indicating that the test vehicle spun inwards.

The asymmetry of the left and right SIS tests could be the result of various factors such as the nonlinearity of the suspension system, asymmetrical loading and suspension compliances, and complex tire mechanics at high dynamic, to name a few. These effects were not measured and modeled in simulation.

For both test directions, the test vehicle could not maintain the constant test speed above 0.55 g of lateral acceleration. However, in the simulation tests, constant maneuver speed was achieved. This was because the powertrain model used in simulation is generic and not specific to the tested SUT.

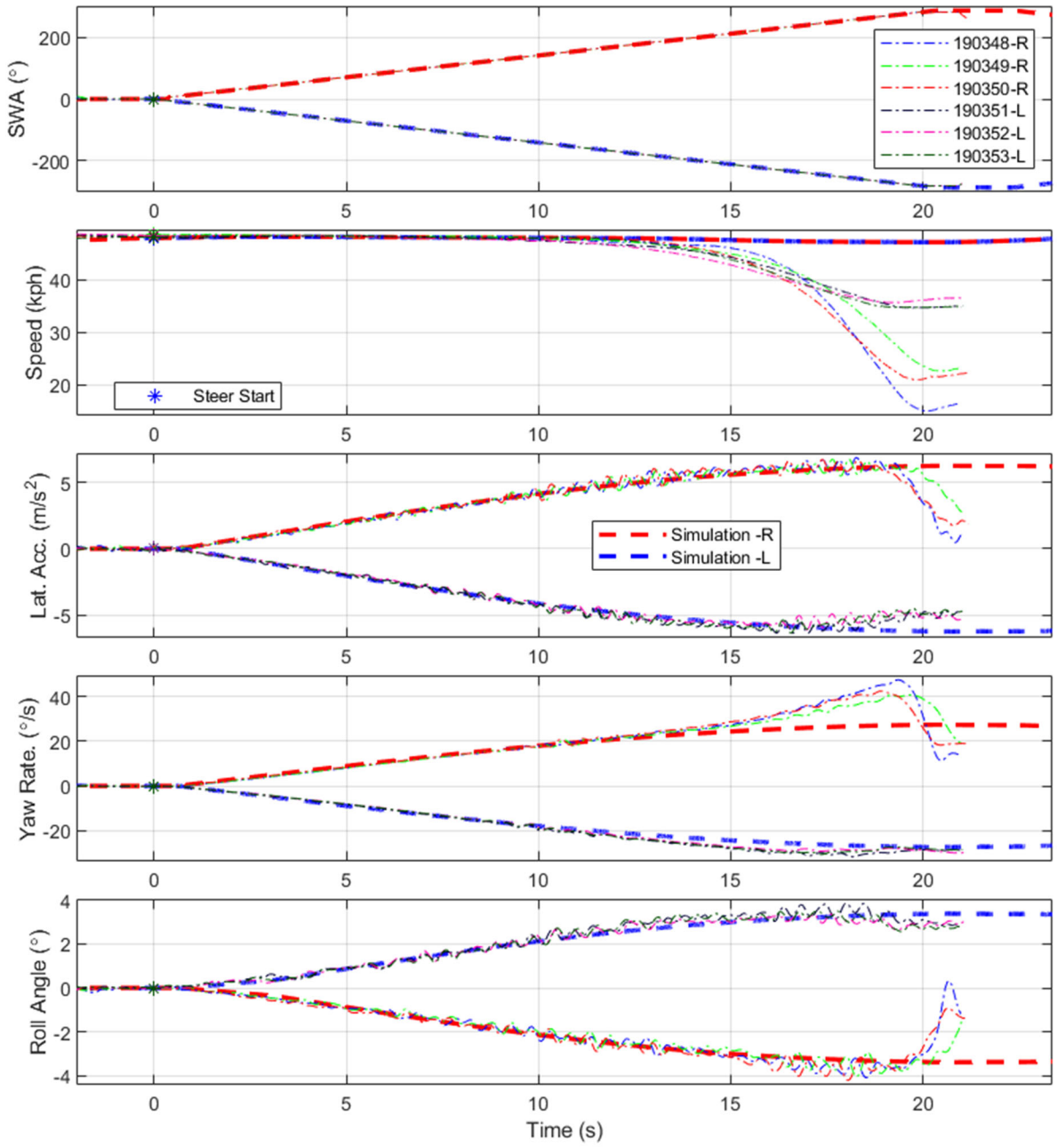

Figure 3-1. SIS Control Inputs and Kinetics at 48 km/h

Table 3-1. General SIS Metrics

u_0 (km/h) & Direction	***@ a_y =0.3g (degrees)***	***Correlation* (R^2)**	**Max. a_y (g)**
Experimental			
48.6-R	103.2	0.97	0.70
48.6-R	98.4	0.97	0.68
48.2-R	101.7	0.98	0.68

u_0 (km/h) & Direction	*@ a_y =0.3g (degrees)*	*Correlation* **(R^2)**	**Max. a_y (g)**
48.2-L	-96.5	0.97	0.65
48.6-L	-101.9	0.99	0.62
48.2-L	-102.3	0.99	0.64
Mean	100.7	0.98	0.66
Standard Deviation	2.61	0.008	0.03
Simulation			
47.9-R&L	99.2	1.0	0.64

Analytical evaluations are used to augment subjective evaluations. Analytical checks should always be performed because direct comparison to experimental data might mask certain types of errors.

Based on the rules of kinematics, the relation shown in Equation 1 should be maintained:

$$a_y = \psi * u \qquad \textbf{Eq. 1}$$

Where,

a_y: Vehicle lateral acceleration (at CG position) (m/s^2)
ψ: Vehicle yaw rate (degrees/s)
u: Vehicle longitudinal speed (m/s)

As a sanity check, the recorded data from both track tests and simulation are validated to ensure they conform to the above equation. Figure 3-2 shows a plot of Equation 1 for both simulation and experiments. The computed correlations were higher than 0.99 (Table 3-2). This indicates that the equations of motions used in simulation are not erroneous, and that the measurements of lateral acceleration, yaw rate, and speed were consistent. Nonconformity to the above equation in the data would indicate incorrect mathematical formulations of motion. In the case of experimental data, it could indicate poor experimental practices, like the acceleration transducer measurements incorrectly/not corrected for the vehicle CG position or accounting for vehicle roll motion by removing the gravitational effects, or the sensors were not properly calibrated. For the experimental data to be used as a "ground truth," it should be thoroughly checked. This simple steady-state equation used in this analysis is a simple approach to gain confidence in both simulation and experimental data.

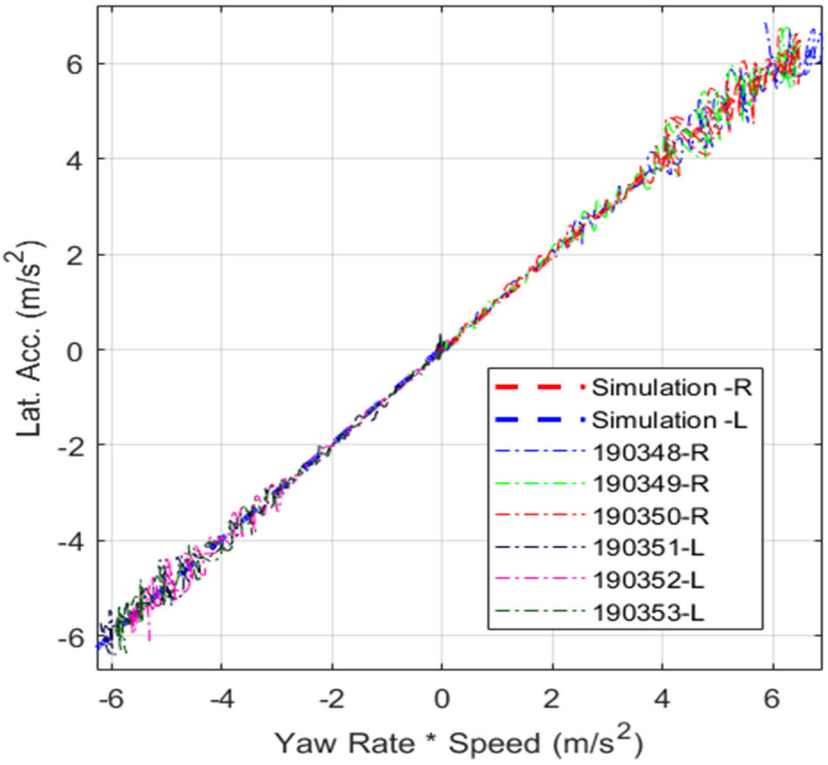

Figure 3-2. Steady-State Lateral Sanity Checks

Table 3-2. Steady-State Sanity Check

u_0 (km/h) & Direction	Correlation Coefficient (R^2) of a_y *vs.* ·
Experimental	
48.6-R	0.994
48.6-R	0.993
48.2-R	0.994
48.2-L	0.993
48.6-L	0.993
48.2-L	0.996
Mean	0.994
Standard Deviation	0.0012
Simulation	
47.9-R&L	1.0

Gradient metrics can also be used for the analytical analysis. In lateral steady-state dynamics, the motion variables are lateral acceleration, yaw rate, and roll angle, while the control inputs are speed and steering angle (handwheel or road wheel angles). These measures help the evaluator to subjectively address if the model is appropriate for the tested vehicle. For example, large discrepancies between measured understeer gradients compared with the simulation would indicate erroneous modeling.

Although instabilities (in general) occur within the non-linear range of vehicle motion, linear analyses for classifying vehicle responses and dynamical properties are needed for a complete systematic characterization. The linear behavior sets the tone of nonlinear responses. Three gradients will be discussed herein; the first is roll gradient, the second is lateral acceleration gradient which is used to compute the understeer gradient, and the third is the yaw rate gradient.

Roll Gradient:
Roll gradient, as shown in Equation 2, is a measure of a vehicle system's resistance to roll motion. Roll gradient is inversely proportional to suspension stiffness. The lower the suspension stiffness the higher the gradient, yet suspensions are designed for a compromise between ride feel and lateral handling performances. A stiffer suspension increases vertical vibrations of the vehicle.

$$\frac{\emptyset}{da_y} = \boldsymbol{m}\frac{\emptyset}{\partial(\sum F_y)} \quad \mathbf{9.} \quad (\boldsymbol{deg/g}) \qquad \textbf{Eq. 2}$$

Where,

- $\emptyset$: Vehicle roll angle (degrees)
- a_y : Vehicle lateral acceleration (g)
- $\sum F_y$: Total summation of lateral forces (N)
- m : Vehicle mass (kg)

Figure 3-3 shows the comparison between simulation and experimental data of roll angle versus lateral acceleration. The results indicate accurate predictions of roll motion. The values of roll gradients and roll angles at steering angles of 100° and 200°, and maximum roll are listed in Table 3-3. The simulated vehicle roll angle underestimated mean measured values by 0.08°, 0.26°, and 0.45° respectively at 100°, 200°, and maximum input of steering angle.

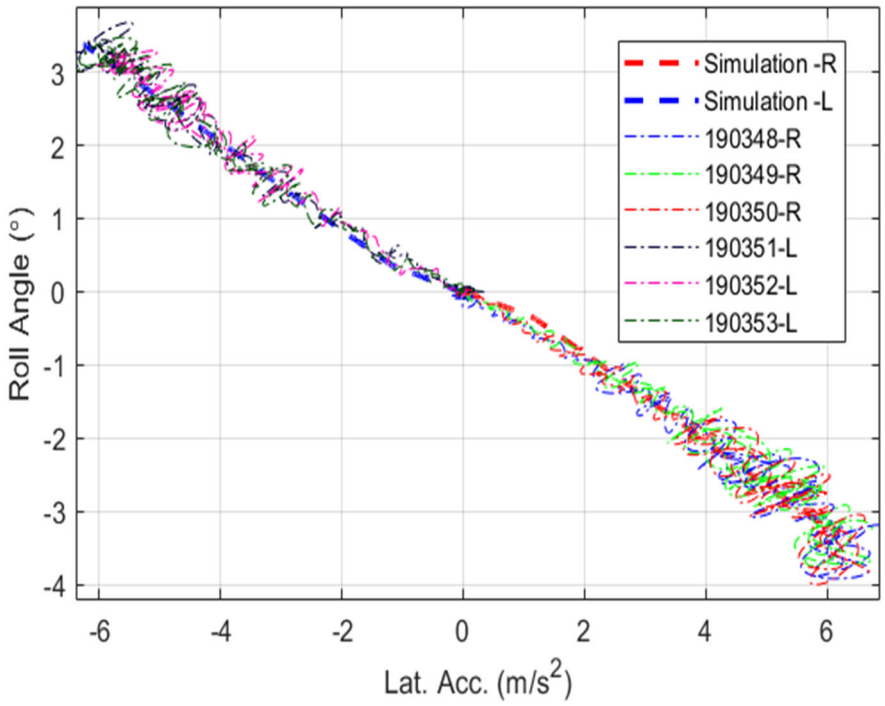

Figure 3-3. Roll Angle Gain

Table 3-3. Roll Angle Metrics

u_0 (km/h) & Direction	Roll Gradient $\frac{\emptyset}{da_y}$ (degrees/g)	Max Roll Angle at θ = 100° (degrees)	Max Roll Angle at θ = 200° (degrees)	Max Roll Angle (degrees)
Experiments				
48.6-R	-4.607	1.38	3.08	4.07
48.6-R	-4.597	1.33	2.93	4.03
48.2-R	-4.816	1.56	3.08	4.20
48.2-L	-4.763	1.54	3.29	3.85
48.6-L	-5.130	1.67	3.12	3.35
48.2-L	-4.859	1.46	3.34	3.49
Mean	-4.795	1.49	3.14	3.83
Standard Deviation	0.196	0.12	0.15	0.34
Simulation				
47.9-R&L	-5.409	1.41	2.88	3.38

Lateral Acceleration Gradient:
Lateral acceleration gradient measurements provide the gradient of lateral acceleration with respect to road wheel steer angle. It is a measure of vehicle's lateral motion sensitivity to steering input, as shown in Figure 3-4. Within the linear range and steady motion, the lateral gradient is expressed using vehicle understeer gradient, vehicle wheelbase, and longitudinal speed, as follows:

$$\frac{d\left(\frac{a_y}{9.81}\right)}{d\delta} = \frac{u^2}{\frac{180}{\pi}L + \frac{K_u}{9.81}u^2} \quad \frac{1}{9.81} \quad (g/deg) \qquad \textbf{Eq. 3}$$

Where,

a_y : Vehicle lateral acceleration (m/s^2)
δ : Road wheel steer angle (degrees)
u : Vehicle longitudinal speed (m/s)
K_u: Vehicle understeer gradient (degrees/g)
L : Vehicle wheelbase (m)
g : Acceleration due to gravity (1 g = 9.81 m/sec^2)

Where the road wheel steer angle δ is the handwheel angle θ divided by the steering ratio K_{SR}, as follows:

$$\delta = \frac{\theta}{K_{SR}} \qquad \textbf{Eq. 4}$$

Where,

δ : Road wheel steer angle (degrees)
θ : Handwheel steer angle (degrees)
K_{SR}: Vehicle steering ratio

The understeer gradient in *deg/g* is estimated for both experimental and simulation data using Equation 5.

$$K_u = 9.81\left(\frac{d\delta}{d(a_y)} - \frac{180L}{\pi u^2}\right) \quad (deg/g) \qquad \textbf{Eq. 5}$$

Where,

a_y : Vehicle lateral acceleration (m/s^2)
δ : Road wheel steer angle (degrees)
u : Vehicle longitudinal speed (m/s)
K_u: Vehicle understeer gradient (degrees/g)
L : Vehicle wheelbase (m)
g : Acceleration due to gravity (1 g = 9.81 m/sec^2)

This understeer gradient is affected by the mass distribution of the vehicle, linear cornering and camber thrust stiffness, wheel base, vehicle roll center, suspension roll steer, lateral load transfer during cornering, lateral force deflection steer (tire carcass stiffness), and the steering system kinetics and compliance properties. If the simulated understeer gradient value is substantially different from measured values, then at least one of the above vehicle properties were either not modeled correctly, or erroneous parameters were used, or both.

Table 3-4 lists the values for the lateral acceleration gradient and the understeer gradient for both simulation and experiments. The understeer gradient is sensitive to vehicle speed. The simulation

result of the lateral acceleration gradient falls closer to the right-side testing experimental values, and the difference with the combined mean for both right and left sides is 0.001 m/s^2/deg. The understeer gradient from simulation is 0.35 deg/g less than the combined mean value.

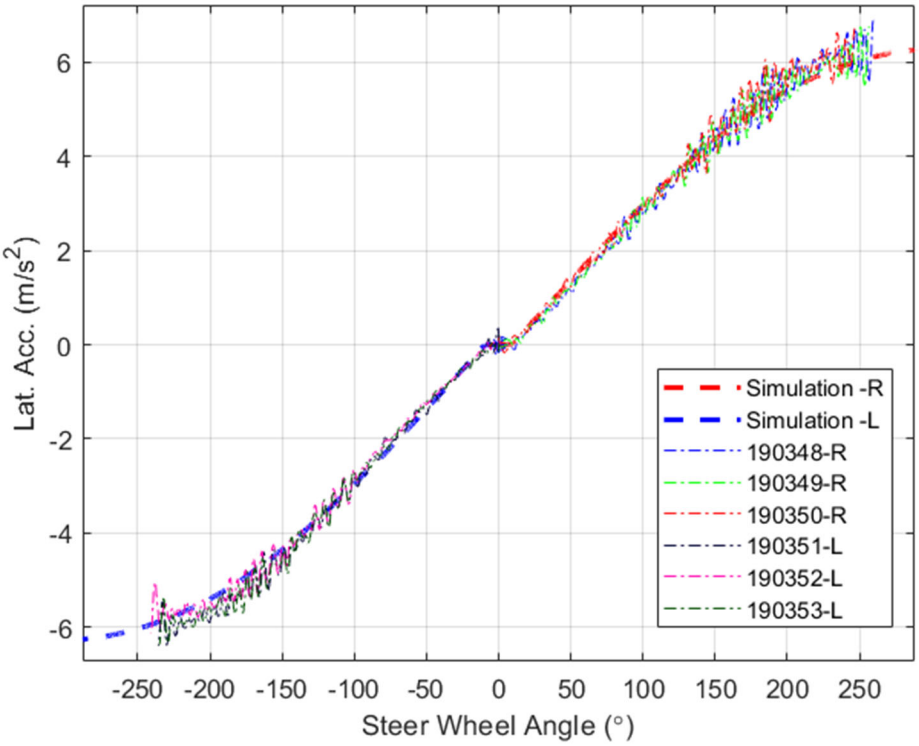

Figure 3-4. Lateral Acceleration Gain

Table 3-4. Lateral Acceleration Gradients

u_0 (km/h) & Direction	**$\frac{da_y}{d\delta}$ (m/s^2/degrees)**	**K_u (degrees/g)**
Experiments		
48.6-R	0.605	2.48
48.6-R	0.607	2.48
48.2-R	0.594	2.82
48.2-L	0.599	2.68
48.6-L	0.590	2.92
48.2-L	0.590	2.95
Mean	0.597	2.72
Standard Deviation	0.0068	0.20
Simulation		
47.9-R&L	0.5974	2.37

Yaw Rate Gain:
The yaw rate gain is a measure of vehicle system planar orientation sensitivity as a response to handwheel steering input. It is estimated by taking the gradient of yaw rate to road wheel steer angle input, and formulated as follows:

$$\frac{\dot{\psi}}{\delta} = \frac{u}{\frac{\pi}{} \frac{K_u}{9.81}u^2} \quad deg/sec/deg) \qquad \textbf{Eq. 6}$$

Where,

- $\dot{\psi}$: Vehicle yaw rate (deg/s)
- δ : Road wheel steer angle (degrees)
- u : Vehicle longitudinal speed (m/s)
- K_u : Vehicle understeer gradient (degrees/g)
- L : Vehicle wheelbase (m)

Figure 3-5 indicates that the simulated yaw rate was accurate within the linear range (up to 20 deg/s of yaw rate).

Table 3-5 displays values for this gradient and confirms the accuracy within the linear range. The yaw rate gradient estimated from simulation is close to the mean value of experimental runs, with a difference of 0.011 deg/s/deg.

The results from the linear analytical comparisons demonstrate that the planar moments and forces on the vehicle from the ground forces were adequately formulated and modeled, and that the center of gravity and suspension parameters were adequate for this model.

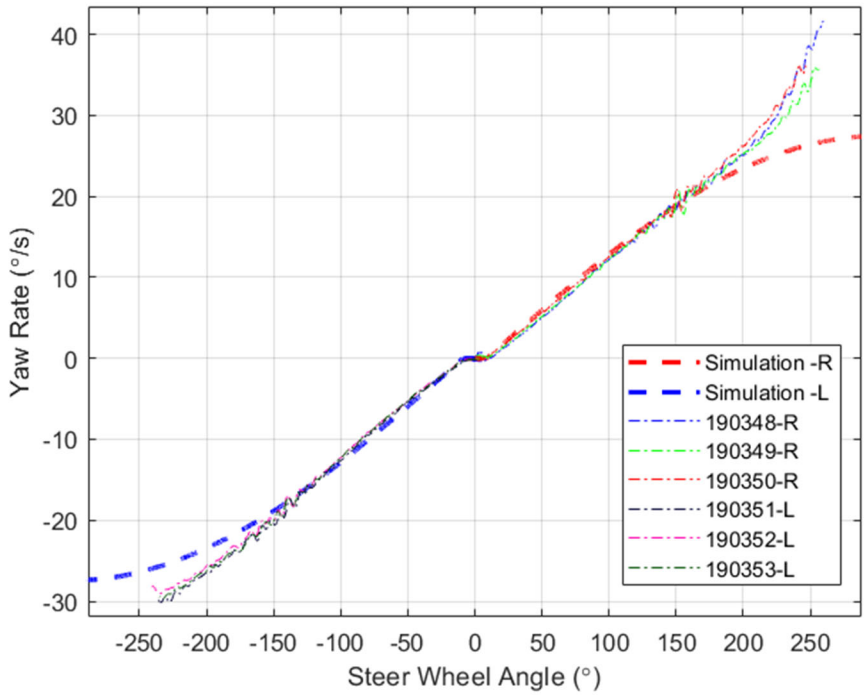

Figure 3-5. Yaw Rate Gain

Table 3-5. Yaw Rate Gradients

u_0 (km/h) & Direction	$\frac{d\dot{\psi}}{d\delta}$ (deg/s/deg)
Experiment	
48.6-R	2.60
48.6-R	2.57
48.2-R	2.54
48.2-L	2.57
48.6-L	2.52
48.2-L	2.52
Mean	2.55
Standard Deviation	0.031
Simulation	
47.9-R&L	2.57

3.1.2 Objective Statistical Metrics

An objective method is a methodology that provides an unambiguous numerical metric that defines model adequacy and accuracy. It is an assessment of model trustworthiness to produce motion results within a specific error tolerance. In this study, three methods were applied; the first is the 95% confidence interval as used in prior research works (Heydinger et al., 1990; Salaani, 1996), the second one is ISO 19364 (2016), and the third one is the ECDF.

3.1.2.1 Confidence Intervals

Random experimental errors can be captured by running repeated tests averaging each data channel in the time domain and computing a statistical CI. There are two significant benefits to this process. First, by repeating each test, the influence of unmeasurable disturbances (e.g., wind gust, variation of friction, surface texture, tire wear and temperature, brake wear and temperature) is greatly reduced. Secondly, it provides a measure of measurement uncertainty. When comparing simulation predictions with experimental measurements, the required accuracy of the simulation predictions can only be assessed relative to experimental measurement uncertainty.

Figure 3-6 shows a comparison between mean experimental results and simulation data. The tested vehicle lateral acceleration, yaw rate, roll angle, and the control inputs (longitudinal speed and steering angle) are averaged over the three test runs for each direction and the mean plotted. The confidence intervals are overlaid on the comparison plots. The analysis is presented here only to demonstrate the concept of confidence intervals, because only three trials were available for each direction. For statistical significance, at least 10 trials are recommended. The simulation results of lateral acceleration, yaw rate, and roll angle were within the 95% CI up to 0.5 g of lateral acceleration. Above this limit, the simulated vehicle speed was outside the experimental 95% confidence intervals, and the simulation results were not close to experimental measures.

The drawback of this validation method is that it requires at least 10 repeated runs. Performing many repeated runs up to the limit of vehicle handling might alter the vehicle system (due to wear) introducing other systemic errors, which makes it difficult to quantify random errors. For example, vehicle tire properties can be altered significantly due to wear from the repeated limit maneuvers.

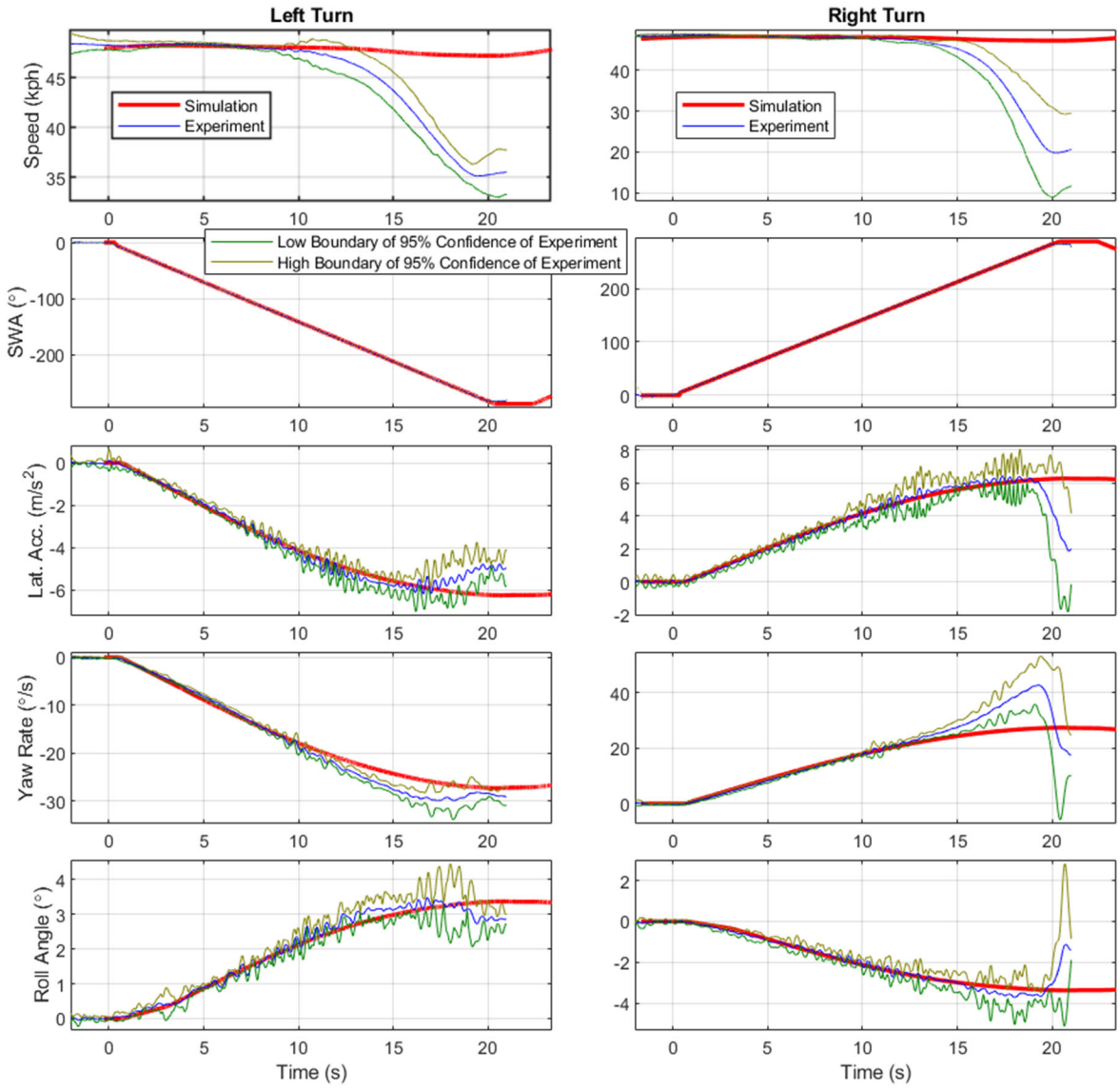

Figure 3-6. SIS CI Validation

3.1.2.2 ISO 19364 Vehicle Dynamic Simulation and Validation – Steady-State Circular Driving Behavior

This section discusses the ISO 19364 (2016) method for comparing computer simulation results from a vehicle model with measured test data for the SIS maneuver.

Simulation results are used to define graphical boundaries for overlaid cross-plots, and the data from physical testing are overlaid to see if the measurements fall within the acceptable ranges. At least three vehicle measurements are used. The cross plots have lateral acceleration in the X-axis and other variables on the Y-axis. The variables are one of the following; steering angle, roll angle, or side slip angle.

The upper boundary points of simulations are calculated as follows:

$$X_T = X - \Delta Y \frac{\varepsilon_X^2}{\sqrt{(\Delta\ \ X)^2+(\Delta\ \ \varepsilon_Y)^2}} \quad \textbf{Eq. 7}$$

$$Y_T = Y + \Delta X \frac{\varepsilon_Y^2}{\sqrt{(\Delta\ \ X)^2+(\Delta\ \ Y)^2}} \quad \textbf{Eq. 8}$$

And the bottom boundary points are,

$$X_B = X + \Delta Y \frac{\varepsilon_X^2}{\sqrt{(\Delta\ \ X)^2+(\Delta\ \ \varepsilon_Y)^2}} \quad \textbf{Eq. 9}$$

$$Y_B = Y - \Delta X \frac{\varepsilon_Y^2}{\sqrt{(\Delta\ \ X)^2+(\Delta\ \ Y)^2}} \quad \textbf{Eq. 10}$$

Where,

X : Lateral acceleration (m/s^2) (same notation is used as the ISO 19364 standard)
Y : Steering angle (deg), or side slip angle (deg), or roll angle (deg)
Δ : Difference in the X-axis variable (lateral acceleration)
Δ : Difference in the Y-axis variable
ε_X : Tolerance in the X-axis variable
ε_Y : Tolerance in the Y-axis variable

The tolerances for each of the cross plots are calculated using an offset and gain with the following formulae,

$$\varepsilon_X = X_{Offset} + X_{gain} * |X| \quad \textbf{Eq. 11}$$

$$\varepsilon_Y = Y_{Offset} \quad Y_{gain} * |Y| \quad \textbf{Eq. 12}$$

Where the parameters for the tolerances are defined in the following table:

Table 3-6. Offsets and Gains Used to Define Tolerances for SIS Tests (ISO 19364)

Variable in Y-axis	X_{Offset} (m/s^2)	X_{gain}	Y_{Offset}	Y_{gain}
Steering Wheel Angle (degrees)	0.1	0.06	5.0	0.03
Side Slip Angle (degrees)	0.1	0.06	0.3	0.04
Roll Angle (degrees)	0.1	0.06	0.2	0.02

Figure 3-7 displays the cross plot of lateral acceleration versus steering angle input. The lateral acceleration measurements fall within the upper and lower bounds of the simulated model which correspond to [-5.18, 5.25] m/s^2. Beyond this range, the lateral acceleration is outside the valid range, according to the recommended ISO tolerance parameters.

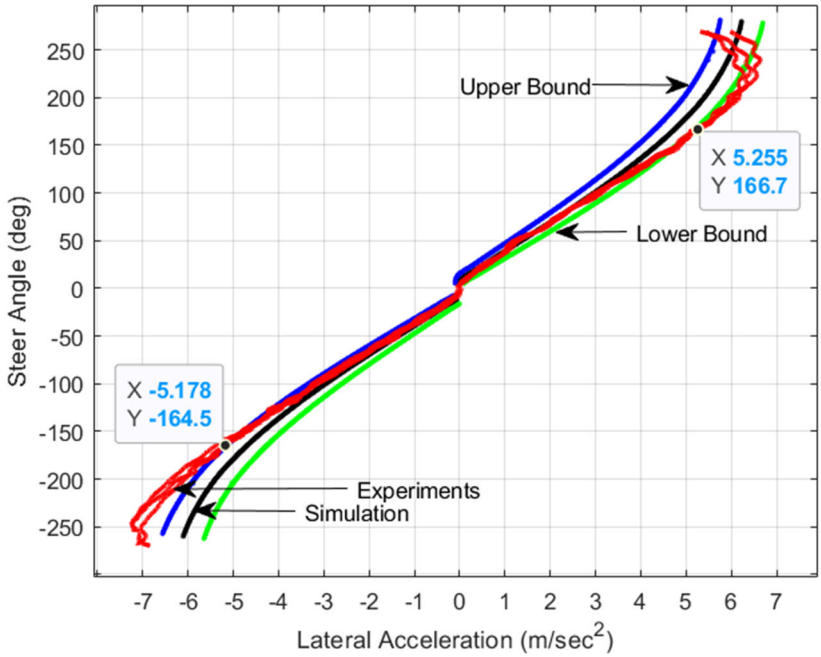

Figure 3-7. Lateral Acceleration – Steering Angle Cross Plot

Figure 3-8 is the cross plot for the lateral acceleration versus roll angle. The figure indicates that roll angle is valid for the complete range of lateral acceleration of [-6, 6] m/s^2, as all measured data fall within the bounds. Outside lateral acceleration limits of [-6, 6] m/s^2 constant vehicle speed were not maintained as Figure 3-9 indicates.

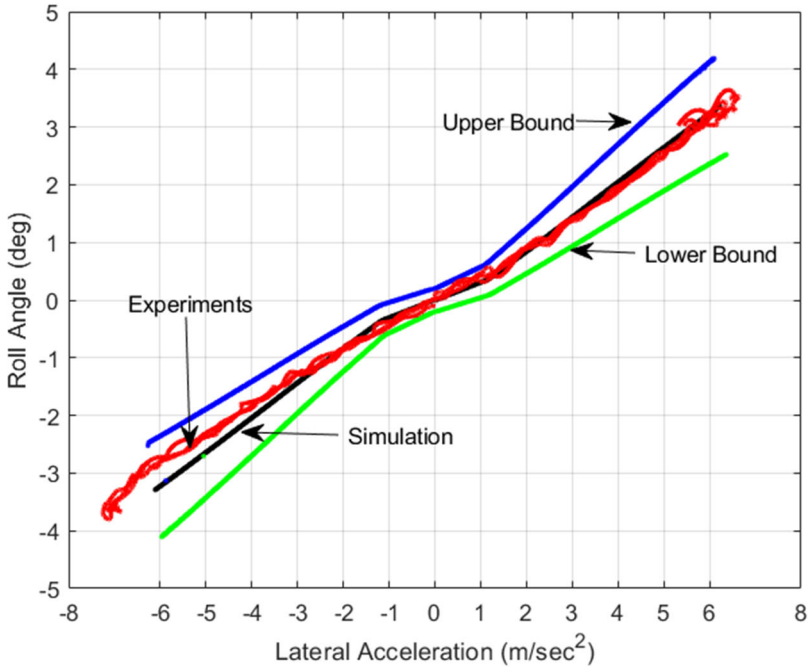

Figure 3-8. Lateral Acceleration – Roll Angle Cross Plot

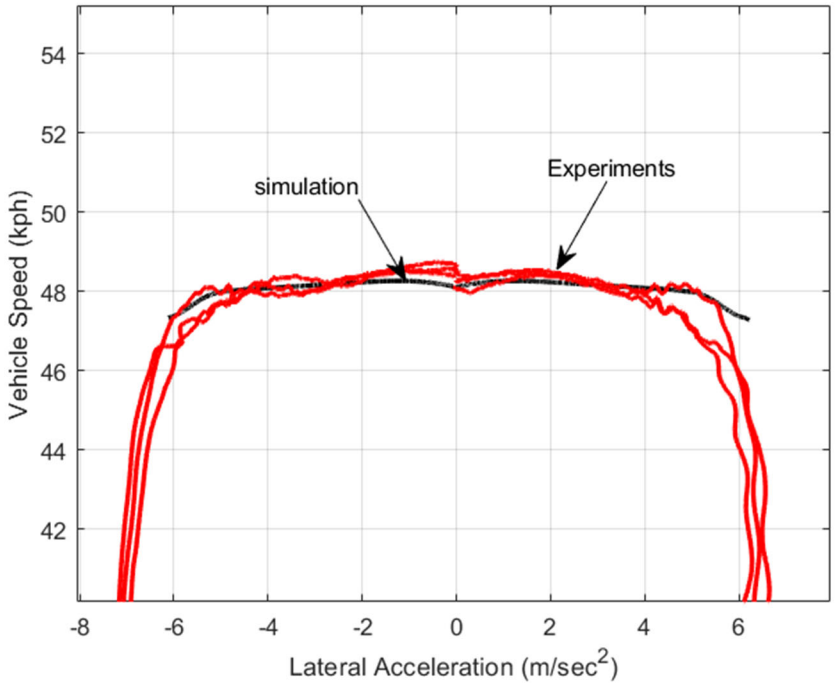

Figure 3-9. Lateral Acceleration – Speed Cross Plot

Vehicle side slip angle was not measured for the test vehicle. To check for directional accuracy the yaw angle rate was compared to a parameter estimated from lateral acceleration tolerances from ISO 19364 (2016). The tolerances defined in Table 3-7 are not part of the ISO 19364 parameters, but estimated (scaled by the report authors) using lateral acceleration X_{Offset} and X_{Gain} parameters as follows,

$$\mathbf{Y_{Offset}} = \frac{\mathbf{X_{Offset}}*}{*} \qquad \textbf{Eq. 13}$$

$$\mathbf{Y_{Gain}} = \frac{\mathbf{X_{Gain}}*}{**} \qquad \textbf{Eq. 14}$$

Where,

X_{Offset} : Lateral acceleration X offset
X_{Gain} : Lateral acceleration X gain
Y_{Offset} : Yaw rate Y offset
Y_{Gain} : Yaw rate Y gain
u : Vehicle speed (m/s)

Table 3-7. Offsets and Gains Used to Define Tolerances for SIS Tests – Yaw Rate

Variable in Y-axis	X_{Offset} (m/s^2)	X_{gain}	Y_{Offset}	Y_{gain}
Yaw rate (degrees/s)	0.1	0.06	0.44	0.13

Figure 3-10 indicates that the yaw rate measurements fall within the simulation tolerance range of [-26.47, 27.65] deg/s. The steering range for this yaw rate validity is [-202, 212] deg.

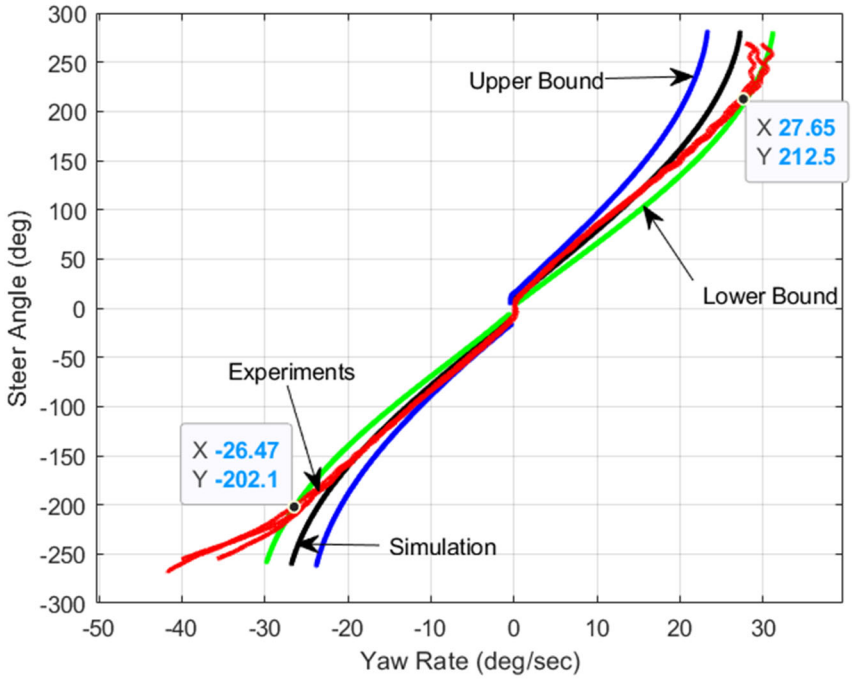

Figure 3-10. Yaw Rate to Steering Angle Input Cross Plot

3.1.2.3 Empirical Cumulative Distribution Function

The ECDF is applied by using mean values of three test runs. In this study, the ECDF is used to evaluate simulation results at three different lateral handling severity stages of the vehicle; linear (up to 0.3g), mid-range (up to 0.4g), and non-linear (up to 0.5g).

The simulation error, $\boldsymbol{\varepsilon}$, is defined by the difference between experiments and simulation of the variable of interest, as follows:

$$\boldsymbol{\varepsilon} = \left|\boldsymbol{Mean\ Variable_{experiment} - Variable_{simulation}}\right| \qquad \textbf{Eq. } 15$$

Validation measurement metrics can be computed with two methods; the first is to compute the error bound ε_b that satisfies a probability higher than a predefined number P, and expressed mathematically with the probability density function $f(.)$ as,

$$\boldsymbol{\varepsilon_b} \qquad > \int_{-\infty}^{\boldsymbol{\varepsilon_b}} \boldsymbol{f(\varepsilon)} \qquad \textbf{Eq. } 16$$

The second method is to define the error bound ε_b and find the corresponding probability P of that error, and expressed mathematically as,

$$\boldsymbol{P} > \int_{-\infty}^{\boldsymbol{\varepsilon_b}} \boldsymbol{f(\varepsilon)} \qquad \textbf{Eq. } 17$$

Both methods are applied in this paper. The results for method 1 (Equation 16) are listed in Table 3-8, with method 2 (Equation 17) in Table 3-9 for the lateral steady-state comparison results. The data showed that simulation predicted results with error bounds for lateral acceleration less than

0.268 m/s^2, yaw rate less than 1.1 degrees/s, and roll angle less than 0.225 degree with a probability nearly 95% for up to 0.5 g. For severity between 0.5-0.6 g of lateral acceleration, the probability is less than 90%, except for roll angle where the accuracy was maintained up to this limit.

Table 3-8. Statistical Measures for Dynamics With Defined Probabilities

Variable	Severity	P > 90%		P > 95%	
		L	R	L	R
Lateral Acceleration Error (m/s^2)	Linear (< 3 m/s^2)	0.145	0.146	0.163	0.167
	Mid (< 4 m/s^2)	0.181	0.154	0.231	0.185
	Non-linear (< 5 m/s^2)	0.209	0.177	0.268	0.212
Yaw Rate Error (Degrees/s)	Linear (< 3 m/s^2)	0.73	0.68	0.76	0.692
	Mid (< 4 m/s^2)	0.722	0.676	0.751	0.689
	Non-linear (< 5 m/s^2)	0.848	0.681	1.116	0.71
Roll Angle Error (Degrees)	Linear (< 3 m/s^2)	0.126	0.126	0.152	0.143
	Mid (< 4 m/s^2)	0.141	0.134	0.159	0.154
	Non-linear (< 5 m/s^2)	0.162	0.15	0.225	0.185

Table 3-9. Probability Measures for Defined Variable Errors

Severity Ay		**L**	**R**	**L**	**R**	**L**	**R**
Linear (<3 m/s^2)	**Variable**	Δ Ay < 0.2 (m/s^2)		Δ Yaw Rate < 0.80 (Degrees/s)		Δ Roll Angle < 0.30 (Degrees)	
	P > (%)	96.4	98.0	97.7	100	100	100
Mid (<4 m/s^2)	**Variable**	Δ Ay < 0.20 (m/s^2)		Δ Yaw Rate < 0.80 (Degrees/s)		Δ Roll Angle < 0.30 (Degrees)	
	P > (%)	92.7	96.8	98.1	100	100	100
Non-linear (<5 m/s^2)	**Variable**	Δ Ay < 0.2 (m/s^2)		Δ Yaw Rate < 0.8 (Degrees/s)		Δ Roll Angle < 0.30 (Degrees)	
	P > (%)	89.0	93.4	87.9	97.7	98.3	100

Table 3-10 is for test-controlled inputs which are for lateral handling speed and steering angle. The errors for P > 95% are small, less than 0.5 km/h for speed, and less than 0.7 degree for steering angle.

Figure 3-11 plots the results for up to 0.3g, Figure 3-12 for up to 0.4g, and Figure 3-13 for up to 0.5g. The ECDF statistics indicate that the model predicted the motion of the tested vehicle with small errors up to 0.5g of lateral dynamics severity.

Table 3-10. Statistical Measures for Controlled Input

Variable	Severity	P > 90%		P > 95%	
		L	R	L	R
Speed (km/h)	Linear (< 3 m/s^2)	0.21	0.54	0.25	0.58
	Mid (< 4 m/s^2)	0.21	0.53	0.25	0.57
	Non-linear (< 5 m/s^2)	0.38	0.52	0.44	0.55
Steering (degrees)	Linear (< 3 m/s^2)	0.5	0.6	0.5	0.7
	Mid (< 4 m/s^2)	0.5	0.5	0.6	0.7
	Non-linear (< 5 m/s^2)	0.5	0.7	0.5	0.7

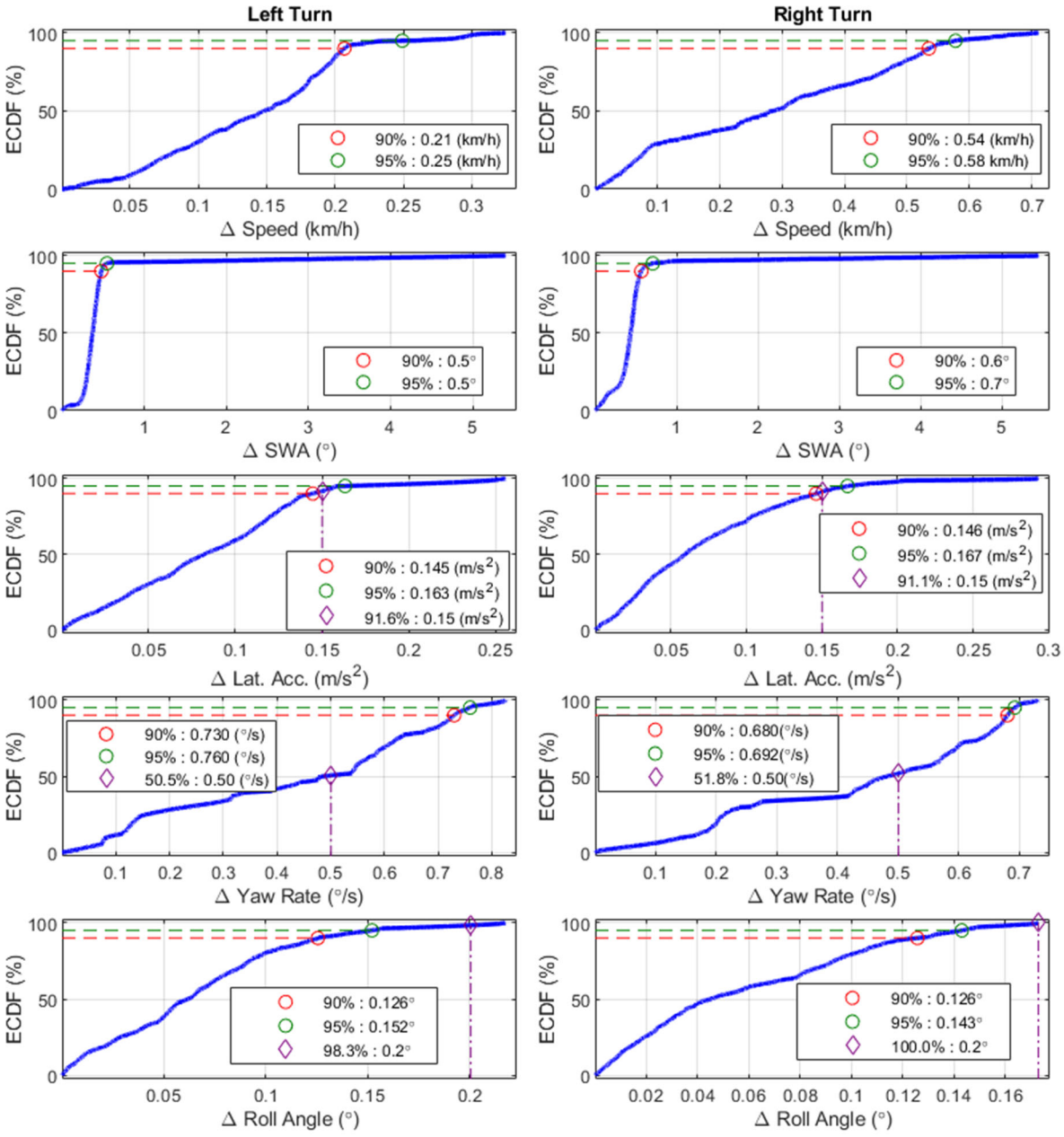

Figure 3-11. ECDF Objective Measures up to 0.3 g of Lateral Acceleration

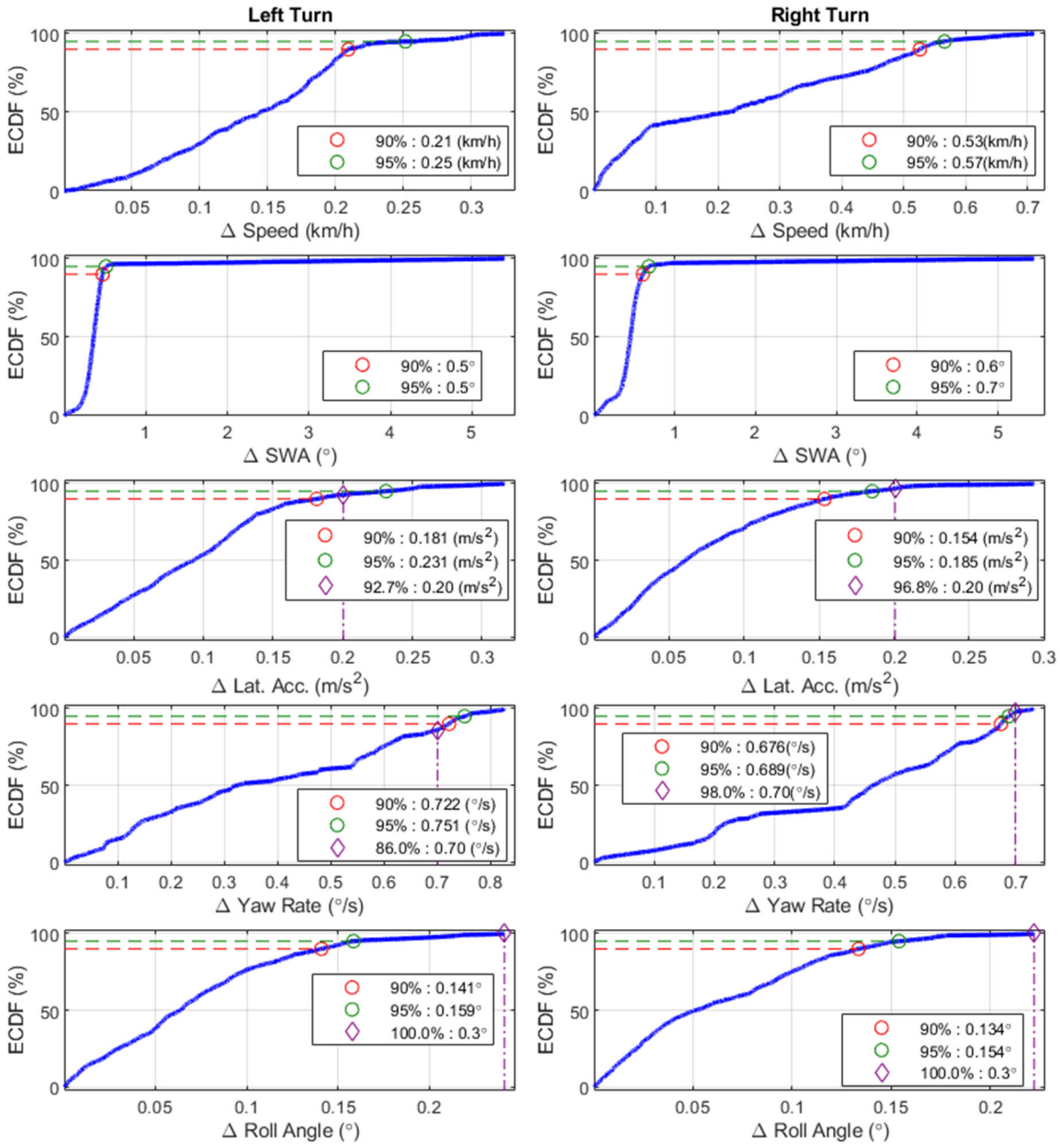

Figure 3-12. ECDF Objective Measures up to 0.4 g of Lateral Acceleration

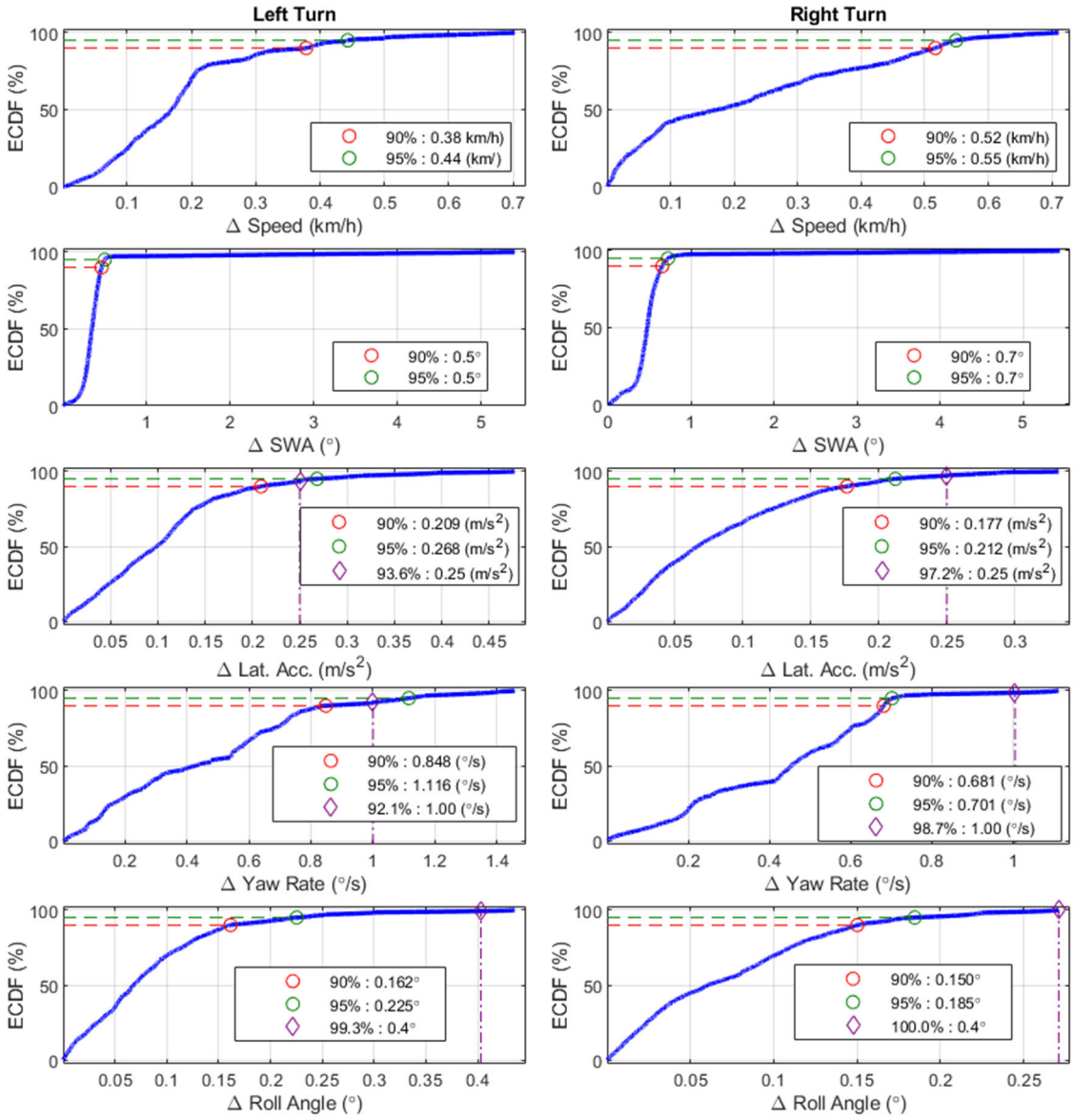

Figure 3-13. ECDF Objective Measures up to 0.5 g of Lateral Acceleration

3.2 Driving Scenario-Based Validation – J-turn (FMVSS No. 136)

The lateral dynamics of the model was further validated using the driving scenario-based approach. The J-turn maneuver was used for this purpose. The J-turn tests were performed following the guidelines established in the FMVSS No. 136 (49 CFR, 2017) test procedures. Simulations were conducted with no ESC and compared with experimental results with ESC disabled. The results from this maneuver should not be interpreted as an evaluation of the truck stability, or adherence to FMVSS No. 136 requirements, as the maneuver was used only for validating vehicle dynamics.

The test consists of driving the truck at a constant speed at the center of the lane through a straight section with a length of 22.9 m (75 feet) that is tangentially connected to a curved lane

section with a radius of 45.7 m (150 feet) measured from the center of the lane. For testing trucks, the lane width is set at 3.7 m (12 feet). The start gate is the tangent point on the radius and is designated as zero degree of radius of arc angle. The end gate is the point on the radius that is 120 degrees of radius arc angle measured from the tangent point. Figure 3-14 shows the course lane, and the paths followed by the test vehicle and simulated one, for both left and right directions.

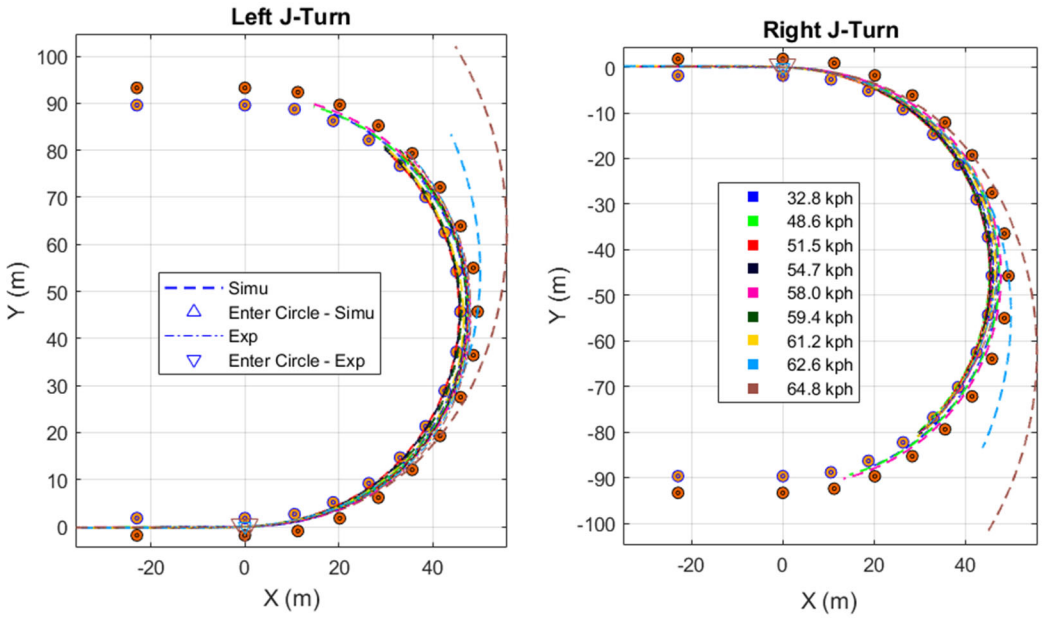

Figure 3-14. Driving Scenario-Based Validation: J-turn Paths for Simulated and Experimental Data

Two series of test runs at increasing entrance speeds were performed with the test vehicle, one series with clockwise steering and the other with counterclockwise steering. Entry speeds started at 32 km/h and were incremented by 2 km/h for each subsequent run until the truck's wheels departed the lanes within the first 120 degrees of radius arc angle. The test driver was instructed to maintain the selected entrance speed through the J-turn maneuver and stay in the lane. The simulated tests used dSPACE ASM path-following algorithm with a constant speed set by a cruise (speed) controller.

Summary results are listed in Table 3-11. Plots of steering wheel angle by the test driver and dSPACE ASM path-following algorithm, vehicle lateral acceleration, yaw rate, and roll angle are shown in Figure 3-15 and Figure 3-16 for both left and right steering directions. This J-turn test is a closed loop test, and the purpose of the simulated driver model was to keep the vehicle following the center lane position while maintaining a constant speed. This model is a generic dSPACE ASM driver model and was not set to mimic test driver control input actions, by producing test driver steering input or throttle and brake inputs.

Evaluations of the graphs indicate that under the speed of 55 km/h, the simulation predictions are similar to experimental results. These tests correspond to peak lateral acceleration of nearly 5.0 m/s^2 or less, which is within the validated range of lateral acceleration severity for the SIS maneuver. This comparison is subjective and performed by inspection of Figure 3-15 and Figure 3-16, and metrics listed in Table 3-11. In this table, three metrics were compared, peak SWA,

peak lateral acceleration, and a Yes/No flag to indicate if the vehicle stayed within the travel lane. A vehicle was defined as staying within the travel lane if none of its wheels crossed the lane boundaries.

At speeds above 55 km/h, the test vehicle was not able to maintain speed during the maneuver in contrast to the driver model in simulation. Hence, a direct comparison with the simulation results is not accurate in this range.

Due to the difference between the test driver and the simulation driver model, only trends and subjective evaluations of vehicle position, lateral acceleration, yaw rate, and roll angle can be performed. Objective evaluations on closed loop simulations are not possible unless the driver model is set to replicate test driver behavior.

Table 3-11. Lateral Dynamics J-Turn Maneuver Results

Entrance Speed (km/h)	**Peak SWA (degrees)**	**Peak Lateral Acc. (m/s^2)**	**Stayed in Lane**	**Peak SWA (degrees)**	**Peak Lateral Acc. (m/s^2)**	**Stayed on Lane**	**Subjective Validity**
	Experiment			**Simulation**			
Left							
32.8	118.2	2.1	Yes	118.9	1.8	Yes	**Yes**
48.6	119.5	4.4	Yes	134.9	4.0	Yes	**Yes**
51.5	119.3	5.1	Yes	142.7	4.6	Yes	**Yes**
54.7	119.1	5.6	Yes	154.7	5.2	Yes	**Yes**
58.0	145	6.3	Yes	171.2	5.8	Yes	No
59.8	134.5	6.5	Yes	182.9	6.1	Yes	No
61.2	149.8	6.9	Yes	249.5	6.5	Yes	No
62.6	123.7	6.7	Yes	700.0	6.3	No	No
64.8	373	7.2	Yes	700.0	6.6	No	No
Right							
32.0	111.5	2.0	Yes	118.9	1.8	Yes	**Yes**
48.2	117.7	4.4	Yes	134.9	4.0	Yes	**Yes**
51.8	119.4	4.9	Yes	142.7	4.6	Yes	**Yes**
54.7	114.3	5.4	Yes	154.7	5.2	Yes	**Yes**
58.0	136.7	6.1	Yes	171.2	5.8	Yes	No
59.4	136.3	6.2	Yes	182.9	6.1	Yes	No
61.2	190.8	6.9	Yes	249.7	6.5	Yes	No
63.0	165.4	6.8	Yes	700.0	6.3	No	No
64.4	249.4	6.8	Yes	700.0	6.6	No	No

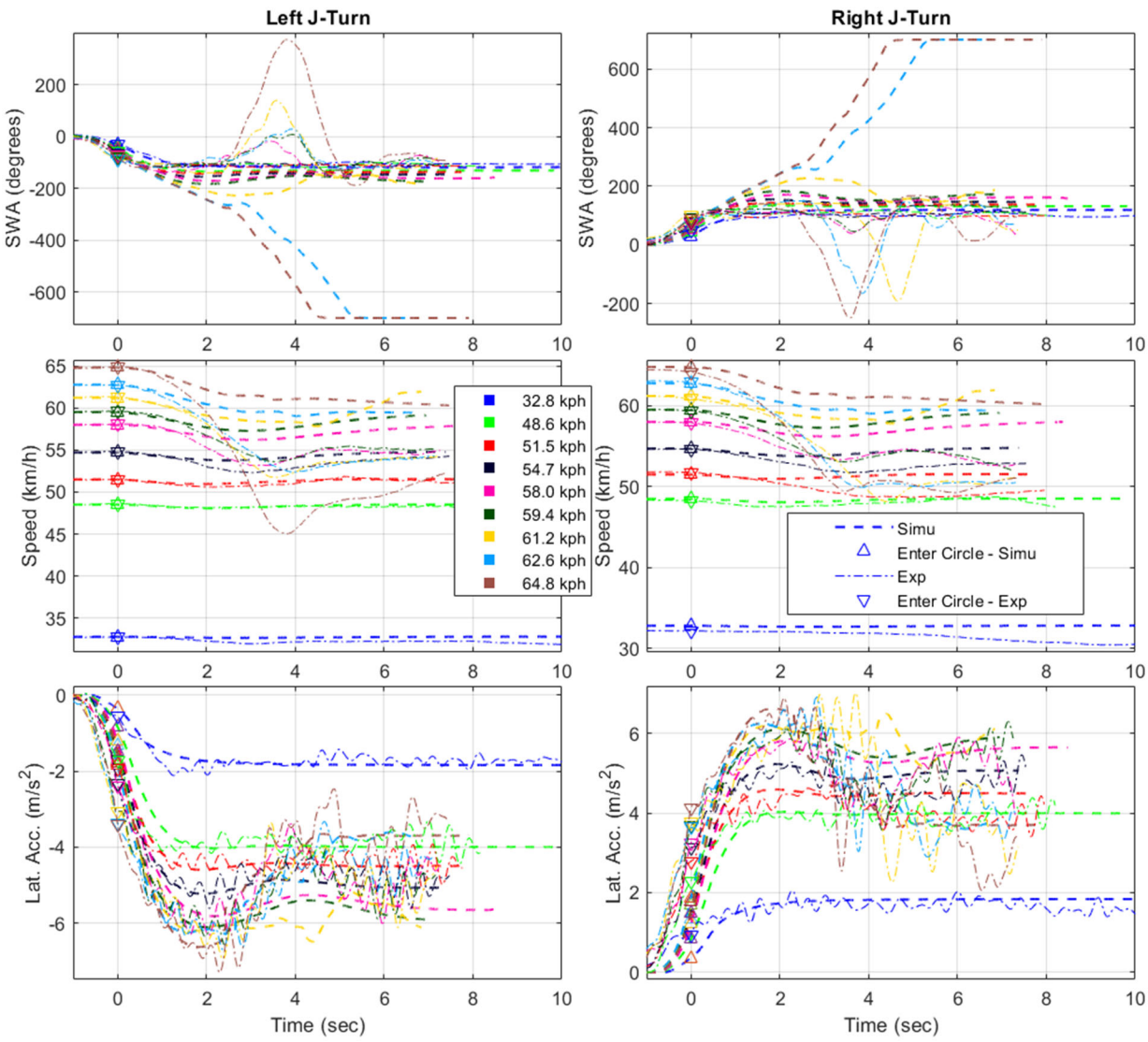

Figure 3-15. Steering Angle, Speed, and Lateral Acceleration for J-Turn Maneuvers

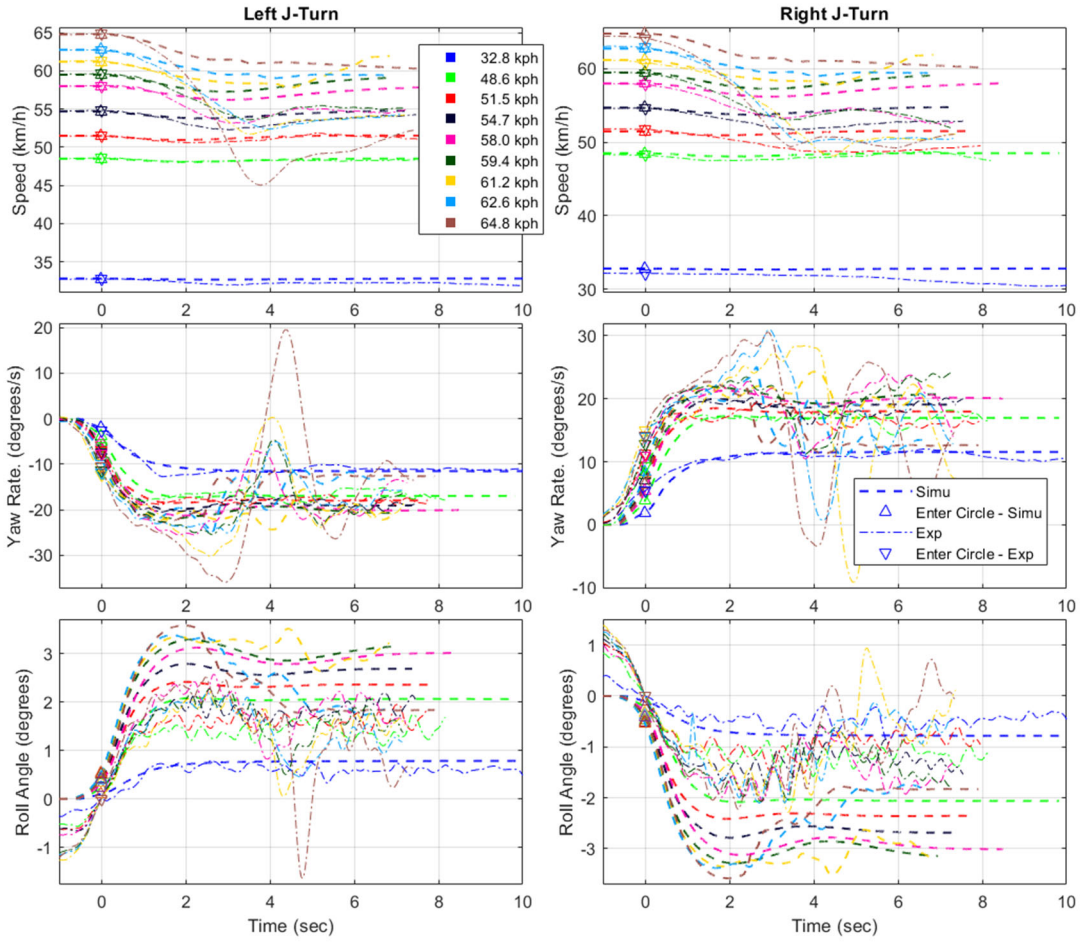

Figure 3-16. Speed, Yaw Rate, and Roll Angle for J-Turn Maneuvers

3.3 Longitudinal Deceleration Performance

These tests were performed using test procedures from the FMVSS No. 121 (49 CFR, 2009) for heavy vehicles with pneumatic brake systems. They were performed after completing the brake burnish procedures described in the laboratory test procedures for two initial speeds of 48.3 km/h (30 mph) and 96.6 km/h (60 mph). Six valid stopping distance test trials were performed at each speed.

3.3.1 Subjective Evaluations

The SUT stopping distance test results are presented in Table 3-12 and Table 3-13. The stopping distance measurements indicate that the SUT meets FMVSS No. 121 (49 CFR, 2009) stopping distance requirements at the tested speeds. The measured mean stopping distance was 15.84 m (51.97 feet) with a standard deviation of 0.36 m (1.18 ft) from 48.3 km/h (30 mph), and 74.1 m (243.11 feet) with a standard deviation of 4.8 m (15.75 ft) from 96.3 km/h (60 mph). The simulated stopping distances for both speeds are 15.69 m (51.48 feet) and 73.29 m (240.45 feet), respectively.

Figure 3-17 and Figure 3-19 show the plots of brake pressure application at the primary line (treadle pressure – pressure at the brake pedal location), front-left, and rear-right pressures at the wheel brake chambers. The HiL simulation used Bendix EC-60 module for ABS activation, while the test vehicle was equipped with a more modern EC-80 controller. Despite this difference, the mean pressure values were close and produced close steady-state decelerations.

Table 3-12. Stopping Distance Test Results – Entrance Speed 96.6 km/h

Test# & Direction	Entrance Speed (km/h)	Stop Distance (m)	Corrected Stop Distance (m)	Stop Duration (s)	Avg. Decel of Brake (m/s^2)	Avg. Decel of Steady Brake (m/s^2)
	Experiments					
1-S	97.7	80.15	78.42	5.83	4.64	4.72
2-S	96.5	81.38	81.47	5.81	4.61	4.71
3-S	98.0	75.20	73.13	5.36	5.08	5.19
4-N	98.0	73.67	71.61	5.16	5.27	5.41
5-S	97.8	72.51	70.75	4.99	5.44	5.57
6-N	97.9	71.12	69.24	4.95	5.47	5.63
Mean	97.6	75.67	74.10	5.35	5.09	5.21
Standard Deviation	0.6	4.19	4.80	0.39	0.38	0.41
	Simulation					
	98	75.42	73.29	5.4	5.04	5.22

Table 3-13. Stopping Distance Test Results – Entrance Speed 48.3 km/h

Test# & Direction	Entrance Speed (km/h)	Brake Stop Distance (m)	Corrected Brake Stop Distance (m)	Brake Stop Duration (s)	Avg. Decel of Brake (m/s^2)	Avg. Decel of Steady Brake (m/s^2)
Experiments						
1-S	49.7	17.25	16.29	2.27	6.09	6.77
2-S	49.7	16.81	15.88	2.21	6.25	6.96
3-S	49.6	17.08	16.17	2.24	6.14	6.85
4-N	49.7	16.33	15.41	2.14	6.46	7.18
5-N	49.4	16.53	15.8	2.2	6.25	6.89
6-N	49.5	16.23	15.47	2.1	6.5	7.31
Mean	49.6	16.71	15.84	2.19	6.28	6.99
Std. Deviation	0.1	0.41	0.36	0.06	0.17	0.21
Simulation						
	49.3	16.39	15.69	2.23	6.13	6.62

Figure 3-18 shows plotted results for the 96.6 km/h (60 mph) test, and Figure 3-20 for the 48.3 km/h (30 mph). The measured brake line pressures revealed more delays than the HiL simulation system but had minimum effects on the overall stopping distance results. The reasons for this

difference can be attributed to the lengths of different pneumatic pressure lines used in the HiL test bench with the actual truck pressure lines, and to a different ECU braking control unit.

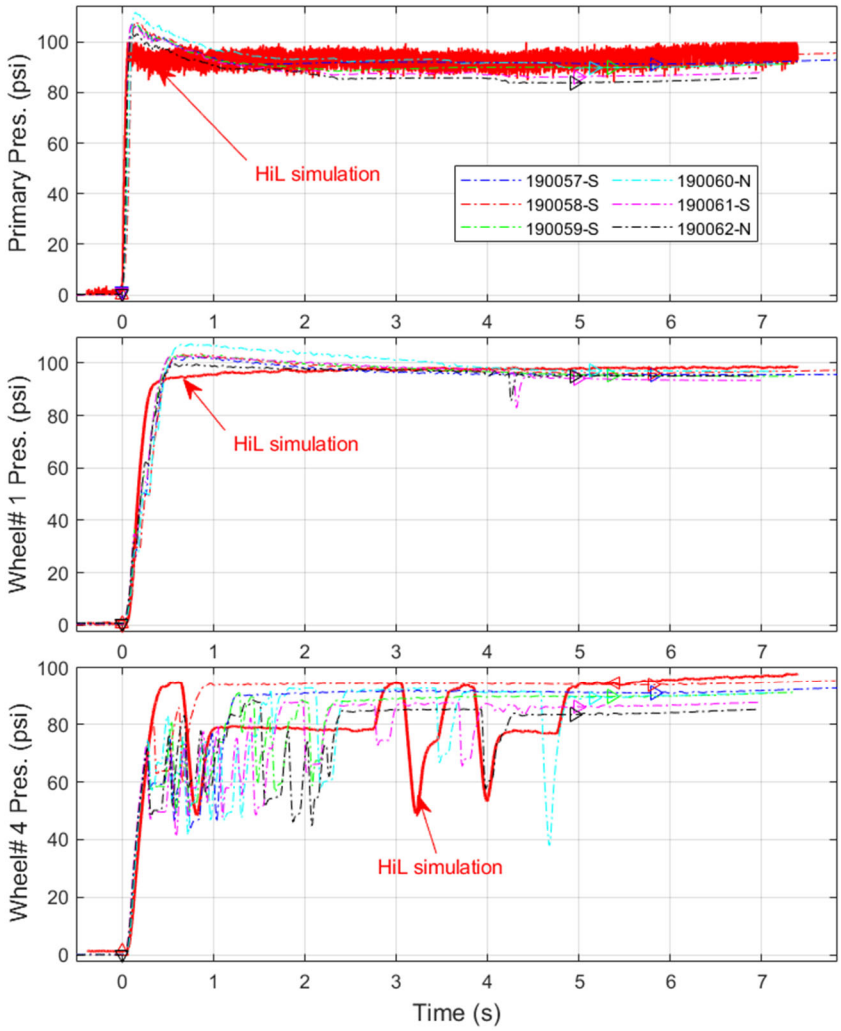

Figure 3-17. Applied Brake Line Pressures – Entrance Speed 96.6 km/h

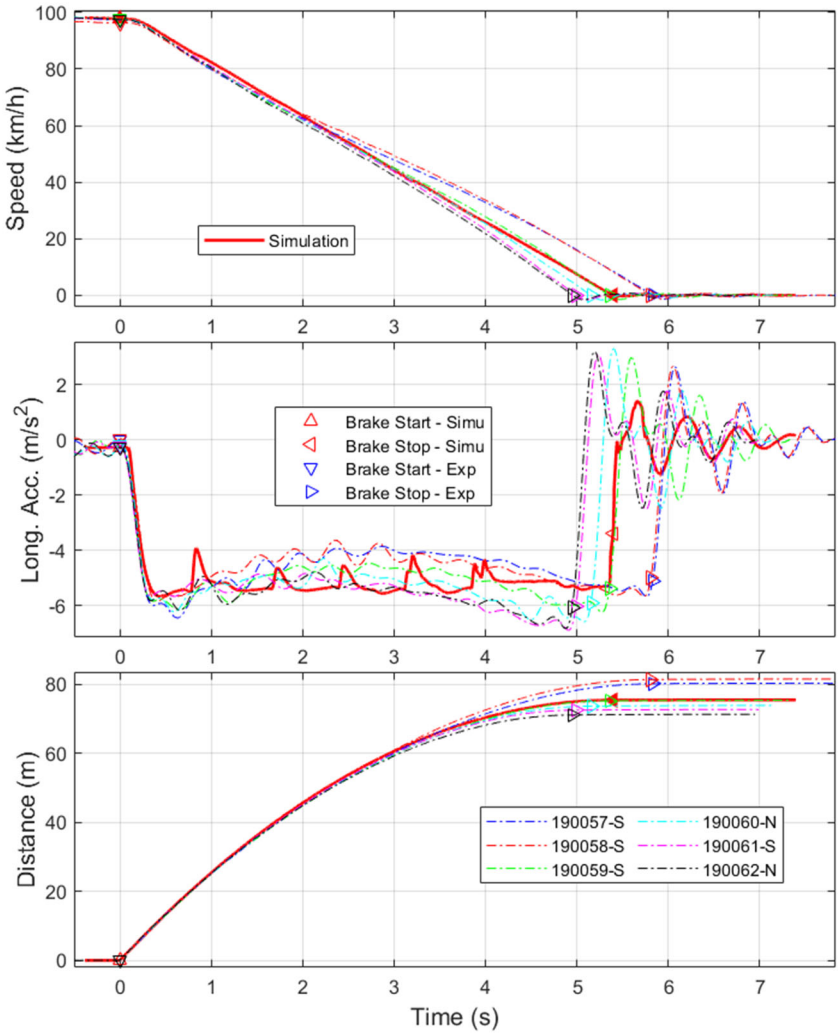

Figure 3-18. Vehicle Kinetics Brake Performances – Entrance Speed 96.6 km/h

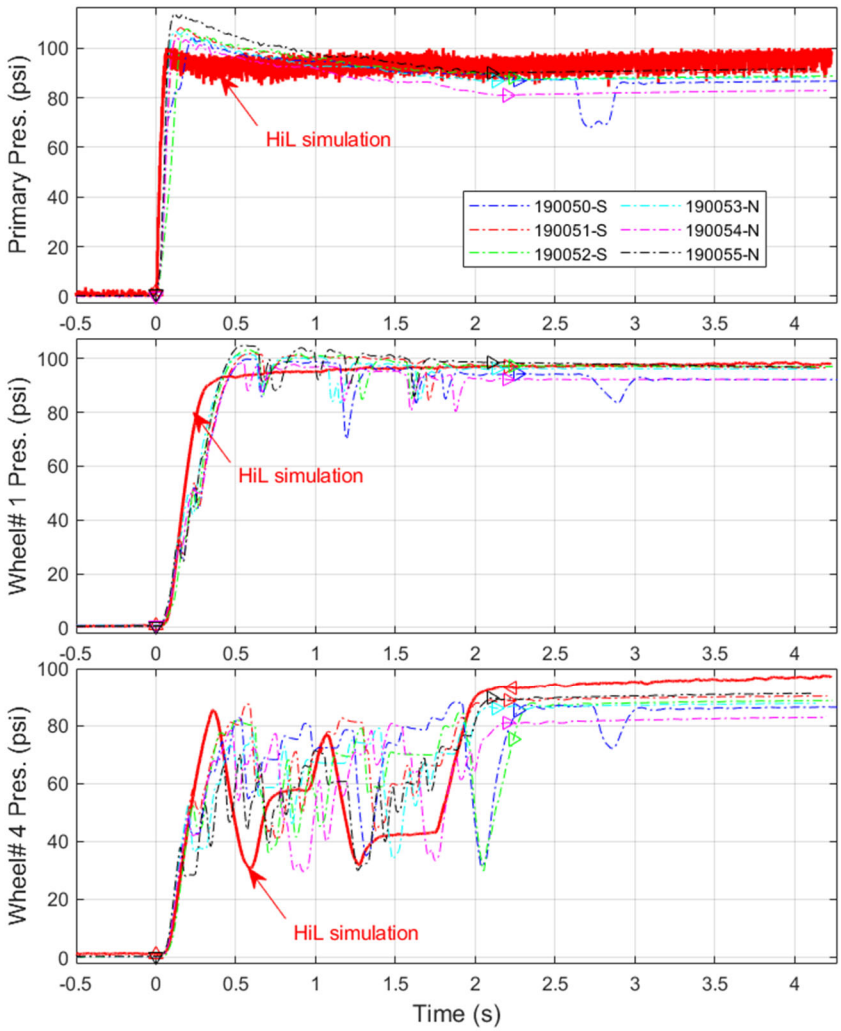

Figure 3-19. Applied Brake Line Pressures – Entrance Speed 48.3 km/h

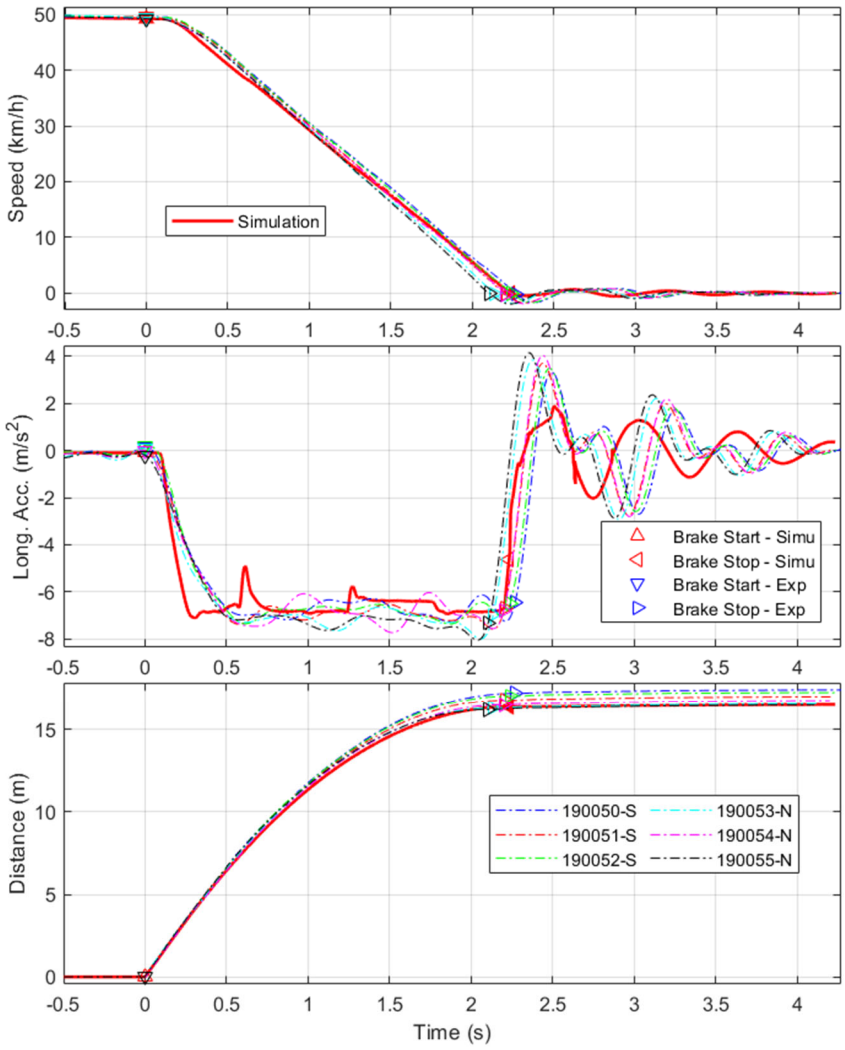

Figure 3-20. Vehicle Kinetics Brake Performances – Entrance Speed 48.3 km/h

Longitudinal stopping distance analytical estimation is used to gain confidence in both simulation and test results, and it is applied with Equation18 (Salaani et al., 2020). This equation uses estimated steady-state deceleration, entry speed, and time delay, as illustrated in Figure 3-21. Table 3-14 and Table 3-15 include comparisons for experimental and simulated stopping distances (S [m]) with the corresponding analytical values (Analytical S [m]). The comparison indicates that experiments and simulation values are very close to the "ideal" estimation. The slight differences are attributed to the estimation of rise time (t_r) and steady deceleration approximations.

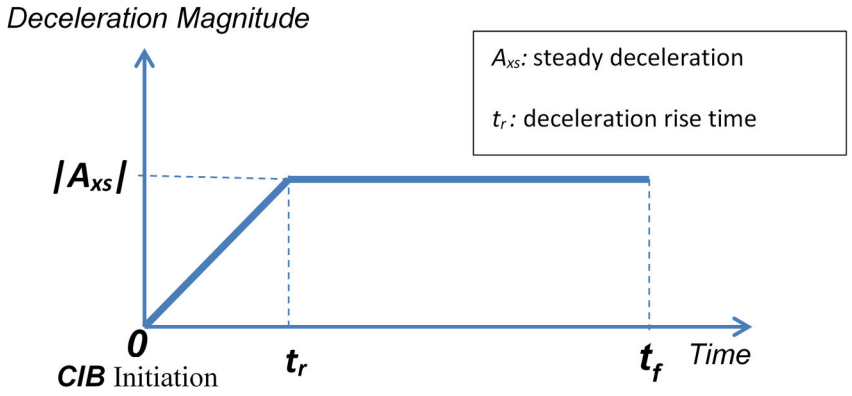

Figure 3-21. Analytical Stopping Distance Evaluations

$$S = \frac{1}{2}u_0 t_r + \frac{1}{2}\frac{u_0^2}{a_{xs}} - \frac{1}{24}a_{xs}t_r^2 \qquad \textbf{Eq. 18}$$

Where,

u_0 : Initial vehicle speed (m/s)
t_r : Deceleration rise time (s)
a_{xs} : Steady deceleration (m/s^2)
S : Stopping distance (m)

Table 3-14. Stopping Distance Evaluations – Entrance Speed 96.6 km/h

Test# & Direction	**u_0 (km/h)**	**t_r (s)**	**a_{xs} (m/s^2)**	**S (m)**	**Analytical S (m)**
1-S	97.7	0.37	4.72	80.2	82.9
2-S	96.5	0.405	4.71	81.4	81.8
3-S	98.0	0.36	5.19	75.2	76.2
4-N	98.0	0.36	5.41	73.7	73.4
5-S	97.8	0.34	5.57	72.5	70.8
6-N	97.9	0.34	5.63	71.1	70.3
Mean	97.6	0.36	5.21	75.7	75.9
Standard Deviation	0.6	0.02	0.41	4.19	5.4
Simulation					
	98.0	0.4	5.22	75.4	76.9

Table 3-15. Stopping Distance Evaluations – Entrance Speed 48.3 km/h

Test# & Direction	u_0 (km/h)	t_r (s)	a_{xs} (m/s²)	S (m)	Analytical S (m)
1-S	49.7	0.61	6.77	17.3	18.1
2-S	49.7	0.58	6.96	16.8	17.5
3-S	49.6	0.62	6.85	17.1	18.0
4-N	49.7	0.61	7.18	16.3	17.4
5-N	49.4	0.68	6.89	16.5	18.2
6-N	49.5	0.57	7.31	16.2	16.7
Mean	49.6	0.61	6.99	16.7	17.7
Standard Deviation	0.1	0.04	0.21	0.41	0.56
Simulation					
	49.3	0.40	6.62	16.4	16.6

3.3.2 Objective Statistical Metrics

CI and ECDF methods were used to provide a numerical assessment of the simulation validation quality in the longitudinal mode and are detailed in the following sections.

3.3.2.1 Confidence Intervals

Figure 3-22 and Figure 3-23 show the CI results for the 48.3 km/h and 96.6 km/h stopping distance tests, respectively. Six experimental runs were used for each speed. For the 96.6 km/h tests, the simulation results were within the 95% CI for speed, longitudinal acceleration, and stopping distance. However, for the 48.3 km/h tests, a discrepancy during 1.0 second of brake activation was noticed. This was due to the difference in pressure rise time between simulation and experiments. For the remaining of brake activation time, all variables were within the 95% CI.

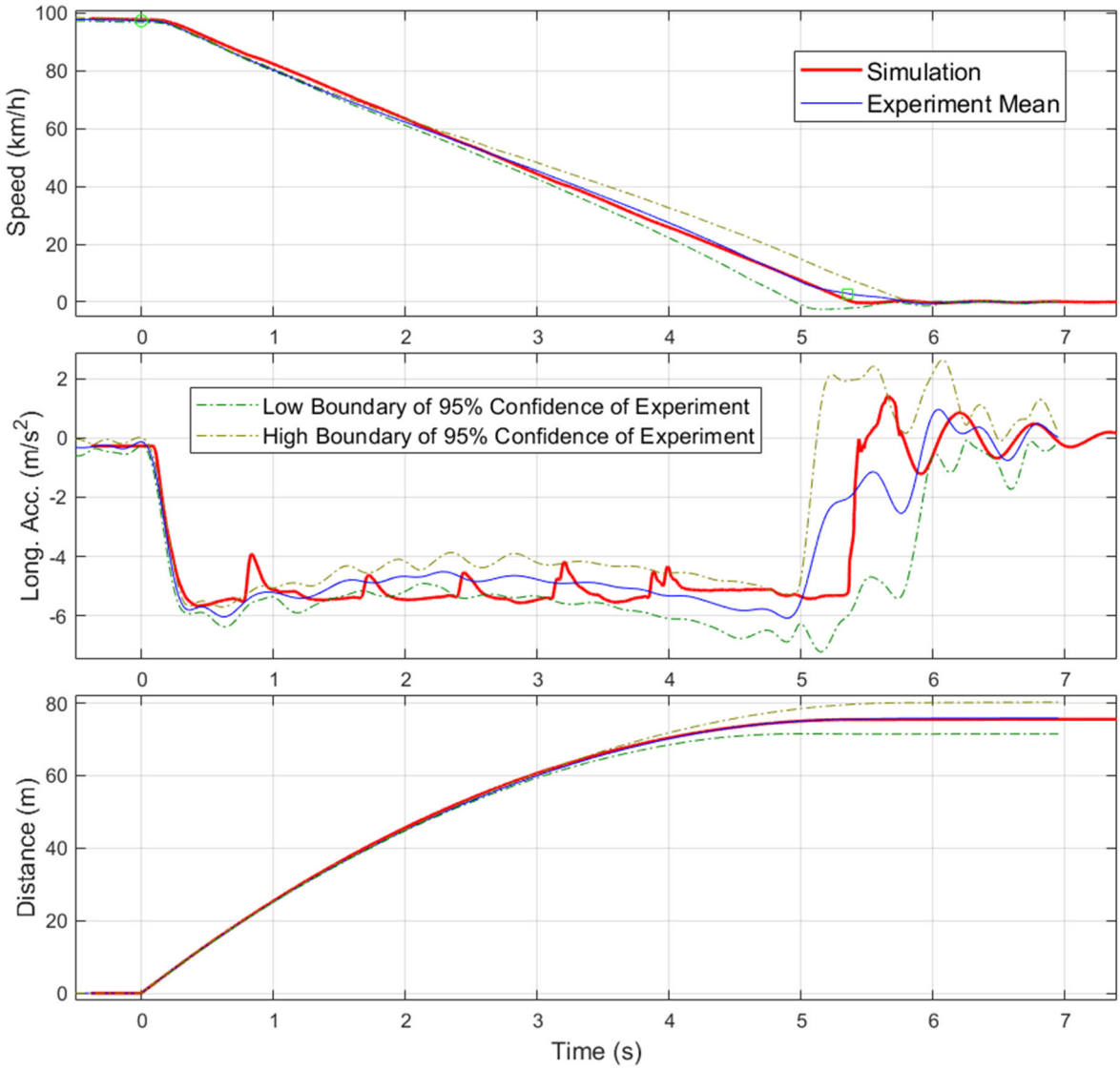

Figure 3-22. Confidence Intervals Comparison – Entrance Speed 96.6 km/h

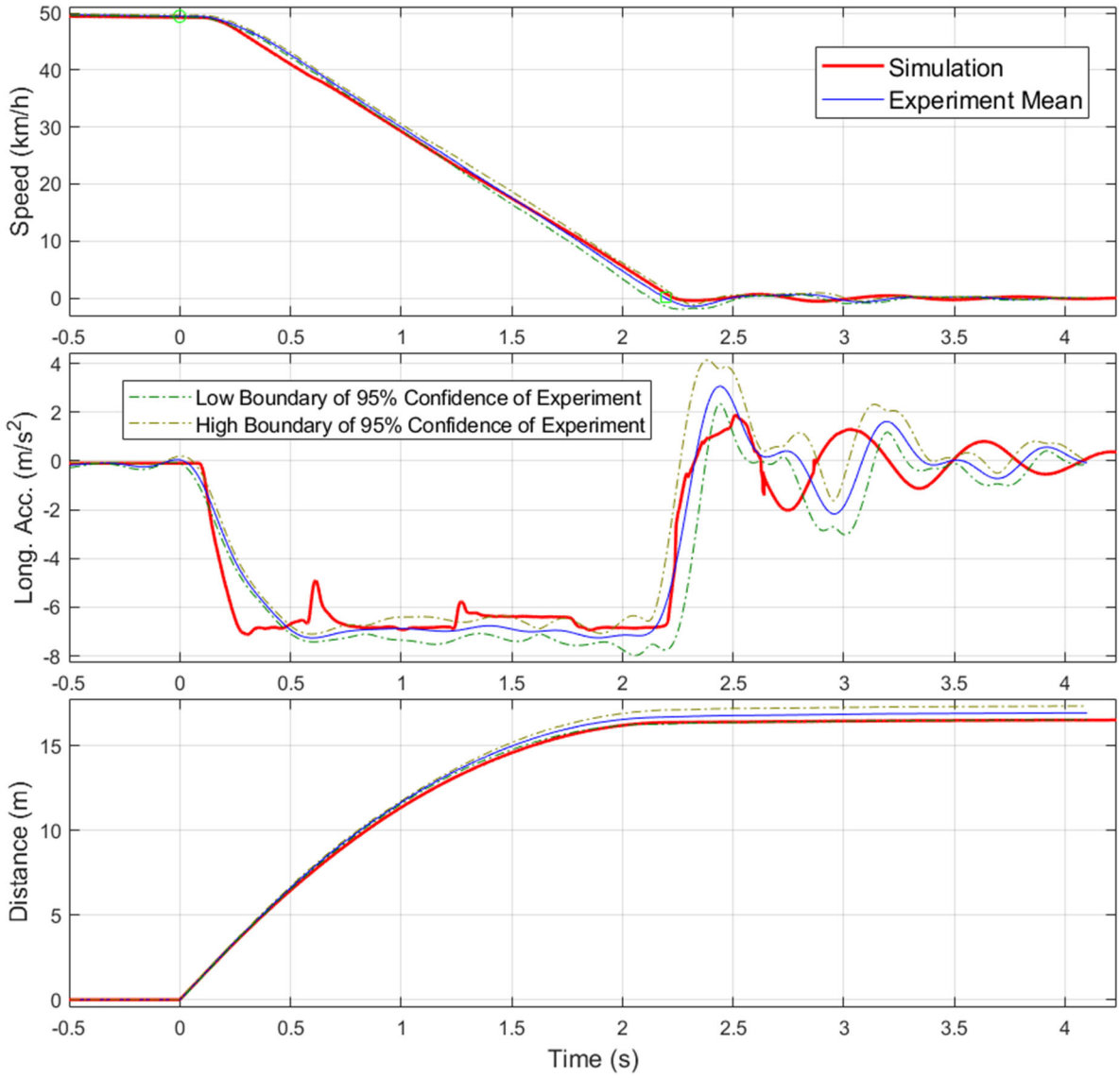

Figure 3-23. Confidence Intervals Comparison – Entrance Speed 48.3 km/h

3.3.2.2 Empirical Cumulative Distribution Functions

The 90% and 95% probabilities of errors between simulation and mean test track values for the longitudinal accelerations, speeds, and distances are listed in Table 3-16, and plotted in Figure 3-24 and Figure 3-25. It is notable that the deceleration error was near 2.1 m/s^2 for the entry speed of 48.3 km/h and 1.41 m/s^2 for the entry speed of 96.6 km/h at a probability above 95%.

Table 3-17 provides a different way for analyzing the ECDF statistical results. In this case, the thresholds for the speed error were set at 2.0 km/h and 1.0 m for the distance error. The data showed that at 48.3 km/h, both speed and stopping distance errors were below the defined threshold (probability of 100%). This means that speed errors are all under 2 km/h and that all distance errors are under 1 m. For entry speed of 96.6 km/h, the speed error probability dropped to 89.5% of the data, falling below the desired error threshold of 2.0 km/h.

This analysis illustrated that it is not necessarily required to model the high frequency modes of a system, like the brakes, to get accurate vehicle stopping performances. What is important are the mean values of the model that are within the frequency spectrum of the desired performance of the vehicle model (meaning this brake system model may not be considered valid for assessing driver/passenger comfort metrics such as jerk).

Other systems, which are not specifically modeled for this vehicle, embrace the same observation, like the powertrain and engine model. A mean-valued engine model is enough to estimate longitudinal braking performances (Salaani & Heydinger, 1998).

Table 3-16. Statistical Measures for Braking Dynamics

Variable	Entrance Speed (km/h)	P > 90%	P > 95%
Longitudinal deceleration (m/s^2)	48.3	1.38	2.09
	96.6	0.84	1.41
Speed (km/h)	48.3	1.46	1.60
	96.6	2.02	2.11
Distance (m)	48.3	0.39	0.40
	96.6	0.73	0.74

Table 3-17. Statistical Measures for Braking Dynamics With Fixed Errors

Variable	Entrance Speed (km/h)	Δ Speed < 2.0 (km/h)	Δ Distance < 1.0 (m)
P > (%)	48.3	100	100
	96.6	89.5	100

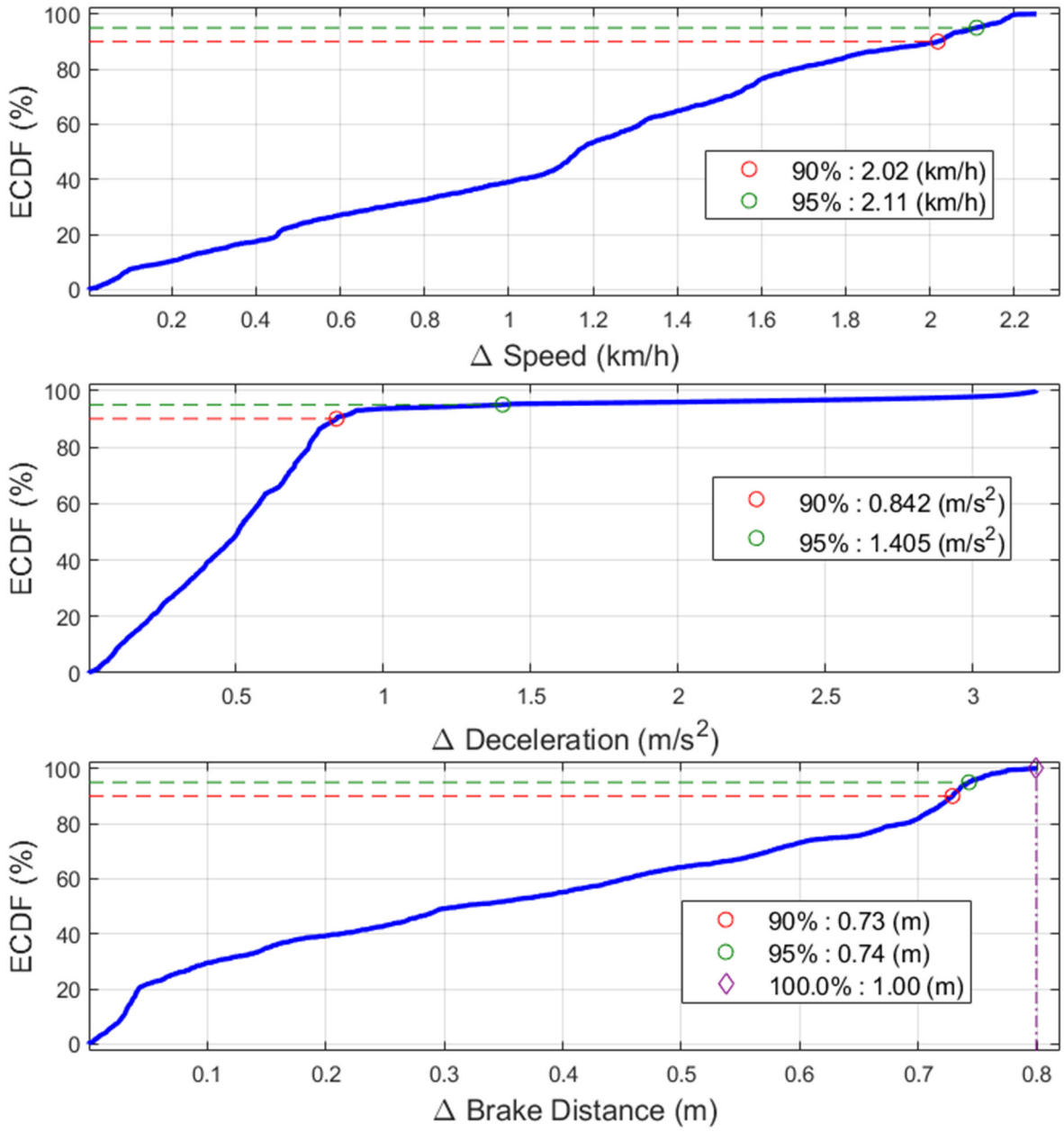

Figure 3-24. Cumulative Distribution Comparisons – Entrance Speed 96.6 km/h

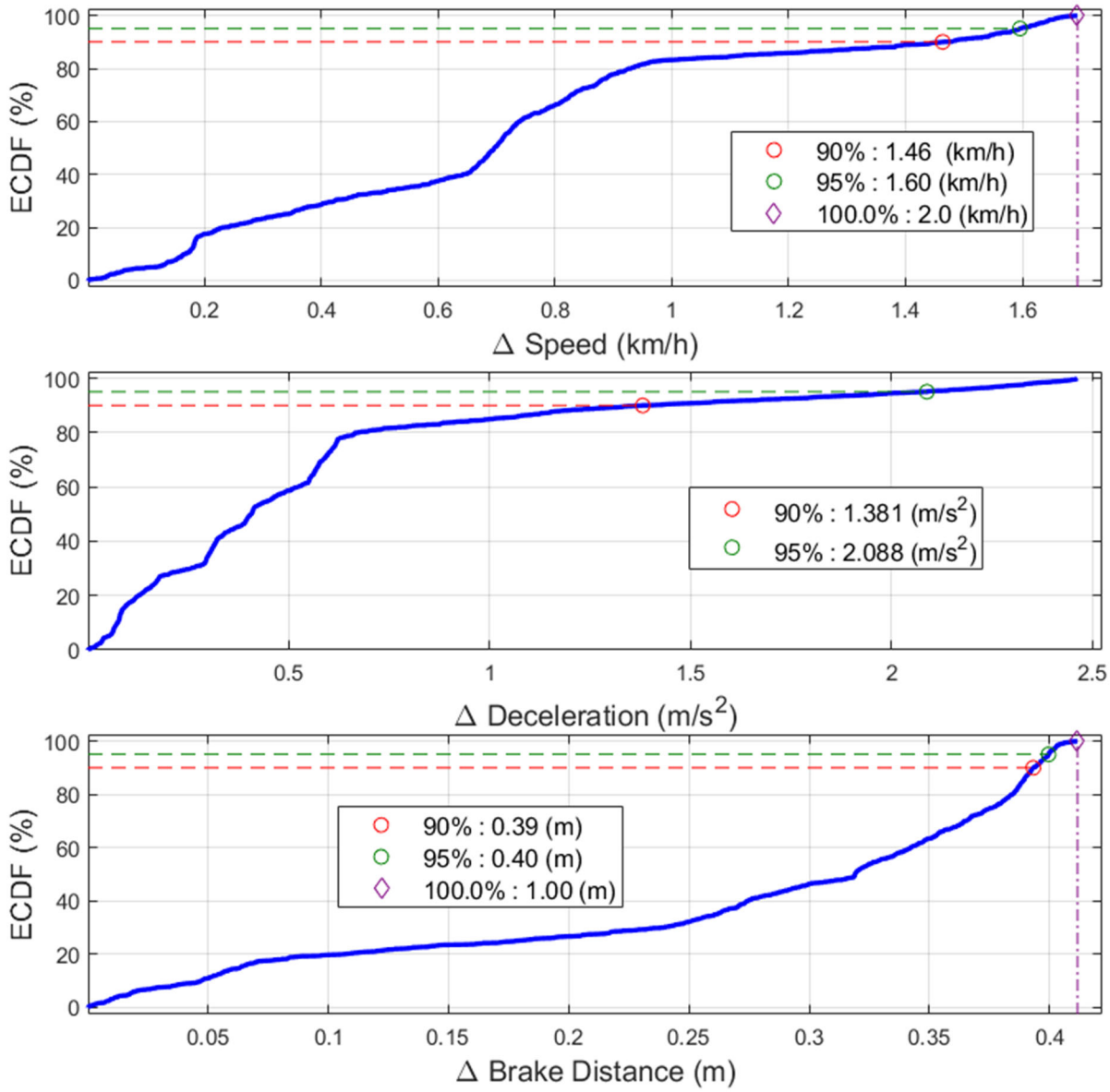

Figure 3-25. Cumulative Distribution Comparisons – Entrance Speed 48.3 km/h

4 Conclusion

This paper discussed modeling and potential validation methods applied to an SUT vehicle dynamics model. Four validation methods from literature were applied and discussed by comparing test track and simulation data: one subjective method, and three objective methods (CI, ISO 19364, and ECDF). For a subjective simulation evaluation, the methodology applied in this report used analytical comparisons within the linear range of vehicle dynamics responses.

Table 4-1 provides a summary of the lateral evaluation and validation, and of how the subjective metric, enhanced with limited analytical metrics, and the objective statistical measures are used to provide information about the trustworthiness of the simulated model. The application of the model is evaluated progressively from the linear trend up to the maximum non-linear state. For the lateral dynamics, the application is defined by lateral acceleration severity with the following ranges: linear range [-0.3, 0.3] g, mid-linear [-0.4, 0.4] g, non-linear [-0.5, 05] g, highly non-linear [-0.6, 06] g, and max-nonlinearity outside the [-0.6, 0.6] g range. For objective evaluations, the ECDF or the ISO 19364 (2016) method can be used. Both methods show consistent results when lateral dynamics are evaluated. However, the advantage of the ECDF is that it does not apply preset definitions of tolerances, which can be different for various vehicle classes and model complexities. In addition, the ECDF can be applied to all measures. Moreover, this method can be applied to test validity at 1, 2, and 3 sigma levels (68%, 95%, and 99.7% CI).

A simulation model may be deemed applicable within a defined range of severity if the ECDF passes the set probability targets. For example, when a variable analyzed with ECDF does not pass the 90% probability threshold, the simulation trustworthiness may not be considered valid, regardless of the trend of the data.

Subjective evaluations listed in Table 4-1 are used to provide confidence in the ECDF metrics. If subjective evaluations state that the trend of the data is not acceptable, then the ECDF metrics should reflect this observation through lower EDCF probability numbers. Otherwise, the metrics are either inaccurate due to low quality data or erroneously computed.

Table 4-1. Performance and Evaluation Guide – Lateral Dynamics

Dynamic Severity	Subjective		CI	ECDF		ISO 19364	Application
	Graphs	Analytical		P>90%	P>95%		
Linear	Good	Good	Yes	Pass	Pass	Yes	Yes
Mid-Linear	Average	NA	Yes	Pass	Pass	Yes	Yes
Non-Linear	Trend–OK	NA	Yes	Pass	Fail	Yes	Limited
Highly Nonlinear	Trend–NO	NA	Fail	Fail	Fail	Fail	Not advised
Max	Trend–NO	NA	Fail	Fail	Fail	Fail	No

For the SUT model tested for validation in this report, a secondary test, the J-turn maneuver, was performed to gain confidence in the validity of the model. The lateral dynamics J-Turn test showed consistent validity within the range of 0.5 g.

For longitudinal dynamics, the ECDF method is the only objective metric that could be properly evaluated, because the CI methodology requires ten runs to achieve statistical significance. The ISO 19364 (2016) validation methodology does not apply for longitudinal dynamics. The ECDF metrics for this analysis are listed in Table 3-16 and Table 3-17; subjective metrics with analytical estimations similar to those listed in Table 3-15 can be used to assess longitudinal dynamics trustworthiness. A summary of the longitudinal dynamics validation results is shown in Table 4-2. This table does not include liner and mid-linear validation ranges because all testing was performed at maximum braking from initial speeds of 48.3 and 96.6 km/h. While this vehicle model was evaluated at maximum braking, it might be necessary to include tests with lower deceleration values to allow assessment of model performance under less severe braking applications. Test track data from linear brake characterization tests (slowly increasing brake force from initial speed) can be applied to evaluate linear and mid-linear longitudinal dynamics. This is not available for the modeled SUT in this report.

The evaluation Table 4-2 for the maximum braking performance indicates that simulation results of longitudinal braking stopping distances were produced within the tolerances of 1.0 m for both tested speeds. The simulated speed profiles were close to experimental results, except for 48.3 km/h during the initial rise time of the longitudinal acceleration. This discrepancy was due to the acceleration differences between simulation and experimental results during the initial application of the brakes. After the period of rise time, the trend of the steady acceleration was similar to experiments. These evaluations show that simulation results of stopping distance and speed may be valid at maximum braking performance. For lower deceleration ranges, depending on the use of the model, the results may be acceptable.

Table 4-2. Performance and Evaluation Guide – Longitudinal Dynamics

Dynamic Severity: Maximum Braking	**Subjective**		**CI**	**ECDF**		**Application**
	Graphs	**Analytical**		**P>90%**	**P>95%**	
Stopping Distance	Pass	Pass	Pass	Pass	Pass	Yes
Speed	Pass	NA	Pass	Pass	Fail	Yes
Acceleration	Trend–OK Except at 48.3 km/h rise time	NA	Fail @ 48.3 km/h at rise time	Fail @ 48.3 km/h	Fail @ 48.3 km/h	Limited

In summary, for the lateral dynamics, the CI, ECDF, and ISO 19364 (2016) methods resulted in consistent validation metrics despite the low number of tests used to apply the CI validation methodology. For the longitudinal dynamics, the ECDF validation methodology was used because of the limited number of tests, and due to the fact that the ISO 19364 method isn't applicable. Moreover, using a common methodology for both the lateral and longitudinal validation process can provide a consistent metric for overall vehicle dynamics.

Referring to the g-g diagram in Figure 1-1, the SUT modeled in this paper was evaluated and considered valid for the following performance ranges: longitudinal acceleration [-0.6, 0] g for maximum braking performance, and lateral acceleration [-0.5 0.5] g. The longitudinal acceleration range has deceleration values only because the powertrain of the tested SUT was not modeled; instead, a generic powertrain model from dSPACE was applied. The vehicle model can

be used to simulate many scenarios, but the range of valid results is limited within operational boundaries defined above with error thresholds discussed in prior sections.

References

49 CFR, Part 571, 571.121, Standard No. 121; Air Brake Systems. (2009).

49 CFR, Part 571 571.126, Standard No. 126; Electronic Stability Control Systems. (2011).

49 CFR, Part 571, 571.136, Standard No. 136; Electronic Stability Control Systems for Heavy Vehicles. (2017).

Allen, R., Rosenthal, T., & Chrstos, J. (1997). A vehicle dynamics tire model for both pavement and off-road sonditions (SAE Technical Paper 970559). SAE International.

Ashley, D. (2003). Jackknife stability of articulated tractor semitrailer vehicles with highoutput brakes and jackknife detection on low coefficient surfaces (PhD dissertation). The Ohio State University.

Garott, R. W., Grygier, P. A., Chrostos, J. P., Heydinger, G. J., & Salaani, K. M. (1997). Methodology for validating the National Advanced Driving Simulator's vehicle dynamics (NADSdyna) (SAE Sp-1228, SAE Paper # 970562). SAE International.

Heydinger, G. J., Garrott, R. W., Chrstos, J. P., & Guenther, D. A. (1990). A methodology for validating vehicle dynamics simulation. Journal of Passenger Cars, 99(6), 126-146.

Heydinger, G. J., Gragier, P. A., & Lee, S. (1993). Pulse testing techniques applied to vehicle handling dynamics (SAE Technical Paper No. 930828). SAE International.

International Organization for Standardization. (2011). Road vehicles - Lateral transient response test methods - Open-loop test methods (ISO Standard No. 7401).

ISO. (2012). Passenger cars - Steady-state circular driving behavior - Open-loop test methods (ISO Standard No. 4138).

ISO. (2016a). Passenger cars - Validation of vehicle dynamic simulation - Sine with dwell stability control testing (ISO Standard No. 19365).

ISO. (2016b). Passenger cars - Vehicle dynamic simulation and validation - Steady-state circular driving behavior (ISO Standard No. 19364).

ISO. (2020a). Passenger cars -- Simulation model taxonomy -- Part 1: Vehicle dynamics maneuver (under development) (ISO Standard No. ISO/AWI 11010-1). Available at www.iso.org/standard/75910.html

ISO. (2020b). Road vehicles --Passenger cars -- Vehicle dynamic simulation and validation -- Lateral transient response test methods (under development) ISO/AWI 22140). Available at www.iso.org/standard/72680.html

Kutluay, E. (2012). Development and demostration of a validation methodology for vehicle lateral dynamics simulation models (Ph.D. dissertation). Technische Universitatt Darmstadt.

NHTSA. (n.d.). Voluntary safety self-assesment (NHTSA web page and portal). Available at www.nhtsa.gov/automated-driving-systems/voluntary-safety-self-assessment

Rao, S. J., Salaani, M. K., Heydinger, G. J., & Guenther, D. (2013). Modeling of a 6x4 tractor and trailers for use in real time hardware in the loop simulation for ESC testing (SAE Technical Paper No. 2013-01-0693). SAE International. Available at https://saemobilus.sae.org/content/2013-01-0693/

SAE International. (2018). Steady-state directional control test procedures for passenger cars and light trucks (SAE Standard J266_201811). Salaani, K. M. (2009). Analytical analysis of tyre forces as a function of normal pressure distributions. International Journal of Heavy Vehicle Systems, 16(1-2).

Salaani, K. M., Heydinger, G. J., & Grygier, P. A. (2003a). Evaluation of heavy tractor-trailer model used in the National Advanced Driving Simulator (SAE Technical Paper 2003-01-1324). SAE International.

Salaani, K. M., Heydinger, G. J., & Grygier, P. A. (2003b). Heavy tractor-trailer vehicle dynamics modeling for the National Advanced Driving Simulator (SAE Technical Paper 2003-01-0965). SAE International.

Salaani, K., Heydinger, G. J., & Grygier, P. A. (2004). Experimental steering feel performance measures (SAE Technical Paper No. 2004-01-1074). SAE International.

Salaani, M. K. (1996). Development and validation of a vehicle model for the National Advanced Driving Simulator. The Ohio State University.

Salaani, M. K., Elsasser, D., & Boday, C. (2020). Heavy vehicles kinematics of automatic emergency braking test track scenario (SAE Technical Paper 2020-01-0995). SAE International.

Salaani, M. K., & Heydinger, G. J. (1998). Powertrain and brake modeling of the 1994 Ford Taurus for the National Advanced Driving Simulator (SAE Technical Paper No. 981190). SAE International.

Salaani, M. K., Heydinger, G. J., & Grygier, P. A. (2002). Modeling and implementation of steering system feedback for the National Advanced Driving Simulator. Journal of Passenger Cars: Mechanical Systems, 111(6), 1767-1775.

Salaani, M. K., Heydinger, G. J., & Grygier, P. A. (2006). Measurement and modeling of tire forces on a low coefficient surface (SAE Technical Paper No. 2006-01-0559). SAE International.

Salaani, M. K., Mikesell, D., Boday, C., & Elsasser, D. (2016). Heavy vehicle hardware-in-the-loop automatic emergency braking simulation with experimental validation. SAE International Journal of Commercial Vehicles, 9(2), 57-62. Available at https://doi.org/10.4271/2016-01-8010

Smith, R. H. (2008). Analyzing friction in the design of rubber products and their paired surfaces. CRC Press.

Starkey, J. M. (1993). The effects of vehicle design parameters on handling frequency response characterestics. International Journal of Vehicle Design, 14(No 5/6). Available at www.inderscienceonline.com/doi/10.1504/IJVD.1993.061850

Appendix A: SUT Vehicle Parameter Settings

SUT dynamics were modeled using ASM by dSPACE Inc., an open Simulink model for real-time automotive applications. Its modular setup makes it possible to combine different model libraries to accommodate different vehicle types. These include truck, trailer, and pneumatics models to cover a diversified range of heavy vehicle cases, which can span from class three to class eight types, with steerable front- and rear-axles, push axles, etc. Switches are included in the model to configure the model to reflect a heavy vehicle model with two axles, twin tires on the rear axle, a rear wheel drive, and an automatic transmission.

The SUT ASM vehicle dynamics parameters were set using ModelDesk from dSPACE. The parameters were set for the vehicle body and wheels, suspension kinematics and compliances, brake, steering, and tire systems. dSPACE offered ASM model data setting with an Excel spreadsheet that lists all the parameters for the vehicle dynamics, as shown in Figure 6-1. No means were offered to convert vehicle dynamics data sets from different simulation software like TruckSIM and TruckMaker to the dSPACE ASM system.

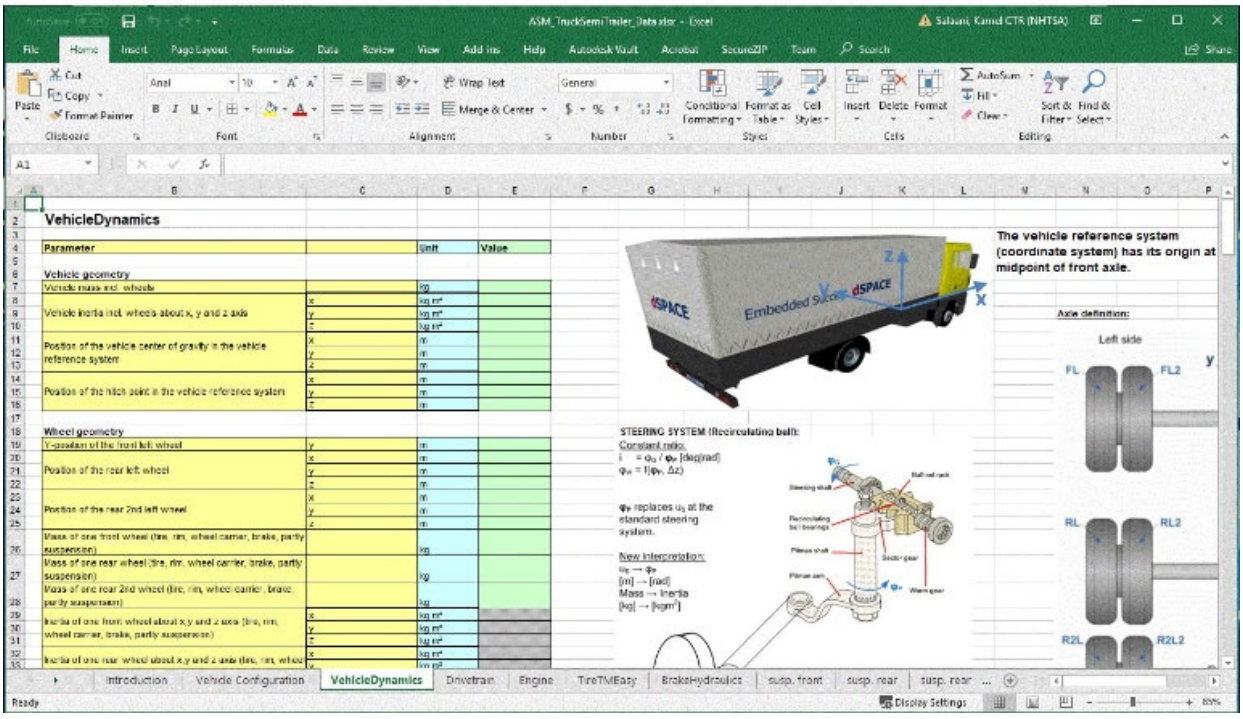

Figure 6-1. ASM Excel Data Sheet

Vehicle Body and Mass Properties

Table 6-1 lists the LLVW mass and inertial properties, and Table 6-2 lists properties of the additional load needed to bring the LLVW vehicle to GVWR loading condition. The vehicle mass, CG longitudinal and lateral positions, additional load mass, and inertial properties were measured. The truck inertial properties and vertical CG position were assumed using

measurements from a 2006 Volvo 6X4 VNL 64T630 obtained at AMSRD-TAR-D, US Army TARDEC.

All the geometric positions listed in data tables (Table 6-1 and Table 6-2) are with respect to the vehicle reference position at the center of the front axle. Each inertial property is with respect to the corresponding body CG. For the additional load, the lateral CG position was positioned at the center to make the vehicle model symmetric which is similar to the actual vehicle.

To check that mass and geometric data entry were entered correctly in the simulation software, a simple static simulation was run, and all vertical loads at the tires were compared with the measured vertical loads from the truck scale. The results indicated that the mass distribution, wheels and axles geometries were accurately modeled in Table 6-3.

Table 6-1. Vehicle LLVW Mass, CG, and Inertia

Type	Values
Total mass (kg)	7107.79
CG X position (m)	-2.116
CG Y position (m)	0.0
CG Z position (m)	0.564
Ixx (kg m^2)	1439.0
Iyy (kg m^2)	8288.6
Izz (kg m^2)	8288.6
Ixz (kg m^2)	1626.0

Table 6-2. Additional Load Mass, CG, and Inertia

Type	Values
Vehicle additional load (kg)	4662.0
CG X position (m)	-4.239
CG Y position (m)	0.0
CG Z position (m)	0.640
Ixx (kg m^2)	2728.94
Iyy (kg m^2)	1331.69
Izz (kg m^2)	2216.75

Table 6-3. Truck Measured/Simulated Corner Weights (kg) at GVWR

Type	Steer – Left	Steer – Right	Rear Drive Axle – Left	Rear Drive Axle – Right	Testing Weight
Measured	2168	1877	3942	3783	11770
Simulated	2022	2022	3862	3862	11768

The wheel and suspension body mass and inertial properties were not measured directly, because they require truck disassembly, but estimates from multi-body dynamics modeling of similar vehicles were used (Salaani et al., 2003a, 2003b; Rao et al., 2013). The left and right wheel masses and inertia are estimated by taking (1/2) of axle mass, and (1/2) of axle inertia (dSPACE manual). Although a solid axle is specified in the ASM document for the tractor suspension model, the data were set through a lumped mass at each vehicle corner position. For lateral motion at high frequency steering input, like a sweep sine steering input or a pulse steer input, the high mass of the wheel and suspension would reduce the vehicle bandwidth responsiveness and decrease the magnitude of the vehicle lateral responses (lateral acceleration and yaw rate). This follows the principle of motion and inertial mechanics: The higher the mass, the lesser the dynamic response bandwidth. The wheel and mass properties used in the simulation are listed in Table 6-4.

Table 6-4. Wheel Mass Inertial Properties

Wheel carrier and body	Values
Front left mass (kg)	187.5
Front left Ixx (kg m^2)	5
Front left Iyy (kg m^2)	6
Front left Izz (kg m^2)	5
Front left rotating (kg m^2)	10
Rear left mass (kg m^2)	317.5
Rear left Ixx (kg m^2)	5
Rear left Iyy (kg m^2)	6
Rear left Izz (kg m^2)	5
Rear left rotating (kg m^2)	20

Tire Mechanics

Vehicle dynamics is essentially the solution of Newton's second law of motion; that is, force equals mass times acceleration. The left side of this equation, force, is predominantly determined by the ground forces generated at the tire contact. If these forces are not modeled accurately, the simulation results become unreliable, with limited use and scope. The simulation is as good as the quality of equations and parameters used to define the force generation process at the tire-ground contact.

ASM offers two tire models. The first model is called the *EasyToUse* (TMeasy) tire model, and the second one is the MagicFormula Model. They are semiempirical tire models for describing lateral and longitudinal forces and self-aligning torque. These tire models generally provide a good agreement of quasi-steady-state tire measurements. The EasyToUse tire model has much simpler empirical formulations, with few parameters, that can be easily understood and formulated to fit experimental data. The SUT tire data were set using the EasyToUse model.

The modeled SUT tires were not measured to determine forces and moments parameters for the EasyToUse ASM tire model, but measured data from tires similar in size and type were used (Salaani et al., 2003a, 2003b). Tire sizes and model are specified in Table 6-5.

Table 6-5. SUT Tires

Steer Axle Tire	11R22.5 Continental HS3 EcoPlus
Drive Axle Tire	11R22.5 Continental HDR2

ASM offers the ability to set four empirical tire data sets that can be used within a single simulation test. This option, of setting 4 sets of tire parameters to simulate different surface conditions that affects not only the friction coefficient, but also the shape of tire forces to slip curves, is an efficient method to address changes to surface conditions. This method of coping with surface conditions is more accurate than merely scaling forces through changes of the coefficient of friction. Changing the coefficient of friction to model different tribological contacts is a nonscientific application of the laws of metallic friction to tires operated on pavements (Smith, 2008). Experimental measurements of tire forces on wet conditions performed at CALSPAN showed that the shape of the force generation is substantially altered due to the presence of water. In wet conditions, changing the coefficient of friction is a scaling approximation, and may not be accurate at the force saturation limits (Salaani et al., 2006).

The tire data are tabulated as follows. Table 6-6 lists the front- and rear-tire geometries, which are easily read from OEM tire description labels.

Table 6-6. Front and Rear Tire Geometry

Type	Values (m)
Unloaded tire radius	0.550
Tire height	0.237
Tire width	0.210
Dual tire distance	0.234

Table 6-7 defines longitudinal and lateral tire force parameters used in the vehicle model database. The various parameters are graphically illustrated in Figure 6-2. These are maximum peak force (F_{max}), slide force at tire saturation (F_{slide}), maximum slip (S_{max}) at which F_{max} occurs, slide slip (S_{slide}) where the forces begin to saturate in sliding mode, and the force to slip slope at the origin. This method of listing forces and slopes at a specific longitudinal and lateral slip values in radians is not intuitive. This table is transformed into Table 6-8, using the same information from Table 6-7, but with parameters that can be set and adjusted based on test surface conditions.

Table 6-7. Tire Force Parameters – Nominal F_z = 27469 N

Parameter	Front/Rear	Longitudinal		Lateral	
		F_z	2* F_z	F_z	2* F_z
F_{max} (N)	Front	22131	40979	21385	35520
	Rear	22489	40019	21385	35520
F_{slide} (N)	Front	21024	38930	19246	31968
	Rear	21365	38018	19246	29810
S_{max}	Front	0.21	0.21	0.20	0.20
	Rear	0.21	0.21	0.20	0.20
S_{slide}	Front	0.80	0.80	1.40	1.40
	Rear	0.80	0.80	1.40	1.40

Parameter	Front/Rear	Longitudinal		Lateral	
		F_z	2* F_z	F_z	2* F_z
Slope (N)	Front	191300	423900	210504	298167
	Rear	181478	390090	210504	298167

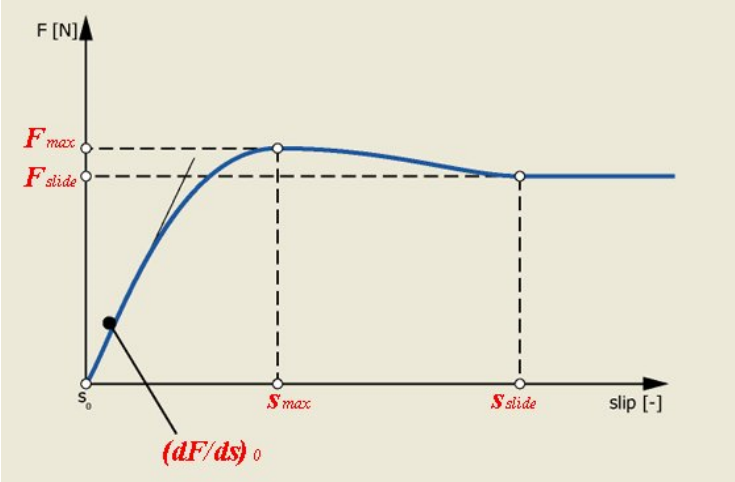

Figure 6-2. ASM Tangential Tire Forces Schematics

Table 6-8 defines tire parameters using three fundamental properties: stiffness, peak, and sliding frictions. In many empirical tire models, these three phases are modeled using third or higher order polynomials expressed in terms of vertical tire loading (e.g., Calspan tire parameters) (Allen et al., 1997; Salaani, 2009). Table 6-7 was transformed by normalizing the forces with respect to the normal force F_z and redefining the longitudinal slip and lateral slip angle into a more usable format, resulting in Table 6-8.

Longitudinal tire force is characterized by normalized longitudinal stiffness $\frac{F_x/\delta\kappa}{F_z}$, peak saturation state (μ_{px}, κ_p), and sliding state (μ_{sx}, κ_s). Tire measurements showed that the tire normalized longitudinal stiffness does not vary much with the change of normal loading, with no data availability, and that a constant normalized stiffness was used. The peak saturation region defined by this set (μ_{px}, κ_p) is load dependent, and a longitudinal slip ratio around 0.2% at the peak was used as no experimental data were available. The peak friction parameter, μ_{px}, is load sensitive. If no tire data are available to set this parameter, it can be estimated from peak longitudinal deceleration using total vehicle weight and road friction coefficient. Sliding slip data point (μ_{sx}, κ_s) is set at 80% of the slip ratio, and the sliding friction coefficient is typically 90% of peak μ_{px} values on asphalt surfaces, based on prior vehicle modeling experiences.

Lateral tire forces are also defined by three fundamental properties; linear stiffness $\frac{F_y}{\alpha}$, peak saturation region (μ_{py}, α_p), and sliding region (μ_{ps}, α_s). Tire lateral stiffness is very sensitive to normal loading, and its variation is not linear in terms of changes in vertical forces. Lateral tire stiffness can be expressed with a third-degree polynomial (Salaani, 2009). The peak saturation region occurs typically at the vicinity of 12° of lateral slip angle, and peak friction values can be

estimated from peak lateral acceleration in a steady turn at a specific loading condition. For the sliding set (μ_{ps}, α_s), the maximum lateral slip angle is set to 80° (theoretically 90° for transversal lateral motion), and peak sliding friction can be set at 90% of peak friction values on asphalt surfaces.

Longitudinal and lateral tire peak and sliding frictions, lateral tire stiffness, and longitudinal tire stiffness are nonlinearly dependent on normal loads. Having two normal loads to define these parameters is a deficiency in the application of this simple tire model in dSPACE ASM system. Modeling tire rubber behavior empirically requires at least four normal load conditions to cover the extent of rubber nonlinearities.

Table 6-8. Tire Force Fundamental Parameters – Nominal F_z = 27469 N

Type		**Longitudinal**		**Lateral**	
		F_z	**2* F_z**	**F_z**	**2* F_z**
F_{max} parameters	**Front**	μ_{px} =0.806	μ_{px} =0.746	μ_{py} =0.778	μ_{py} =0.646
	Rear	μ_{px} =0.819	μ_{px} =0.728	μ_{py} =0.778	μ_{py} =0.646
F_{slide} parameters	**Front**	μ_{sx} =0.765	μ_{sx} =0.709	μ_{sy} =0.70	μ_{sy} =0.582
	Rear	μ_{sx} =0.778	μ_{sx} =0.692	μ_{sy} =0.70	μ_{sy} =0.542
S_{max} parameters	**Front**	κ_p =0.21 %	κ_p =0.21 %	α_p =11.46°	α_p =11.46°
	Rear	κ_p =0.21 %	κ_p =0.21 %	α_p =11.46°	α_p =11.46°
S_{slide} parameters	**Front**	κ_s =0.80 %	κ_s 0.80 %	α_s =80°	α_s 80°
	Rear	κ_s =0.80 %	κ_s =0.80 %	α_s =80°	α_s =80°
Slope parameters	**Front**	$\frac{F_x/\kappa}{F_z}$ =6.964 N/N	$\frac{F_x/\kappa}{F_z}$ =7.716 N/N	$\frac{F_y}{\alpha}$ =3674 N/degrees	$\frac{F_y}{\alpha}$ =5204 N/degrees
	Rear	$\frac{F_x/\kappa}{F_z}$ =6.607 N/N	$\frac{F_x/\kappa}{F_z}$ =7.101 N/N	$\frac{F_y}{\alpha}$ =3674 N/degrees	$\frac{F_y}{\alpha}$ =5204 N/degrees

Table 6-9 lists the parameters for the aligning moment used in the tire model, and an illustration of these parameters is shown in Figure 6-3. The normalized pneumatic trail n/L data was estimated from the same tire data used for longitudinal and lateral forces. The dSPACE tire model uses a linear approximation with respect to normal load variation, and it is a reasonable approximation for the pneumatic trail based on prior tire modeling experiences.

Table 6-9. Tire Aligning Moments – Nominal F_z = 27469 N

Parameter	**Type**	**F_z**	**2*F_z**
n/L	Front	0.15	0.38
	Rear	0.15	0.38
S_{max}	Front	0.20 (α_p =11.46 degrees)	0.20 (α_p =11.46 degrees)
	Rear	0.20 (α_p =11.46 degrees)	0.20 (α_p =11.46 degrees)
S_{slide}	Front	0.50 (α_s =28.65 degrees)	0.50 (α_s =28.65 degrees)
	Rear	0.50 (α_s =28.65degrees)	0.50 (α_s =28.65 degrees)

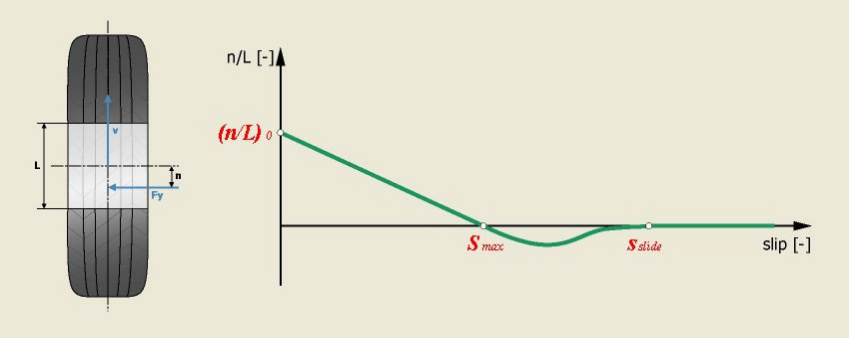

Figure 6-3. ASM Aligning Moment Schematics

Values for the tire structural stiffnesses are shown in Table 6-10 and illustrated in Figure 6-4. The vertical stiffness is a typical value that is used for one-point vertical contact model with the road surface, and for normal pressure of 0.76 MPa (110 psi). This parameter is typically measured during suspension compliance tests. The initial values for the lateral damping and stiffness were adopted from (Salaani et al., 2003, 2003b) and modified slightly to improve simulation results.

Table 6-10. Tire Structural Stiffness Front and Rear

Parameter	Longitudinal	Lateral	Vertical
Damping N/(m/s)	1600	400	800
Stiffness (N/m)	300000	80000	1190000

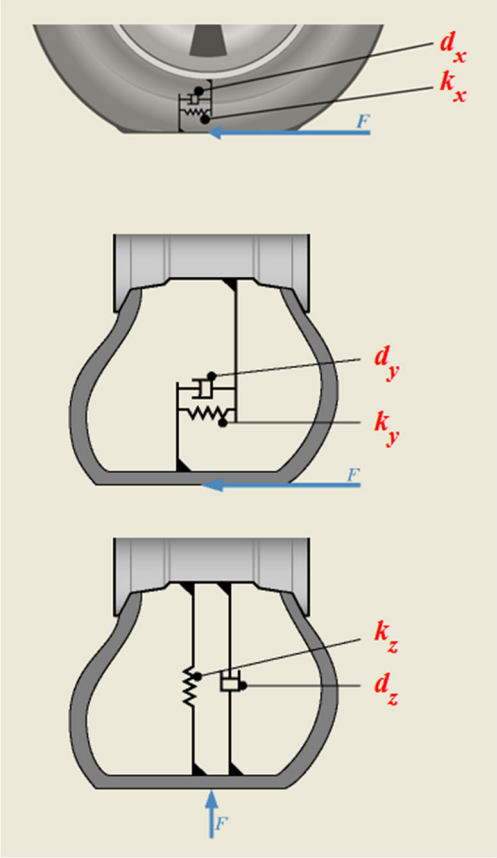

Figure 6-4. Tire Structural Rigidity Schematics

The tire model (TMEasy) used in modeling the SUT is limited and has two fundamental shortcomings to properly define the force generation process of tires. These shortcomings affect vehicle dynamics simulation predictions at high dynamic transient states, or at the high nonlinear range. It is unlikely possible to accurately model vehicle dynamics behavior in the high non-linear range (typically higher than 0.5 g) with these shortcomings.

The first is the absence of enough data points to accurately define tire friction and stiffness. Tire peak and sliding frictions and linear stiffness are load dependent and not linear. A more accurate description is to add more columns of loads (at least 4) in ASM tire modeling that span 25% to 200% of the tire nominal load.

The second is the absence of lateral tire relaxation length, or lateral force delay. The relaxation length is a property of viscoelasticity of pneumatic tires that defines the delay of lateral force build up and stress relaxation, and it is speed dependent. Similarly, the longitudinal relaxation length is not part of the data set, but this has lesser effects on overall vehicle dynamics than the lateral relaxation length. Numerous published results used either first- or second-order differential equations to model this dynamic delay, as it is present on most commercial vehicle dynamics software and accepted as a standard practice (e.g., SAE J266).

Suspension – Forces, Compliances, and Geometry

The suspension kinematics, compliances, and forces are configured in the model with look-up tables. The kinematics are defined by the relative wheel center position and by its orientation, along with the spring, damper, and stabilizing bar displacements (deflection) and rate of displacements. This type of data is generally generated by K&C (kinematics and compliances) testing, or by a multibody dynamics software simulation of suspension joints like ADAMS/car suspension kit. Without experimental K&C suspension data, or multibody simulation data, reasonable assumptions were used to arrive at models. These are described in detail in the following subsections.

Axle Compliances – Forces and Moments

Compliances result from flexibility and deflection of the vehicle suspension components. These deflections cause some additional steering angle and camber changes (orientations about the wheel longitudinal axis) at the wheel. These affect the force generation process at the tire/ground contact. The simulation model implements these deflections with a look-up table. This method of applying changes in wheel orientations kinetically is sufficient for accurately simulating vehicle motion within the frequency spectrum (less than 4 Hz) of vehicle motion. Suspension compliances and flexibility have a higher frequency than vehicle motion, and the inclusion of high stiffness elements in the suspension would impede real-time numerical computation practicality.

ASM provides three tables to implement suspension compliances: axle displacements and rotations (Table 6-11), wheel camber compliances (Table 6-12), and wheel toe (steer) compliances (Table 6-13). The values in these tables were not measured directly but were adjusted from different data sets provided by the ASM example model to make the simulation closer to experiments. The front axle has more flexibility than the rear because of the steering linkages. Also, longitudinal and lateral compliances were added.

Table 6-11. Axle Compliances

Type	Front	Rear
Longitudinal displacement to longitudinal force dx/dfx (mm/KN)	0.33	0.0
Lateral displacement to lateral force dy/dfy (mm/KN)	0.17	0.13
Toe (steer) rotation to Z-moment dGamma/dTz (degrees/KN)	0.0	0.0
Toe (steer) rotation to Fy force dGamma/dfy (degrees/KN)	0.0	0.0

Table 6-12. Wheel Camber Compliances

Type	Front	Rear
dCamber/dfx (degrees/KN)	0.0	0.0
dCamber/dfy (degrees/KN)	0.33 10e-3	0.0
dCamber/dTx (degrees/KN)	0.33 10e-3	0.0
dCamber/dTz (degrees/KN)	0.0	0.0

Table 6-13. Wheel Toe Compliances

Type	Front	Rear
dToe/dfx (degrees/KN)	0.0	0.0
dToe/dfy (degrees/KN)	-0.05	0.0
dToe/dTx (degrees/KN)	0.0	0.0
dToe/dTz (degrees/KN)	0.17	0.17

Suspension Forces

Suspension forces resulting from the spring and damper deflections are applied at the wheel center, and not at their actual positions on the vehicle between the chassis and the axle, (see Figure 6-5). Figure 6-6 displays front and rear spring forces versus deflections. The front suspension stiffness is 281 KN/m, and rear suspension stiffness is 153 KN/m; both were measured for a similar SUT (2011 International Durastar 4300M7 SBA 4x2). Bump stops were added to limit the roll angle, and those were set several times stiffer than the spring stiffness and were not measured. They were set to limit suspension travel and match the maximum measured roll angle during lateral dynamics testing. The stabilizer bar for the front is 72 KN-m/deg and neglected at the rear. The bump stops and stabilizer bar values were set by making a comparison between simulation roll angle and experimental measures. The damping forces for the front and rear used were from ASM heavy truck nominal values supplied by dSPACE.

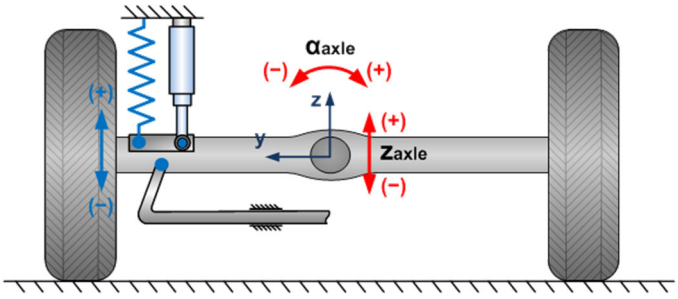

Figure 6-5. Suspension Spring and Damper Schematic

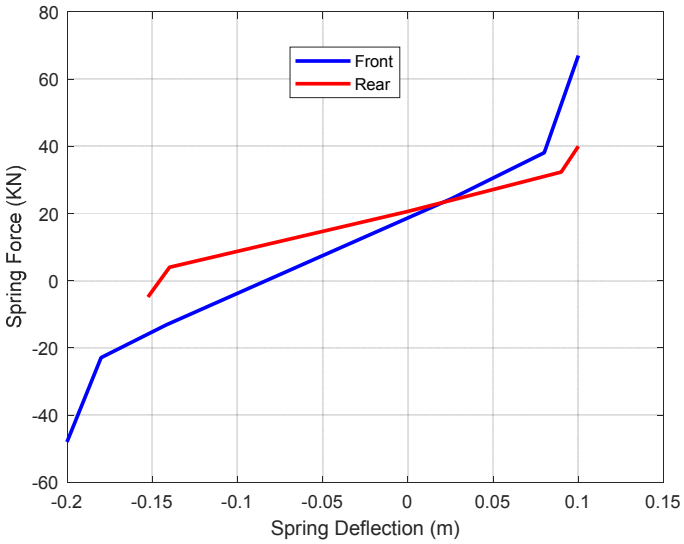

Figure 6-6. Front and Rear Suspension Force versus Deflection

Suspension Geometry

Table 6-14 lists the positions of the front- and rear-left suspensions with respect to the model vehicle reference coordinate system, which is at the center of front axle and vehicle center position. The right suspension positions are symmetrical to the left. The suspension positions are wheel center positions in simulation.

Table 6-14. Suspension Position in Vehicle Coordinate System

Type	Values
Front left wheel – lateral (m)	1.016
Front left wheel – longitudinal (m)	0.0
Front left wheel – vertical (m)	0.0
Rear left wheel – longitudinal (m)	-4.496
Rear left wheel – lateral (m)	0.94
Rear left wheel – vertical (m)	0.0

With no measured spatial data for the wheel motion, nor a 3-D multibody dynamics model of the truck suspension geometry available (Figure 6-7), the axle displacement data are the nominal data from dSPACE ASM model of similar vehicle type. In the modeling process, the default values were used as a starting point to see how well the model performed in comparison with the test track data. When not in agreement, adjustments were made either based on suspension measurements or vehicle dynamics experience.

Front axle wheel longitudinal and lateral positional changes with respect to pitman arm rotation were set to zero (zeros in the tabular data), the same for the caster and camber rotation (zeros in the tabular data). The only input that needed to be set was the gamma rotation (toe steer), as shown in Figure 6-8. The table for that is set as gamma rotation (steer rotation) angle versus pitman arm rotation. This part is discussed next as part of steering system parameters setting. The rear wheel displacements were set to zero, because they are part of the rear rigid axle.

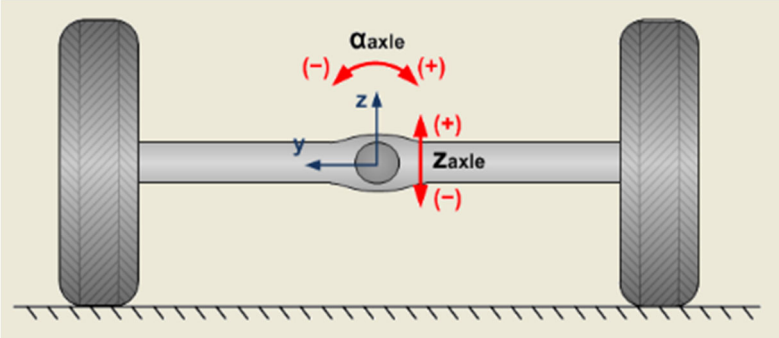

Figure 6-7. Axle Spatial Movement

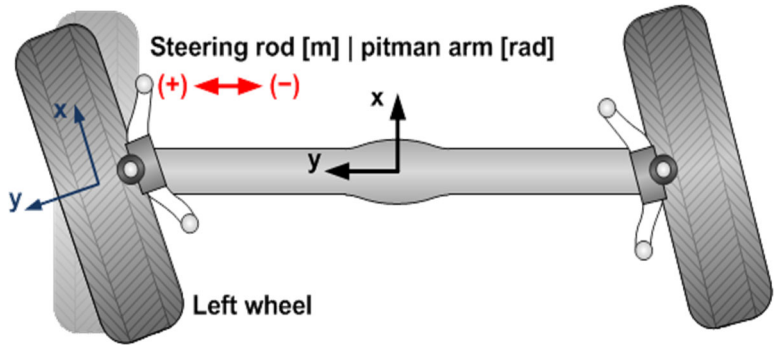

Figure 6-8. Left Wheel Displacement to Pitman Arm Rotation

Steering System

The tested SUT is equipped with a pitman-arm power steering system, shown in Figure 6-9. Only the parameters that affect the kinetic motion of the road wheel to handwheel steering were modified. The system was not evaluated and validated for a closed driver in the loop testing, where torque feedbacks at the steering handwheel and on-center steering performances needed to be compared with experimental measures. Parameters related to the forces and friction of the steering linkage and power assist were not modified from the nominal steering data set supplied with ASM software for heavy truck.

The steering ratio between the handwheel and road wheel was measured to be 18.3 degrees/degree, and the steering dead band at the handwheel measurement was 7.5 degrees. The Ackermann steering effect was measured by rotating the handwheel steering from 620 degrees to -620 degrees and measuring road wheel angles.

The steering system compliances were not defined here and were set to zero. These compliances were accommodated at the suspension/axle compliances discussed earlier.

Table 6-15 lists the steering system parameters used for the SUT model. The model kinetic steering system uses the rotation from steering system pitman arm to road wheel, and it is part of the suspension geometric setting. The model default parameter for the ratio of handwheel to pitman arm rotation is used to calculate pitman arm to road wheel rotation (Figure 6-10) from the measured handwheel to road wheel steering data.

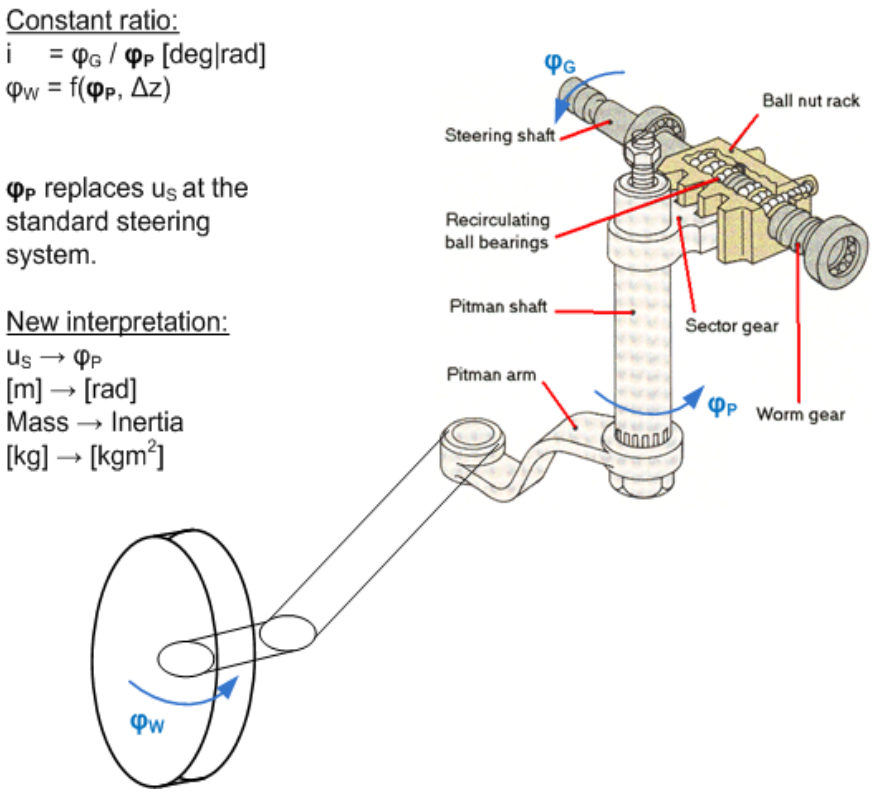

Figure 6-9. Pitman Arm Steering System Schematic

Table 6-15. Steering System Model

Type	Symbols	Values
Measured or Calculated at VRTC		
Total steering ratio: handwheel to road wheel	φ_G/φ_W	18.2 degrees/degrees
Pitman – to road wheel	$\varphi_P/\ \varphi_W$	Tabular data – Figure 6-10
Dead band	φ_G	7.5 degrees
ASM Default Parameter		
Steering wheel to pitman arm rotation	φ_G/φ_P	7142.86 degrees/rad

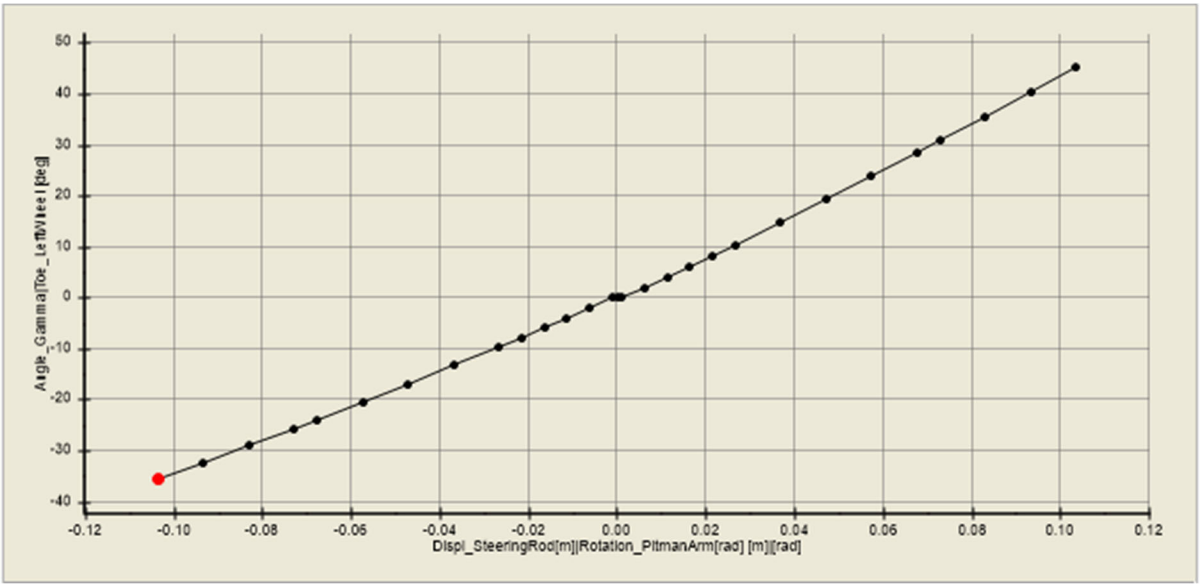

Figure 6-10. Pitman Arm to Left Wheel Rotation

Note: The x-axis has displacement steering rod because dSPACE uses a single normalized model for steering rod and pitman arm steering systems.

Brake System

The model used the HiL brake system developed at NHTSA, as shown in Figure 6-11 and Figure 6-12. The system hardware is detailed in several publications (Salaani et al., 2016), and the discussion herein is focused on brake model setting parameters and Simulink interface. The hardware is slightly adjusted to accommodate a two-axle truck system. The ASM Simulink model is modified to accommodate hardware in the loop simulation to integrate brake line pressures at the wheel chambers and the electronic control units. For this simulation, the Bendix EC-60 is used to primarily activate the ABS system during hard braking, with no stability and control effects.

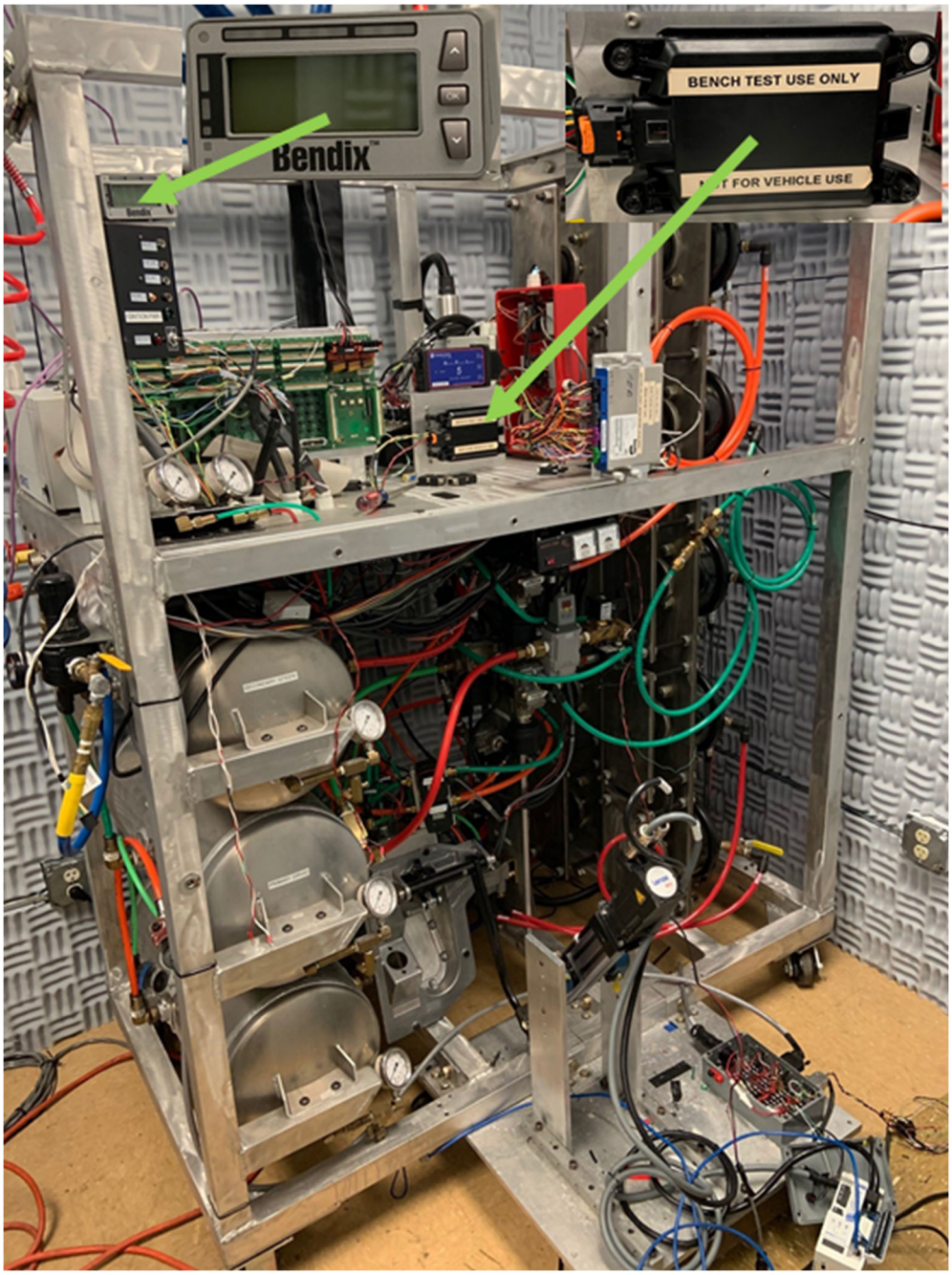

Figure 6-11. VRTC HiL System With Bendix Display and Radar Insets

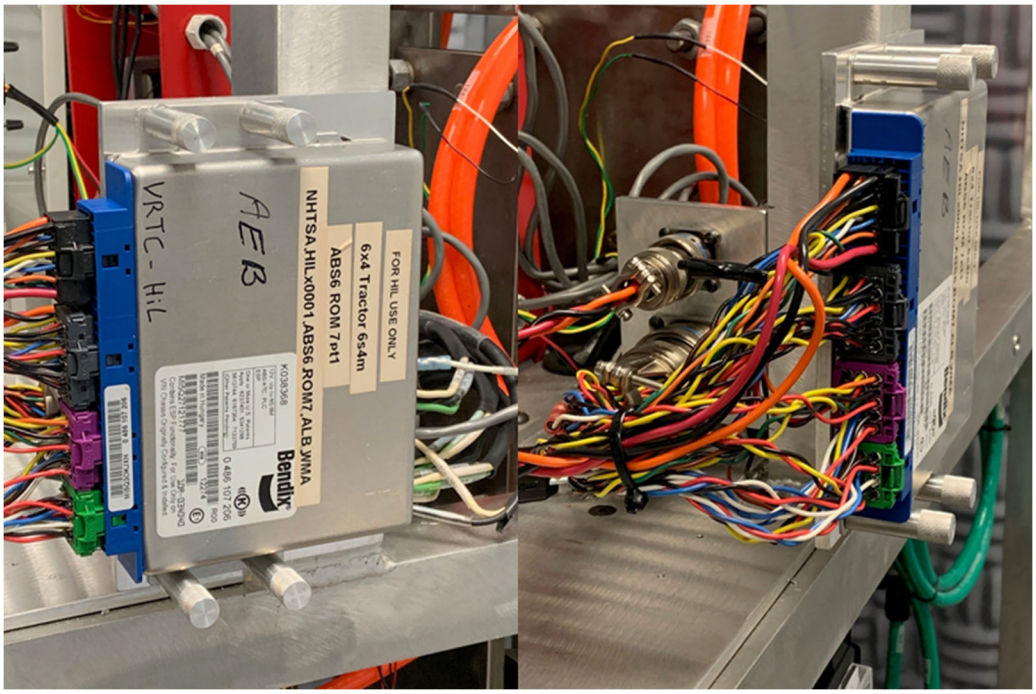

Figure 6-12. VRTC HiL Braking System – ECU and Connection

The ASM dSPACE Simulink model (see Figure 6-13), peripheral I/O and MDL (dSPACE vehicle, environment, sensors, models), was modified to use the testbench brake system. The system was modified to handle model only brake system or testbench model with automated switches at the simulation interface.

The front and rear brake line pressures were measured at the brake chamber inlet pressure position, processed through calibration and signal conditioning (Figure 6-14), and used with vehicle speed to calculate brake torques using 2-D table lookup from Simulink (Figure 6-15). The performances of heavy truck brake torque were speed dependent, and the parameters and scaling guidance were adopted from prior NHTSA research (Ashley, 2003). The values of the brake torque curves were adjusted to identify simulation braking responses (acceleration, speed, and stopping distance) during deceleration events closer to experimental measurements. A first order dynamic was used with a time delay of 0.05 seconds at each brake line to accommodate additional brake delays and to filter brake line data from measurement noise. The Simulink model is shown in Figure 6-16.

The dSPACE ASM pneumatic brake model was not applied in this SUT model because it required numerous brake component parameters not available for the tested SUT. For vehicle dynamics handling and control, a simple model from a system performance approach as applied in the simulated SUT is enough to produce reasonably accurate braking performance without the burdens of detailed brake component data.

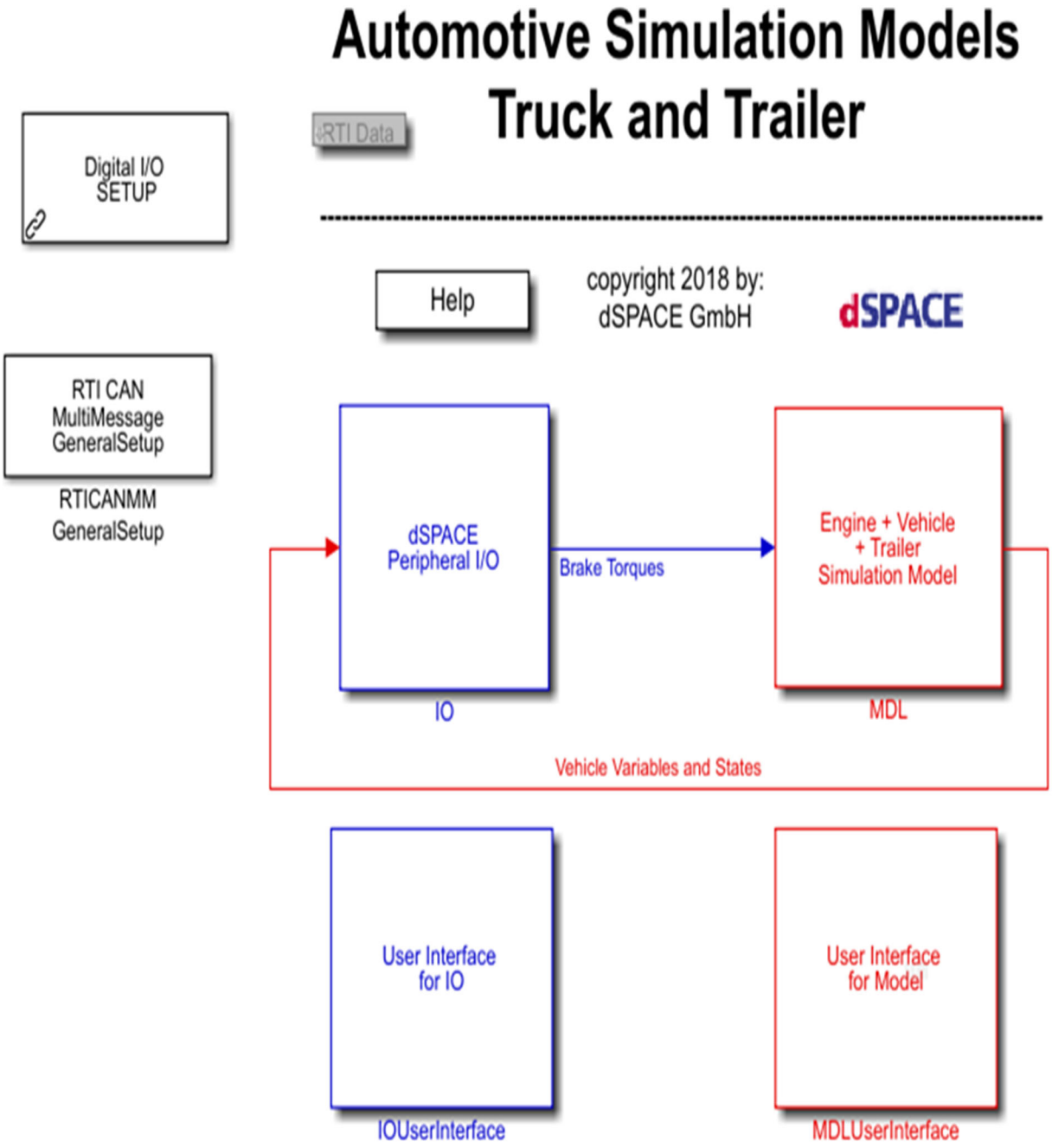

Figure 6-13. ASM Simulink Model

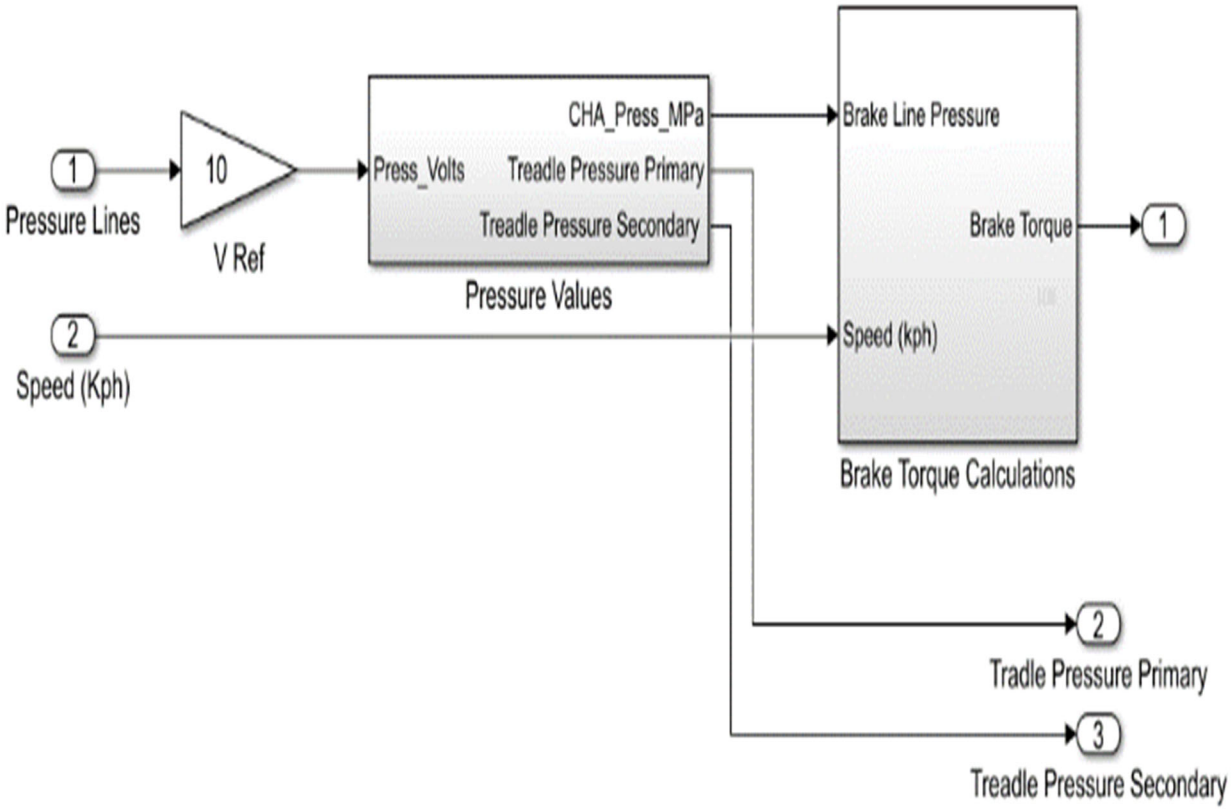

Figure 6-14. Brake System for HiL System

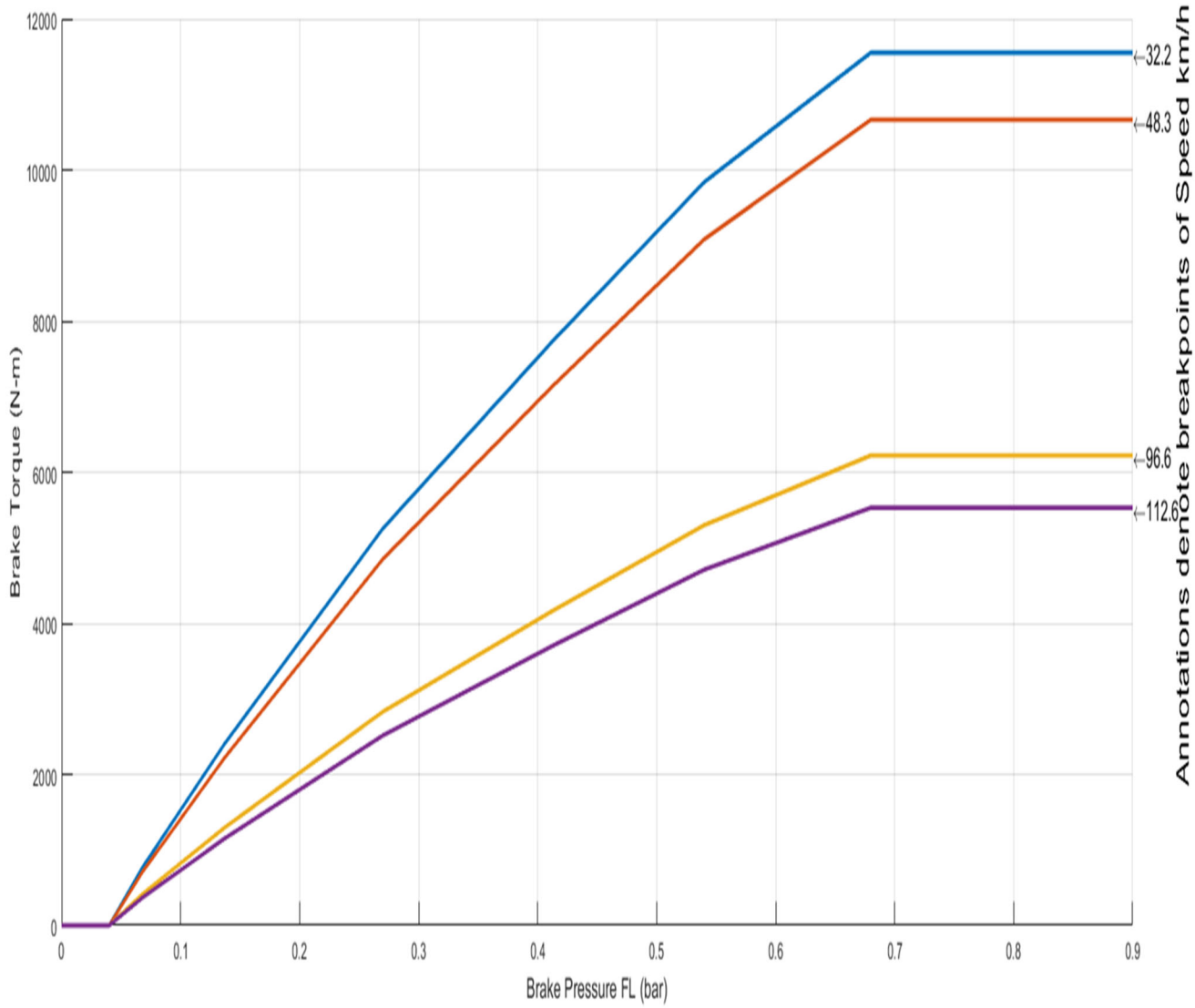

Figure 6-15. Brake Torque Parameters

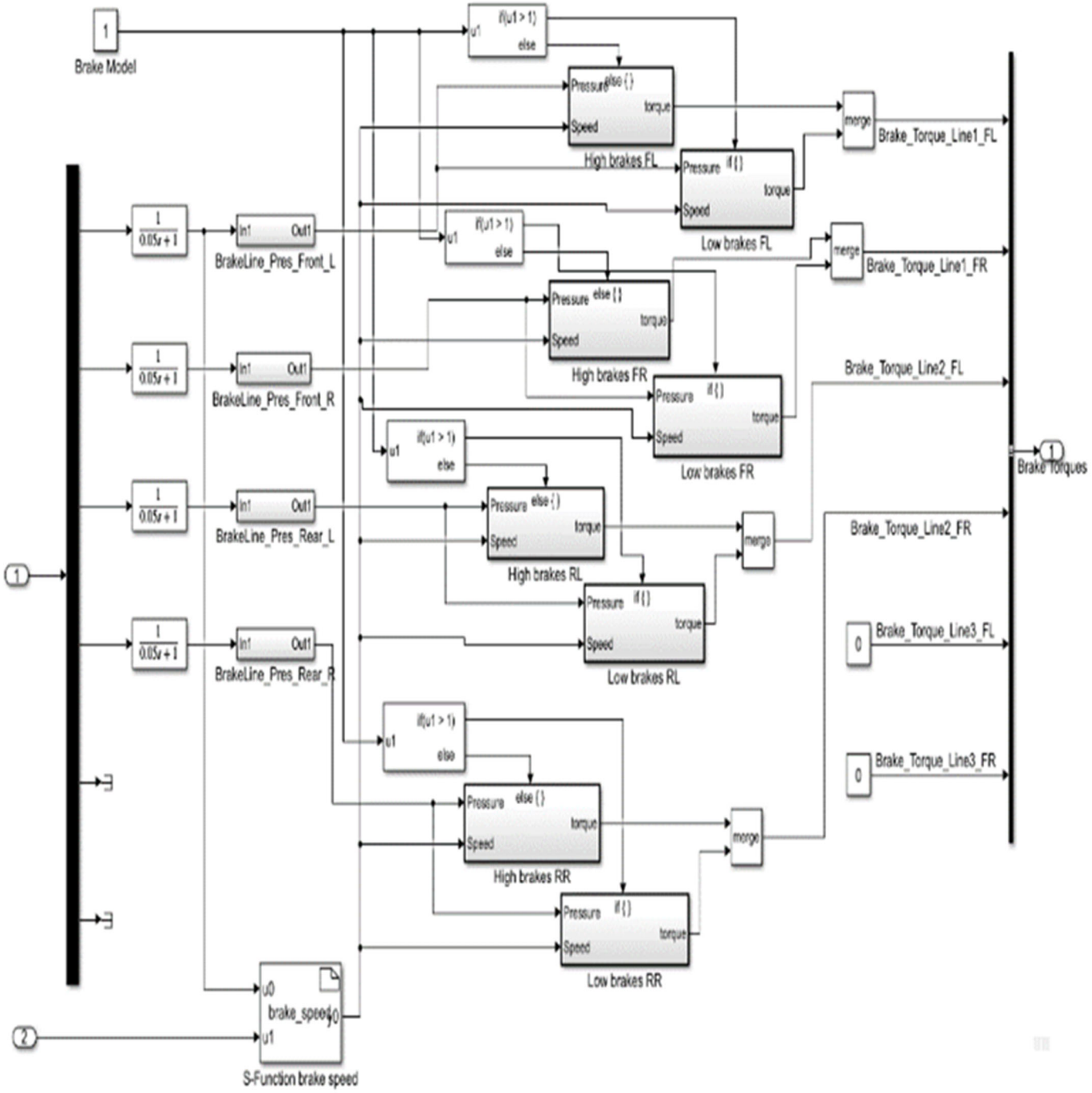

Figure 6-16. Simulink Brake Model

Aerodynamics & Powertrain

The aerodynamics and vehicle powertrain data sets were not modified from the original ASM software. The powertrain model supplied with ASM is a rear wheel drive system with an automatic transmission. The powertrain model was not fully evaluated since the validation tests were either conducted at a constant speed, coast down, or brake stops.

DOT HS 813 177
September 2021

U.S. Department
of Transportation

**National Highway
Traffic Safety
Administration**

15328-090221-v3